Charles University in Prague
Faculty of Mathematics and Physics

DOCTORAL THESIS

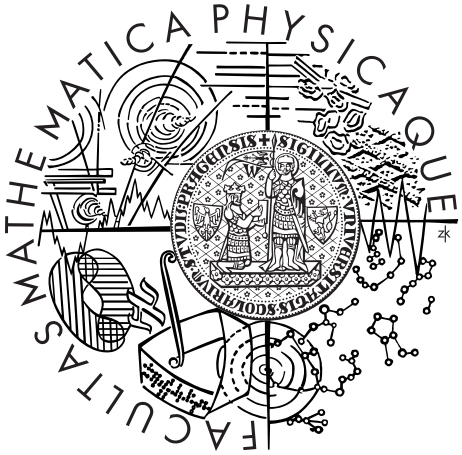

Jan Šimák

Solution of inverse problem for a flow around an airfoil

Department of Numerical Mathematics

Supervisor: Prof. RNDr. Miloslav Feistauer, DrSc., dr. h. c.
Study programme: Mathematics
Specialization: Scientific and Technical Calculations

Prague 2014

I would like to thank my supervisor, Prof. RNDr. Miloslav Feistauer, DrSc., dr. h. c., for his invaluable help with my doctoral thesis. I would also like to thank my colleagues from Aerospace Research and Test Establishment in Prague for their support and valuable advice, namely RNDr. Jaroslav Pelant, CSc. Last but not least, I would like to thank my family for the great support and patience.

I declare that I carried out this doctoral thesis independently, and only with the cited sources, literature and other professional sources.

I understand that my work relates to the rights and obligations under the Act No. 121/2000 Coll., the Copyright Act, as amended, in particular the fact that the Charles University in Prague has the right to conclude a license agreement on the use of this work as a school work pursuant to Section 60 paragraph 1 of the Copyright Act.

In ..... date ..... signature of the author

Název práce: Řešení inverzní úlohy obtékání leteckého profilu

Autor: Mgr. Jan Šimák

Katedra: Katedra numerické matematiky

Vedoucí disertační práce: prof. RNDr. Miloslav Feistauer, DrSc., dr. h. c., Katedra numerické matematiky MFF UK

Abstrakt: Metoda popsaná v této práci se zabývá řešením inverzní úlohy obtékání leteckého profilu. Slouží k návrhu tvaru profilu na základě zadaného rozložení rychlosti či tlaku po délce tětivy. Metoda je založena na hledání pevného bodu operátoru, který kombinuje přibližný inverzní a přímý operátor. Přibližný inverzní operátor, odvozený na základě teorie tenkých profilů, přiřazuje k zadanému rozložení příslušný tvar. Výsledný tvar je pak konstruován pomocí střední čáry a tloušťkové funkce. Přímý operátor představuje určení rozložení rychlosti či tlaku na povrchu profilu. Lze využít rychlý, zjednodušený model potenciálního proudění řešeného pomocí Fredholmovy integrální rovnice, případně pomalejší, ale přesnější model RANS rovnic s k-omega modelem turbulence. Metoda je určena pro subsonické proudění.

Klíčová slova: Inverzní úloha, návrh profilu, vazké proudění, model turbulence.

Title: Solution of inverse problem for a flow around an airfoil

Author: Mgr. Jan Šimák

Department: Department of Numerical Mathematics

Supervisor: prof. RNDr. Miloslav Feistauer, DrSc., dr. h. c., Department of Numerical Mathematics

Abstract: The method described in this thesis deals with a solution of an inverse problem for a flow around an airfoil. It can be used to design an airfoil shape according to a specified velocity or pressure distribution along the chord line. The method is based on searching for a fixed point of an operator, which combines an approximate inverse and direct operator. The approximate inverse operator, derived on the basis of the thin airfoil theory, assigns a corresponding shape to the specified distribution. The resulting shape is then constructed using the mean camber line and thickness function. The direct operator determines the pressure or velocity distribution on the airfoil surface. We can apply a fast, simplified model of potential flow solved using the Fredholm integral equation, or a slower but more accurate model of RANS equations with a k-omega turbulence model. The method is intended for a subsonic flow.

Keywords: Inverse problem, airfoil design, viscous flow, turbulence model.

Contents

1. Introduction

The development of computers since the middle of the last century allows their gradual integration into the problems of aerodynamics. Before the arrival of sufficiently powerful computers, a wind tunnel or knowledge gained from practical tests had been a major source of information. Of course, these experiments were supported by various theoretical models used to understand the principles of the fluid flow. The Navier-Stokes equations describing the flow of viscous fluids, which we still come out from, were derived in the original form already in 1822. The Euler equations for an ideal fluid were derived even a century before. However, their complexity did not allow their direct use in solving general problems of aerodynamics. From these reasons, simplified flow models, which could be solved analytically if possible, were developed.

Only with the increase in computational power, it was possible to solve these equations numerically. A new field called Computational Fluid Dynamics, CFD, was established. Step by step, numerical simulations of the flow began to be applied and they allowed obtaining new ideas about the complexity of the flow. Their development still continues as computers are faster and faster. And also the quality of the methods is improving. They became an equivalent variant to experimental measurements and in some cases even replaced them. However, the need for a comparison of the obtained results with experimental data is still here.

The development of numerical methods is also reflected in the design of airfoils. Previously, individual shapes had to be tested in a wind tunnel and on the basis of measurements of pressure and forces acting on the airfoil and using a flow visualization, convenient designs were selected. This meant a real manufacture of experimental airfoils and therefore from the financial and time reasons, it was possible to test only a few candidates. Today, this process can be replaced just by numerical simulations. This eliminates the consuming production of many modified airfoils and also the preparation of their measurements. Using the speed of computers, much more designs can be tested during the same time. The experimental verification is thus left only for promising candidates.

The problem of an aerodynamic design can be hold from two different perspectives. One is a shape optimization, when we require achievement of optimal values of variables describing the performance of an airfoil. The second way is to find a shape of an airfoil which corresponds to predetermined properties. This approach is called an inverse problem.

In the case of the shape optimization, an initial shape is iteratively changed to achieve the desired improvements. These may be for example a reduction of the drag coefficient while maintaining the constant lift coefficient. To do this it is necessary to add some constraints on the geometry, such as a minimum and maximum thickness of the final airfoil. Otherwise an infeasible shape could be obtained. A shape optimization uses various optimization algorithms to search through the design space, such as gradient-based methods, simplex methods,

genetic algorithms or other techniques. These algorithms usually require large number of evaluating of airfoil characteristics, i.e. evaluations of the flow. In the case of more complex CFD models, it leads to a large time demands. In addition, for most of these algorithms it is not guaranteed they find the global optimum.

For a shape optimization it is also extremely important to choose the right cost function or optimization criteria. Their determination usually requires some experience from previous similar problems. As shown for example in [1], a single-point optimization can indeed improve the performance for the selected flow regime, but for other regimes may be considerably worse. To overcome this drawback, a multipoint optimization can be involved, which requires meeting optimization criteria for multiple regimes. However, this may lead to a slower convergence and also when given mutually incompatible criteria, it may result in an unacceptable shape of the airfoil. On the other hand, if the optimization problem is well defined, the resulting airfoil has better properties than the original shape.

1.1 Inverse problem

In the case of an inverse problem we are trying to find a shape of an airfoil that corresponds to some prescribed requirements. These requirements are usually a given velocity or pressure distribution along the surface of the airfoil. Then using iterative methods a new shape is searched for, which corresponds to this distribution. Most of inverse methods use some relationship between a shape and the corresponding distribution which specifies the further changes of the shape. In the result, much less computations of the flow are required than in the case of a shape optimization which searches through the entire design space. That means a reduction of the time consumption.

The main problem of inverse methods is determining the desired distribution of velocity or pressure. Although when using optimization methods the optimization criteria must be correctly specified, their determining is still easier. The prescribed distribution must agree to required properties of the new airfoil and that requires some previous experience in this field. In addition, it is difficult to determine in advance whether for the chosen distribution an appropriate airfoil shape exists or whether it has reasonable geometric properties. The inverse problems are often ill-posed. More preferred than design an entirely new velocity or pressure distribution is to come out from an already known distribution of an existing airfoil. Then using appropriate adjustments, for example using an optimization process, a new shape with enhanced performance is obtained.

First attempts to solve an inverse problem of a flow around an airfoil were based on a solution of potential flow using a conformal mapping, where the shape of the airfoil was transformed into a unit circle and using a complex analysis a problem for a velocity potential was solved. With a convenient formulation of Theodorsen [2] this method could be rewritten for the purpose of the inverse method. For example, some NACA airfoils [3] were designed on that basis. The

method was further developed by many authors, including Lighthill [4], who showed in his work that the prescribed velocity or pressure distribution cannot be completely arbitrary. He derived three integral conditions to ensure the uniformity of the free stream and that the corresponding airfoil will be of a closed shape.

In the following time, more sophisticated methods appeared such as Takanashi [5] using the approach of a predictor/corrector type, which is based on the difference between the specified and calculated distribution that determines the way the geometry is modified. The correction is defined by the solution of the Dirichlet boundary value problem which is solved by using a transonic integral equation method. Takanashi used a three-dimensional full potential equation written in a form for a perturbation velocity potential. The method is thus able to design airfoils in a transonic regime. A quite similar method was suggested by Campbell and Smith [6].

A possible disadvantage of some inverse methods is that they are single-point. This means that the shape corresponds to a given distribution for a particular angle of attack. In practice, however, operation in a wider range of angles is usually required. We thus have the same problem as the single-point optimization tasks, for which the performance in an off-design regime can degrade. This fact should be taken into account and it is recommended to analyse the resulting design. Some inverse methods are therefore trying to do a multi-point design, e.g. Eppler [7]. In this particular case, the surface of the airfoil is divided into several parts on which individual distributions for different angles of attack are prescribed. Also mixed methods were derived, which combine already given parts of the airfoil along with parts that are designed using the specified velocity distribution, such as proposed by Drela [8].

An another approach for solving inverse problems suggested Garabedian and McFadden [9]. In this method, the change of airfoil coordinates is determined by using a differential equation based on the difference between the current and target pressure. At the end of the last century the inverse problem started to be also combined with minimization algorithms, such as control theory [10] using gradient methods or even methods using genetic algorithms, which can provide a very comprehensive shape design. However, genetic algorithms, for example, are very time consuming, especially when combined with CFD methods, and so they should be used only when it is really needed. From the newer methods it is possible to mention the method of constrained direct iterative surface curvature (CDISC) by Campbell [11].

1.2 Presented method

The method described in this work is intended to solve an inverse problem of a subsonic flow. Like other inverse methods, it uses the difference between the calculated and the target distribution of velocity or pressure to identify further

changes. The main idea is to derive an approximate inverse operator that assigns to a given distribution a corresponding shape of the airfoil. Because this inversion is based on a simplified flow model, the resulting shape does not completely comply with the required properties. Therefore, using an iterative process, the whole procedure is repeated until a correct result is achieved. A parameter that controls the shape of the airfoil is thus a so-called fictitious distribution of velocity or pressure.

The method consists of two main parts, an approximate inverse operator and direct operator that evaluates the velocity/pressure distribution along the airfoil surface. The advantage is that these two operators are independent and it is thus possible to consider different flow models according to our needs. Thus, we can solve the problem for incompressible potential flow or an improved model for compressible viscous flow with a turbulence model.

The initial principle of this method was proposed in a work by Pelant [12]. Later, the author of this thesis adapted this method for solving incompressible and compressible flow in the master thesis [13]. The method in that formulation allowed the design of symmetric and asymmetric airfoils for a potential flow and of symmetric airfoils for a compressible inviscid flow described by the Euler equations [14]. The main problem was in the coupling of the inverse operator with the angle of attack. The direct operator was later modified to allow determination of the suitable angle of attack and thus to be able to design asymmetric airfoils [15]. Modification of the approximate inverse operator in such a way that it allowed design from a specified pressure distribution, made us possible to deal with problems of viscous laminar flow [16] and finally using a suitable model to solve turbulent flow problems [17].

This thesis summarizes and extends results obtained so far on this method. It allows us to solve inverse problems of a flow around an airfoil for subsonic turbulent flow. By eliminating somewhat restrictive conditions on the angle of attack, we can prescribe a pressure or velocity distribution for the selected angle of attack, as shown in the practical part.

2. Solution of the flow

The crucial part in the mentioned inverse design method is the prediction of the flow on the modelled surface. Based on these values, parameters describing the quality of the resulting airfoil can be evaluated. The expected properties of the method are reliability, robustness and speed.

2.1 Potential flow

The simplest model of a flow that can be used for our purposes, is a potential flow model. This model represents a very simplified description of a steady incompressible flow where the fluid viscosity is neglected. Another characteristic of this model is the neglecting of the vorticity. It is clear that this model is able to describe the physical nature of the air flow around an airfoil only to a limited extent. Under the assumption of the incompressibility it is applicable mainly to lower speed flows. In practice, there is usually stated a limit of the airflow to the free stream Mach number $M_\infty = 0.3$ up to which the model gives adequate results. The Mach number is the ratio of the local speed and the local speed of sound. This means, in its basic form, it is impossible to detect density changes such as shock waves. Moreover, the assumption of zero viscosity leads to entirely neglect the boundary layer, which influences the estimate of the drag of the airfoil. Also, the flow separation cannot be captured. From these reasons, the basic model was extended by many authors. In the literature, there can be found all sorts of modifications and corrections using additional equations which can more or less reliably capture these phenomena. The potential flow model is used for example by the software XFOIL by M. Drela [18], which is aimed at the analysis and design of subsonic isolated airfoils. It uses the panel method to simulate the inviscid flow and an integral boundary layer formulation to capture viscous effects on the airfoil surface.

On the other hand, the advantage of this model is its simplicity. The potential flow model allows us to obtain solutions in much less time than the commonly used more complex models. Therefore, in some cases it may happen that this model is the best candidate to use. A typical example is a task of optimization when it is necessary to test a large number of designed candidates and the time saving is more than welcome.

2.1.1 Solution using a Fredholm integral equation

Our goal is to determine a velocity field $\mathbf{v} = (v_x, v_y)$ in an area around a given airfoil. Suppose that at a sufficient distance from the given airfoil, the flow is unaffected by this airfoil and therefore the velocity vector could be considered as a constant. Let us denote it as $\mathbf{v}_\infty$. This free stream velocity, as we call it, can

also be written in the form

$$\mathbf{v}_\infty = v_\infty \left(\cos \alpha_\infty, \sin \alpha_\infty\right), \tag{2.1.1}$$

where the symbol α_∞ is the angle of attack of the airfoil.

Due to finding the solution, we convert our problem into the field of complex numbers. A complex number z is typically defined as $z = x + \mathrm{i}y$. The real and imaginary part of z are denoted by $\mathrm{Re}(z)$ and $\mathrm{Im}(z)$. The set of all complex numbers will be denoted by $\mathbb{C}$ and the closed complex plane will be denoted as $\mathbb{S} = \mathbb{C} \cup \{\infty\}$. The airfoil exposed to the flow is represented by a complex-valued curve $\psi : \mathbb{R} \to \mathbb{C}$, $\psi(t) = \psi_1(t) + \mathrm{i}\psi_2(t)$ for $t \in [0, d]$. The symbol d is the length of ψ. About this curve, we assume that it is a closed positively oriented (counterclockwise) Jordan curve. The image of this curve is denoted by $\langle\psi\rangle = \{\psi(t); t \in [0, d]\}$. Further assume that it is continuous up to the second order derivatives including the curve endpoints. The domain of the flow is then the exterior of the curve, i.e. $\Omega = \mathrm{Ext}\,\psi$. Further, we will define the complex-valued function $\sigma(z)$ on $\langle\psi\rangle$ such that

$$\sigma\left(\psi\left(t\right)\right) = \psi'(t), \quad \forall t \in [0, d]\,. \tag{2.1.2}$$

Due to the choice of parametrization of the curve it is necessarily true that $|\psi'(t)| = 1$.

By converting the velocity vectors $\mathbf{v}$ and $\mathbf{v}_\infty$ into the complex field we obtain complex-valued velocity functions

$$F(z) = v_x(x, y) - \mathrm{i}v_y(x, y), \quad z \in \Omega, \tag{2.1.3}$$

$$w_\infty = v_\infty \cos \alpha_\infty - \mathrm{i}v_\infty \sin \alpha_\infty. \tag{2.1.4}$$

According to our assumptions that we put on the flow, the following relationships derived from the continuity equation and the condition for an irrotational flow are true,

$$\frac{\partial v_x}{\partial x} + \frac{\partial v_y}{\partial y} = 0, \tag{2.1.5}$$

$$\frac{\partial v_y}{\partial x} - \frac{\partial v_x}{\partial y} = 0, \quad \text{in } \Omega. \tag{2.1.6}$$

Hence F is necessarily a holomorphic function in Ω (because the so-called Cauchy-Riemann conditions are satisfied) and it is also continuous on $\overline{\Omega} = \Omega \cup \langle\psi\rangle$.

For the next steps we will need the following definition:

Definition. *We define a set $H(\mu, D)$ of complex-valued functions defined on a subset $D \subset \mathbb{C}$ such that for every $\varphi \in H(\mu, D)$, $\mu > 0$ the following is true:*

$$(\exists A > 0)\,(\forall z, z_0 \in D)\,(|\varphi(z) - \varphi(z_0)| \leq A\,|z - z_0|^\mu)\,.$$

The set $H(D) = \bigcup_{\mu \in (0,1]} H(\mu, D)$ is called a class of Hölder's functions.

The problem we need to solve can be formulated:
Find a function F defined on $\overline{\Omega}$, satisfying the following conditions:

$$F \text{ is continuous on } \overline{\Omega}, \tag{2.1.7}$$

$$F \text{ is holomorphic on } \Omega, \tag{2.1.8}$$

$$F|_{\langle\psi\rangle} \in H(\langle\psi\rangle), \tag{2.1.9}$$

$$F(\infty) = w_\infty, \tag{2.1.10}$$

$$\operatorname{Im}\left(F(z)\sigma(z)\right) = 0 \ \text{ on } \ \langle\psi\rangle\,. \tag{2.1.11}$$

The condition (2.1.11) says that the velocity in the normal direction to the airfoil is zero.

Due the validity of the conditions (2.1.7) and (2.1.8), this function can be written according to [19] in the form

$$F(\zeta) = F(\infty) - \frac{1}{2\pi\mathrm{i}} \int_\psi \frac{F(z)}{z-\zeta} dz, \ \zeta \in \Omega. \tag{2.1.12}$$

Further it is possible to introduce a function f defined on $\langle\psi\rangle$ which represents the tangential component of the velocity on the airfoil. This function satisfies $f(z) = F(z)\sigma(z)$, $z \in \langle\psi\rangle$ due to the condition (2.1.11). We require that this function is real-valued and also $f \in H(\langle\psi\rangle)$. In addition, if this function satisfies that

$$\lim_{\zeta\to z_0} \left(w_\infty - \frac{1}{2\pi\mathrm{i}} \int_\psi \frac{f(z)}{\sigma(z)(z-\zeta)} dz \right) = \frac{f(z_0)}{\sigma(z_0)} \tag{2.1.13}$$

for $\zeta \in \Omega$, $z_0 \in \langle\psi\rangle$, it is possible to extend the function F defined by (2.1.12) onto the closure of the domain Ω as follows,

$$F(\zeta) = \begin{cases} w_\infty - \frac{1}{2\pi\mathrm{i}} \int_\psi \frac{f(z)}{\sigma(z)(z-\zeta)} dz & \text{in } \Omega, \\ \frac{f(\zeta)}{\sigma(\zeta)} & \text{on } \langle\psi\rangle\,. \end{cases} \tag{2.1.14}$$

The function F defined in this way will necessarily satisfy the given conditions (2.1.7)–(2.1.11). The flow field in the whole region Ω is thus determined only by the velocity distribution on the airfoil and by the free-stream velocity.

To continue, we need the following statement from [20]:

Theorem 1. *Let ψ be a smooth positively oriented Jordan curve and $z_0 \in \langle\psi\rangle$. Let $\varphi \in H(\langle\psi\rangle)$ be a function defined on the curve ψ. Then the Cauchy type integral*

$$H(\zeta) = \frac{1}{2\pi\mathrm{i}} \int_\psi \frac{\varphi(z)}{z-\zeta} dz, \quad \zeta \in \mathbb{C} - \langle\psi\rangle$$

has the limits

$$H^i(z_0) = \lim_{\substack{\zeta\to z_0 \\ \zeta\in \operatorname{Int}\psi}} H(\zeta) = \frac{1}{2}\varphi(z_0) + \frac{1}{2\pi\mathrm{i}} \int_\psi \frac{\varphi(z)}{z-z_0} dz$$

and

$$H^e(z_0) = \lim_{\substack{\zeta\to z_0 \\ \zeta\in \operatorname{Ext}\psi}} H(\zeta) = -\frac{1}{2}\varphi(z_0) + \frac{1}{2\pi\mathrm{i}} \int_\psi \frac{\varphi(z)}{z-z_0} dz.$$

The Cauchy type integrals are considered in the sense of the Cauchy principal value:

$$(PV)\int_{\psi}\frac{\varphi(z)}{z-\zeta}dz=\lim_{\epsilon\to 0}\int_{\psi-B(\zeta,\epsilon)}\frac{\varphi(z)}{z-\zeta}dz,\quad \zeta\in\langle\psi\rangle\,, \tag{2.1.15}$$

where $B(\zeta,\epsilon)=\{z\in\mathbb{C};\|z-\zeta\|\leq\epsilon\}$. If the integral exists in the usual sense, then its value equals the principal value. From this reason we will omit the (PV) notation.

According to this theorem, it is possible to take the limit in the condition (2.1.13). Thus, we obtain the condition

$$f(z_0)+\frac{1}{\pi\mathrm{i}}\int_{\psi}\frac{f(z)}{\sigma(z)}\frac{\sigma(z_0)}{z-z_0}dz=2\sigma(z_0)w_\infty,\quad z_0\in\langle\psi\rangle\,. \tag{2.1.16}$$

This equation for the unknown function f can be split in the real and imaginary part. It can be proven that f is the solution of the real part of the equation if and only if f is the solution of the imaginary part (see [21]). Therefore it is quite sufficient to be concerned further only with the real part

$$f(\psi(\tau))+\frac{1}{\pi}\int_0^d \mathrm{Im}\left(\frac{\psi'(\tau)}{\psi(t)-\psi(\tau)}\right)f\left(\psi(t)\right)dt=\mathrm{Re}\Big(2w_\infty\psi'(\tau)\Big),\quad \tau\in[0,d]\,. \tag{2.1.17}$$

This equation is the Fredholm integral equation of the second kind with the continuous kernel. The imaginary part forms the Fredholm integral equation of the first kind, which is more difficult to solve. With this step we moved back into the field of real numbers.

The solution of the equation (2.1.17) can be written in the form $f=f_0+\alpha f_1$, where f_0 is a particular solution to this equation, f_1 is a non-zero solution of the corresponding homogeneous equation and α is a real parameter. From this it also follows that the solution under the given conditions (2.1.7)–(2.1.11) is not unique. To achieve uniqueness it still needs to add some additional condition. One possibility, which is based on natural requirements for the flow around an airfoil, is a condition prescribing circulation,

$$\mathrm{Re}\left(\int_{\psi}F(z)dz\right)=\int_0^d f\left(\psi(t)\right)dt=\Gamma,\quad \Gamma\in\mathbb{R}. \tag{2.1.18}$$

The value of this parameter Γ will be determined later in Section 2.1.3.

2.1.2 Potential of the velocity

Since the function F defined by (2.1.14) is continuous in $\overline{\Omega}$ and holomorphic in Ω, there is a complex function Φ_c defined on $\overline{\Omega}$ such that $\Phi_c'(\zeta)=F(\zeta)$. This primitive function to F is called a potential to the velocity. Because of the properties of primitive functions, it follows that

$$\Phi_c(z_2)-\Phi_c(z_1)=\int_{\psi_{z_1,z_2}}F(z)dz=\int_a^b F(\psi(t))\sigma(\psi(t))dt \tag{2.1.19}$$

for arbitrary two points $z_1, z_2 \in \langle\psi\rangle$, $z_1 = \psi(a)$, $z_2 = \psi(b)$. As a result of the condition (2.1.11) we get $\mathrm{Im}\,(\Phi_c(z)) = const.$ on $\langle\psi\rangle$. Therefore,

$$\frac{d\,\mathrm{Re}\,(\Phi_c(\psi(t)))}{dt} = f(\psi(t)). \tag{2.1.20}$$

In other words, the velocity distribution on the airfoil is determined by the real part of the complex-valued potential Φ_c. In the following we will denote this real part by the symbol Φ.

The potential Φ_c can also be expressed as

$$\Phi_c(\zeta) = w_\infty\zeta + \frac{1}{2\pi\mathrm{i}}\int_\psi F(z)\log(z-\zeta)dz. \tag{2.1.21}$$

Since the logarithm of a complex number can be written as $\log(z) = \ln|z| + \mathrm{i}\arg(z)$, where the function arg denotes the argument (angle) of a complex number, the real part of the potential can be expressed as

$$\Phi(\zeta) = \mathrm{Re}\,(w_\infty\zeta) + \frac{1}{2\pi}\int_0^d f(\psi(t))\arg\left(\psi(t)-\zeta\right)dt, \quad \zeta\in\Omega. \tag{2.1.22}$$

Now it is better to stop here for a moment. The complex-valued logarithm is generally defined as a set $\log w = \{z\in\mathbb{C};\ w = \exp z\}$. It is clear that for given w it yields infinitely many values, each differing by multiples of $2\pi\mathrm{i}$. This is why the principal value of the complex-valued logarithm is usually defined: $\log w = \{z = x+\mathrm{i}y;\ x\in\mathbb{R},\ y\in(-\pi,\pi],\ w=\exp z\}$. The function $\arg(\psi(t)-\zeta)$ in a variable t is generally discontinuous and may contain jumps. Nevertheless, it is relatively easy to overcome this problem with a suitable choice of the logarithm values and hence consider it as a continuous function of $t\in[0,d]$.

The integral in equation (2.1.22) can be reformulated by the use of the per-partes method,

$$\begin{aligned}\int_0^d f(\psi(t))\arg\left(\psi(t)-\zeta\right)dt = &\Big(\Phi(\psi(d)) - \Phi(\psi(0))\Big)\arg\left(\psi(0)-\zeta\right)\\ &-\int_0^d\left(\Phi(\psi(t))\frac{d\arg\left(\psi(t)-\zeta\right)}{dt}\right)dt\end{aligned} \tag{2.1.23}$$

and further by the limit to the airfoil,

$$\begin{aligned}\Phi(\psi(\tau)) = &\,2\,\mathrm{Re}\,(w_\infty\psi(\tau)) + \frac{1}{\pi}\Gamma\arg\left(\psi(0)-\psi(\tau)\right)\\ &-\frac{1}{\pi}\int_0^d\left(\Phi(\psi(t))\frac{d\arg\left(\psi(t)-\psi(\tau)\right)}{dt}\right)dt, \quad \tau\in[0,d].\end{aligned} \tag{2.1.24}$$

The circulation $\Gamma = \big(\Phi(\psi(d)) - \Phi(\psi(0))\big)$ fully complies with the previously specified condition (2.1.18). Due to the continuity of the second derivative $\psi''(\tau)$, the derivative

$$\frac{d\arg\left(\psi(t)-\psi(\tau)\right)}{dt} = \frac{1}{2}\,\mathrm{Im}\left(\frac{\psi''(t)}{\psi'(t)}\right) \tag{2.1.25}$$

is also continuous. The solution of the equation (2.1.24) is again unique.

The function $\arg(\psi(t)-\psi(\tau))$ is continuous on the set $[0,d]\times[0,d]$ except the points $t=\tau$. At these points the function has a jump of size $-\pi$. Therefore, the continuous kernel of the integral equation is defined as

$$K\big(\psi(t),\psi(\tau)\big)=\begin{cases}\dfrac{1}{\pi}\arg\big(\psi(t)-\psi(\tau)\big) & \text{for } t<\tau,\ t,\tau\in[0,d),\\ & \text{or } \tau=d, t\in(0,d),\\ \lim\limits_{\substack{\tau_1\to 0_+\\ \tau_2\to d_-}}\dfrac{1}{\pi}\arg\big(\psi(\tau_1)-\psi(\tau_2)\big) & \text{for } t=0,\ \tau=d,\\ \dfrac{1}{\pi}\arg\big(\psi(t)-\psi(\tau)\big)+1 & \text{for } t>\tau,\ t,\tau\in(0,d],\\ & \text{or } \tau=0, t\in(0,d),\\ \lim\limits_{\substack{\tau_1\to d_-\\ \tau_2\to 0_+}}\dfrac{1}{\pi}\arg\big(\psi(\tau_1)-\psi(\tau_2)\big)+1 & \text{for } t=d,\ \tau=0,\\ \lim\limits_{\tau_1\to\tau_-}\dfrac{1}{\pi}\arg\big(\psi(\tau_1)-\psi(\tau)\big) & \text{for } t=\tau\in(0,d],\\ \lim\limits_{\tau_2\to 0_+}\dfrac{1}{\pi}\arg\big(\psi(0)-\psi(\tau_2)\big) & \text{for } t=\tau=0.\end{cases} \tag{2.1.26}$$

It is obvious that

$$\frac{dK(\psi(t),\psi(\tau))}{dt}=\frac{1}{\pi}\frac{d\arg(\psi(t)-\psi(\tau))}{dt}. \tag{2.1.27}$$

The solution of the equation (2.1.24) for the unknown velocity potential Φ on the airfoil can be written by the superposition of potentials in the form

$$\Phi(\psi(\tau))=\Phi^x(\psi(\tau))v_\infty\cos\alpha_\infty+\Phi^y(\psi(\tau))v_\infty\sin\alpha_\infty+\Gamma\Phi^\Gamma(\psi(\tau)) \tag{2.1.28}$$

using the fact that the complex-valued velocity at infinity is given by (2.1.4).

The respective equations for solving the individual components have the form

$$\Phi^x(\psi(\tau))=2\,\mathrm{Re}\,(\psi(\tau))-\int_0^d\left(\Phi^x(\psi(t))\frac{dK(\psi(t),\psi(\tau))}{dt}\right)dt, \tag{2.1.29}$$

$$\Phi^y(\psi(\tau))=2\,\mathrm{Im}\,(\psi(\tau))-\int_0^d\left(\Phi^y(\psi(t))\frac{dK(\psi(t),\psi(\tau))}{dt}\right)dt, \tag{2.1.30}$$

$$\Phi^\Gamma(\psi(\tau))=K(\psi(0),\psi(\tau))-\int_0^d\left(\Phi^\Gamma(\psi(t))\frac{dK(\psi(t),\psi(\tau))}{dt}\right)dt. \tag{2.1.31}$$

Meaning of these components is such that the first one represents a velocity potential for a unit velocity of the free stream in the direction of the axis x, the next one for a unit velocity in the direction of the axis y and finally the last component is a velocity potential for a zero velocity of the free stream and with the unit circulation.

In the text above, the solution of the velocity potential on a given airfoil using Fredholm integral equations was briefly derived. In the next section, the numerical method of finding the solution will be shown.

2.1.3 Computation of the solution

In the previous section, integral equations for the velocity potential on the specified airfoil were derived. Now it is needed to show how these equations can be effectively solved. To establish a method for finding the numerical solution, it is convenient to rewrite the equations in a vector form

$$\mathbf{\Phi}(\psi(\tau)) = \mathbf{p}(\tau) - \int_0^d \left(\mathbf{\Phi}(\psi(t)) \frac{dK(\psi(t), \psi(\tau))}{dt} \right) dt, \quad \tau \in [0, d]\,, \tag{2.1.32}$$

where the vectors have components

$$\mathbf{\Phi}(\psi(\tau)) = \left(\Phi^x(\psi(\tau)), \Phi^y(\psi(\tau)), \Phi^\Gamma(\psi(\tau)) \right)^T, \tag{2.1.33}$$

$$\mathbf{p}(\tau) = \left(2\,\mathrm{Re}(\psi(\tau)), 2\,\mathrm{Im}(\psi(\tau)), K(\psi(0), \psi(\tau)) \right)^T. \tag{2.1.34}$$

The easiest way how to evaluate the integral contained in this equation is the application of a quadrature formula. First, we choose $m+1$ points from the interval $[0, d]$, where $m \in \mathbb{N}$ is an even number. These points will be denoted by $0 = t'_0 < t'_1 < \ldots < t'_m = d$. Then the integral in (2.1.32) can be approximated by the sum

$$\int_0^d \left(\mathbf{\Phi}(\psi(t)) \frac{dK(\psi(t), \psi(\tau))}{dt} \right) dt \approx \sum_{\substack{e=1 \\ e \text{ is odd}}}^{m-1} \Phi(\psi(t'_e)) \int_{t'_{e-1}}^{t'_{e+1}} \left(\frac{dK(\psi(t), \psi(\tau))}{dt} \right) dt =$$

$$= \sum_{\substack{e=1 \\ e \text{ is odd}}}^{m-1} \Phi(\psi(t'_e)) \Delta_e(\tau), \tag{2.1.35}$$

where $\Delta_e(\tau) = K(\psi(t'_{e+1}), \psi(\tau)) - K(\psi(t'_{e-1}), \psi(\tau))$.

If we now denote

$$\phi_i = \mathbf{\Phi}(\psi(t'_i)), \tag{2.1.36}$$

$$p_i = \mathbf{p}(t'_i), \tag{2.1.37}$$

$$\Delta_{e,i} = \Delta_e(t'_i) \text{ for } e \neq i, \tag{2.1.38}$$

$$\Delta_{i,i} = \Delta_i(t'_i) + 1, \tag{2.1.39}$$

then it is possible to convert the integral equation (2.1.32) into a system of linear algebraic equations. This will be achieved by substituting for $\tau = t'_1, t'_3, \ldots, t'_{m-1}$, so we get a system for a total of $m/2$ unknowns ϕ_i. The system has the form

$$\sum_{\substack{e=1 \\ e \text{ is odd}}}^{m-1} \phi_e \Delta_{e,i} = p_i, \quad i = 1, 3, \ldots, m-1. \tag{2.1.40}$$

Solving this system, we get values of individual components of the velocity potential at the airfoil points $\psi(t'_1), \psi(t'_3), \ldots, \psi(t'_{m-1})$. Because of the potential properties (2.1.20), the sought velocity distribution f on the surface of the airfoil is obtained by the differentiation of the individual components of Φ^x, Φ^y, Φ^Γ with

respect to the variable t (i.e. $d\Phi^x/dt = f^x$, $d\Phi^y/dt = f^y$, $d\Phi^\Gamma/dt = f^\Gamma$). Putting them together, we get

$$f(\psi(t)) = f^x(\psi(t))v_\infty \cos\alpha_\infty + f^y(\psi(t))v_\infty \sin\alpha_\infty + \Gamma f^\Gamma(\psi(t)), \tag{2.1.41}$$

where $t \in [0, d]$.

From this equation it is clear that the magnitude of the velocity on the airfoil depends among other on the size and direction of the free stream velocity and also on the circulation Γ. Free stream parameters are the part of the assignment, it remains to determine the parameter Γ. Its determination is related to the geometrical shape of the airfoil, because the circulation determines the position of stagnation points. For a completely natural condition it can be set that the stagnation point is located on the trailing edge of the airfoil. In the case that the ending points of the curve ψ are located on the trailing edge, we are interested in the point $\psi(0)$. In the case of an airfoil with a rounded trailing edge we require that $f(\psi(0)) = 0$, in the case of an airfoil with a sharp trailing edge that the velocity at this point is bounded (finite). This condition is called the Kutta condition.

Under this condition, the following relationship can be derived for the circulation Γ:

$$\Gamma = -v_\infty \frac{\left(f^x(\psi(t'_1)) + f^x(\psi(t'_{m-1}))\right)\cos\alpha_\infty + \left(f^y(\psi(t'_1)) + f^y(\psi(t'_{m-1}))\right)\sin\alpha_\infty}{f^\Gamma(\psi(t'_1)) + f^\Gamma(\psi(t'_{m-1}))}, \tag{2.1.42}$$

which ensures the correct position of the stagnation point.

The coordinates of the airfoil ψ in the $\mathbb{R}^2$-plane are given by $\psi_1(t)$ and $\psi_2(t)$, $t \in [0, d]$. For the purpose of the inverse design method, we suppose that the chord line of the airfoil lies on the x-axis and that the leading edge is situated in the origin. That means $\psi(t_0) = 0$ for some $t_0 \in (0, d)$ and this point divides the airfoil into the upper and lower part. The length of the chord line will be denoted by C (i.e. $\psi(0) = \psi(d) = C$). We define two functions $f_u, f_l : [0, C] \to \mathbb{R}$ such that

$$f_u(\psi_1(t)) = f(\psi(t)) \text{ for } t \in [0, t_0]\,, \tag{2.1.43}$$

$$f_l(\psi_1(t)) = f(\psi(t)) \text{ for } t \in [t_0, d]\,. \tag{2.1.44}$$

The absolute values $|f_u|$, $|f_l|$ will be called a velocity distribution on the upper and lower part of the airfoil. We can similarly define f_u^x, f_l^x, f_u^y, f_l^y, f_u^Γ, f_l^Γ. The procedure described in this section that assigns the velocity distribution to the airfoil ψ is called the direct operator $\mathbf{P}$.

Examples of individual particular solutions to the NACA0012 airfoil are shown in Figure 2.1. Composing them according to the formula (2.1.41), it is possible to get the velocity distributions on the airfoil for different angles of attack and free stream velocity. Comparison of the obtained results with the results of the compressible inviscid flow model (see Section 2.2) is in Figure 2.2.

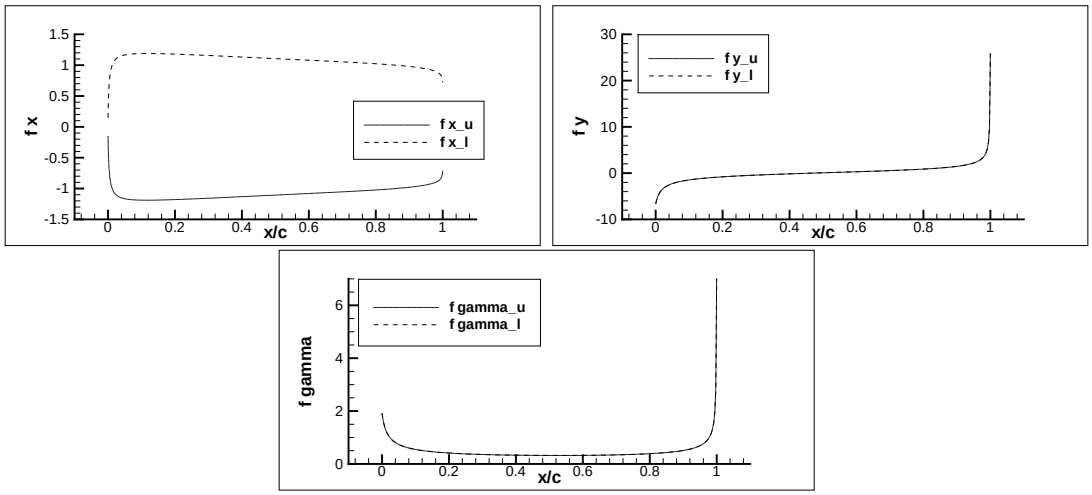

Figure 2.1: Particular solutions of velocity distribution f^x, f^y and f^Γ corresponding to NACA0012 airfoil.

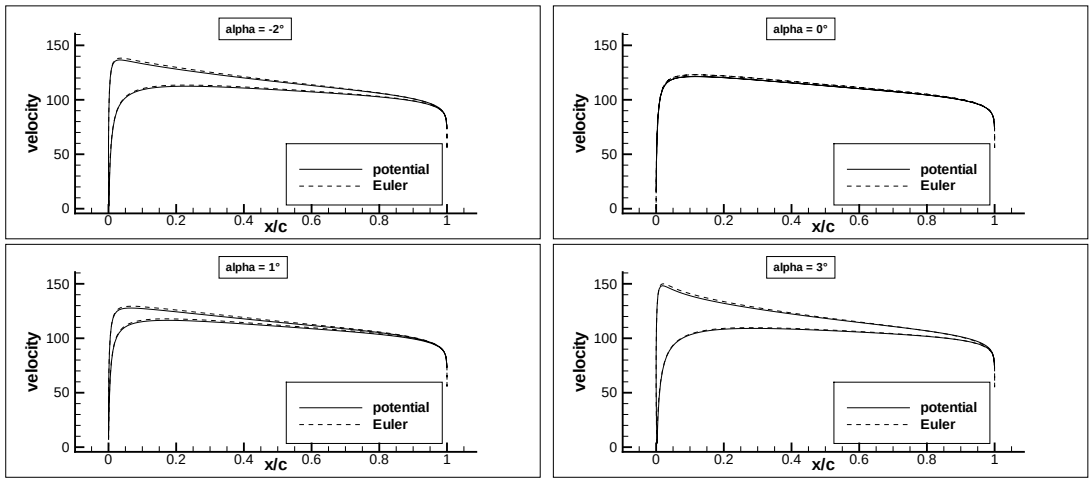

Figure 2.2: Velocity distribution on NACA0012 airfoil for $M_\infty = 0.3$ obtained by a composition of particular solutions, compared with a solution of the Euler equations for a compressible flow.

2.1.4 Compressibility correction

At higher speeds, the effect of compressibility of air starts to be significant and thus the incompressible model exhibits an increased error. The pressure on the airfoil is usually expressed as the dimensionless pressure coefficient c_p which relates the local static pressure p with the dynamic pressure of the free stream and is defined as

$$c_p = \frac{p - p_\infty}{\rho_\infty v_\infty^2/2}. \tag{2.1.45}$$

The symbols p_∞ and ρ_∞ are static pressure and density of the free stream. We are dealing with an incompressible, irrotational and steady flow. Therefore we can use the Bernoulli equation to express the incompressible pressure coefficient

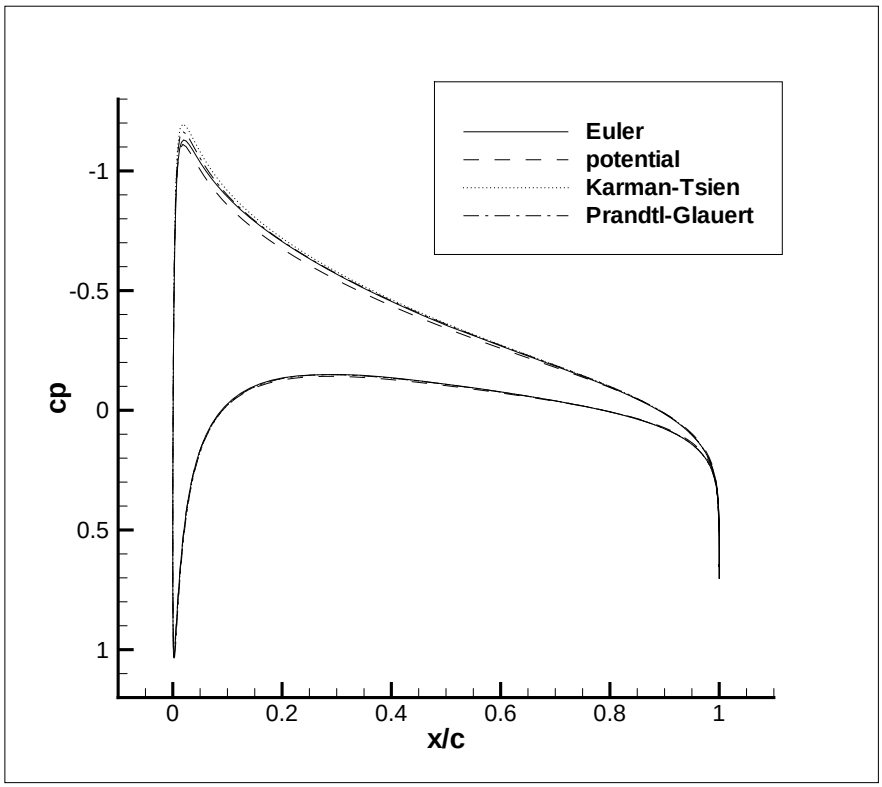

Figure 2.3: Comparison of pressure coefficient c_p of a compressible and a potential incompressible flow (c_p, c_p^{PG}, c_p^{KS}) around NACA0012 airfoil, $\alpha_\infty = 3°$, $M_\infty = 0.3$.

directly from the local speed $v = \sqrt{v_x^2 + v_y^2}$ and the free stream:

$$c_p = 1 - \left(\frac{v}{v_\infty}\right)^2. \tag{2.1.46}$$

At speeds up to $M_\infty = 0.3$ this compressibility effect is negligible, as shown by comparing the results with the results of the compressible model of an inviscid flow described by the system of the Euler equations (described in the next section) in Figure 2.3. It describes the flow around the NACA0012 airfoil at the free stream velocity $v_\infty = 102.05\ m \cdot s^{-1}$ and the angle of attack $\alpha_\infty = 3°$. This corresponds exactly to the value of $M_\infty = 0.3$.

However, when the velocity increases the compressibility affects the flow more and more. Its influence can be imitated using empirically derived corrections [22]. One of them is the Prandtl-Glauert compressibility correction,

$$c_p^{PG} = \frac{c_p}{\sqrt{1 - M_\infty^2}}. \tag{2.1.47}$$

Another possibility is the compressibility correction by Karman-Tsien,

$$c_p^{KS} = \frac{c_p}{\sqrt{1 - M_\infty^2} + \frac{c_p}{2}\left(1 - \sqrt{1 - M_\infty^2}\right)}. \tag{2.1.48}$$

Comparison of the results of incompressible flow with results of the compressible flow (inviscid Euler equations and viscous turbulent flow, see Sections 2.2 and 2.3)

with the free stream velocity $v_\infty = 198.9\ m \cdot s^{-1}$ and $\alpha_\infty = 3°$ (corresponding to $M_\infty = 0.6$) is shown in Figure 2.4. The results show a fairly good agreement when using a correction. The correction by Karman-Tsien shows better results, although it tends to slightly overestimate pressure in the area of large compression near the leading edge. Both corrections behave quite well until the minimum value of the local pressure coefficient (given by (2.1.47) and (2.1.48)) comes close to the critical value c_p^*. In this situation, the compressible flow approaches locally the sonic flow and thus the corrections are no longer valid. The value c_p^* for air ($\gamma = 1.4$) is given by:

$$c_p^* = \frac{1}{0.7M_\infty^2}\left(\left(\frac{1}{1.2} + \frac{M_\infty^2}{6}\right)^{3.5} - 1\right). \tag{2.1.49}$$

In our cases, for $M_\infty = 0.3$ is $c_p^* = -6.95$ and for $M_\infty = 0.6$ is $c_p^* = -1.29$.

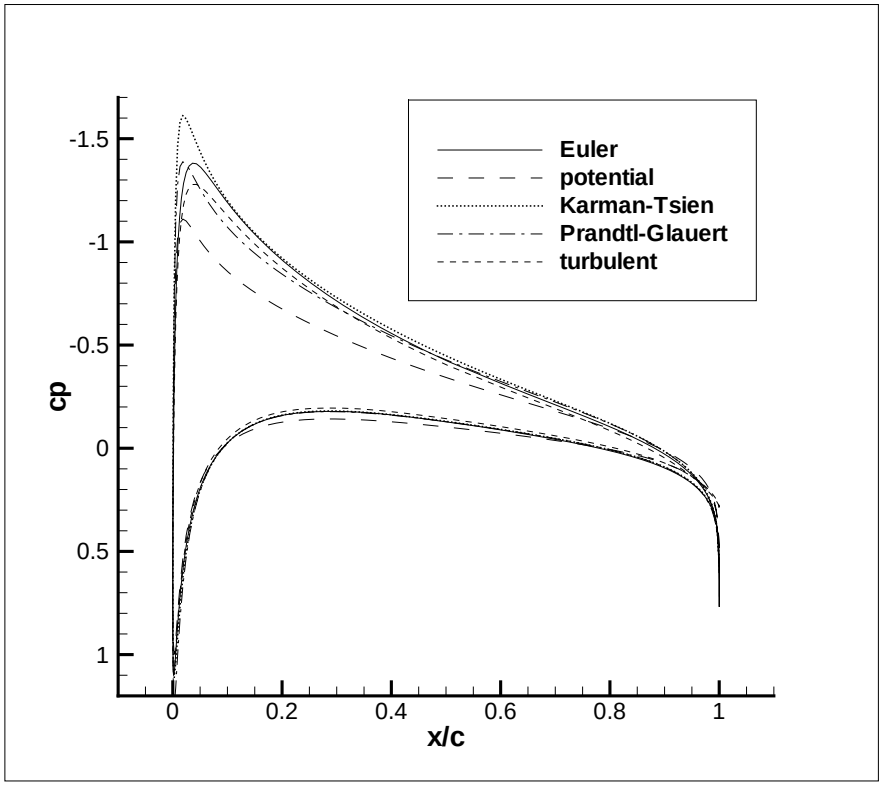

Figure 2.4: Comparison of c_p, c_p^{PG}, c_p^{KS} pressure coefficients of a compressible and a potential incompressible flow around NACA0012, $\alpha_\infty = 3°$, $M_\infty = 0.6$.

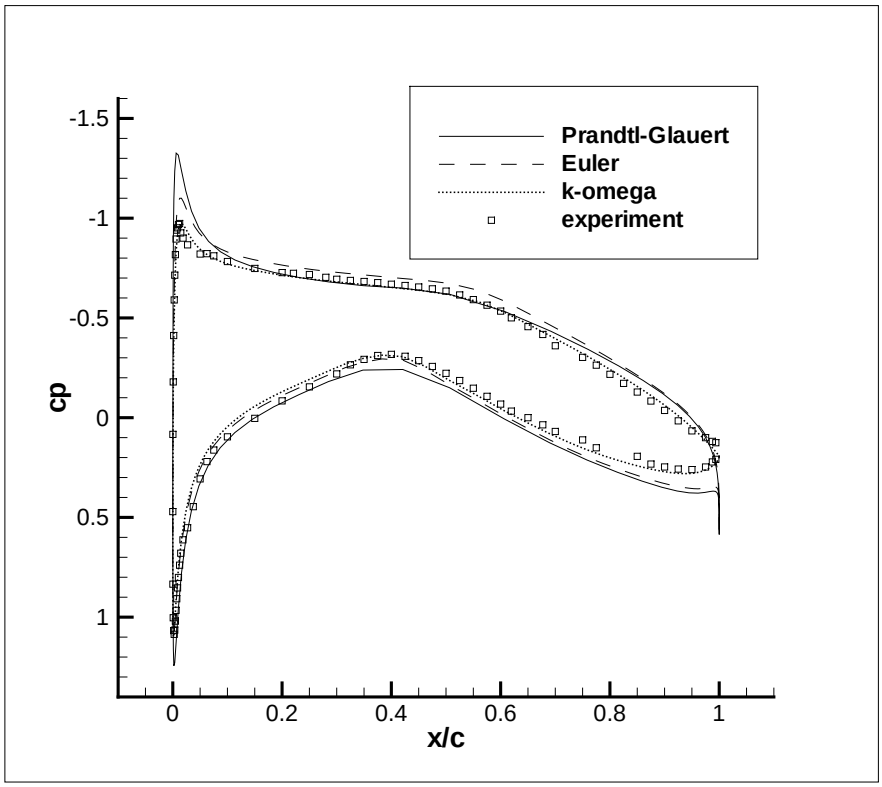

Figure 2.5: Comparison of pressure coefficient for compressible and corrected potential incompressible flow around RAE2822, $\alpha_\infty = 1.96°$, $M_\infty = 0.604$, results compared with data from AGARD test case 3 [23].

2.2 Description of a motion of a viscous fluid

The model described in the previous chapter is a simplification of the reality. The real flow of fluid is compressible, it contains vortices from microscopic to macroscopic scales and of course, it is influenced by the internal friction of gas molecules. Furthermore, the flow is generally non-stationary although it can be, under certain circumstances, regarded as constant in time.

The general description of a flow is commonly based on the formulation of the law of conservation of mass, conservation of momentum and conservation of energy. The flow is generally a three-dimensional problem, however, it can be simplified for the needs of our inverse problem. We assume an idealized, sufficiently long wing of a constant cross-section, situated perpendicular to the stream. Let the x_3-axis of the Cartesian coordinate system be parallel to the wing. Then the region in the middle of the wing span is not influenced by the flow at the wing tip. Hence, the derivatives $\partial/\partial x_3$ can be considered zero and the flow treated as a two-dimensional problem. This greatly simplifies the task from the perspective of the computational complexity. To preserve the generality, however, the mathematical model is derived for a fully three-dimensional flow.

Due to the nature of our problem, we can neglect any external forces acting on the fluid, such as gravity, and also neglect heat sources within the flow. The only heat sources, which are considered, are caused by the internal friction or by the airfoil itself. This leads to the expression of the continuity equation

$$\frac{\partial \rho}{\partial t} + \operatorname{div}(\rho \mathbf{v}) = 0, \tag{2.2.1}$$

the equations of motion (Navier-Stokes eqs.)

$$\frac{\partial(\rho v_i)}{\partial t} + \operatorname{div}(\rho v_i \mathbf{v}) = -\frac{\partial p}{\partial x_i} + \operatorname{div}(\boldsymbol{\mathcal{T}})_i, \quad i = 1, 2, 3 \tag{2.2.2}$$

and finally the energy equation

$$\frac{\partial E}{\partial t} + \operatorname{div}\left((E + p)\mathbf{v}\right) = \operatorname{div}(\boldsymbol{\mathcal{T}}\mathbf{v}) - \operatorname{div}\, \mathbf{q}_L. \tag{2.2.3}$$

We use the following notation: $\mathbf{x} = (x_1, x_2, x_3)$ are spatial coordinates, t denotes time, ρ density, $\mathbf{v} = (v_1, v_2, v_3)$ velocity vector, p static pressure, E total energy, e specific internal energy, T absolute temperature, $\mathbf{q}_L$ thermal flux, $\boldsymbol{\mathcal{T}}$ viscous stress tensor, k_c coefficient of thermal conductivity, R gas constant, C_p specific heat at constant pressure, C_v specific heat at constant volume, γ Poisson adiabatic constant, λ and μ are the first and second viscosity coefficients.

The heat transfer inside the fluid is expressed by the Fourier law

$$\mathbf{q}_L = -k_c \nabla T. \tag{2.2.4}$$

The air can be regarded as a perfect gas, so it is a Newtonian fluid. For Newtonian fluids, the viscous stress tensor $\boldsymbol{\mathcal{T}}$ is proportional to the deformation velocity tensor $\boldsymbol{\mathcal{D}}$ and thus can be expressed by the relation

$$\boldsymbol{\mathcal{T}} = (\lambda \operatorname{div} \mathbf{v})\, \boldsymbol{I} + 2\mu \boldsymbol{\mathcal{D}}, \tag{2.2.5}$$

where $\boldsymbol{I}$ is an identity matrix. For monoatomic gases, $\lambda = -2/3\mu$ and this condition is usually used even for more complicated gases. The viscosity coefficient μ is also called the dynamic viscosity. The deformation velocity tensor depends on the velocity gradients and can be written in the form

$$\boldsymbol{\mathcal{D}} = \frac{1}{2}\left(\nabla \mathbf{v} + (\nabla \mathbf{v})^T\right). \tag{2.2.6}$$

In order to complete the system (2.2.1)–(2.2.3), additional equations from the thermodynamics have to be included. The gas is characterized by the equation of state $p = p(\rho, T)$ and by the relation for the specific internal energy $e = e(\rho, T)$. Since we consider a perfect gas, these equations have the form

$$p = RT\rho \tag{2.2.7}$$

and

$$e = C_v T. \tag{2.2.8}$$

From this, it is possible to derive the expression for the total energy

$$E = \frac{p}{\gamma - 1} + \frac{1}{2}\rho \left|\mathbf{v}\right|^2. \tag{2.2.9}$$

The experiments show that the coefficients C_p and C_v are almost constant for a wide range of temperatures. They are related to the gas constant R by

$$R = C_p - C_v \tag{2.2.10}$$

and to the Poisson constant by

$$\gamma = \frac{C_p}{C_v} \geq 1. \tag{2.2.11}$$

The dynamic viscosity coefficient μ depends on the temperature of the air. One possibility how to relate the viscosity and temperature is by the Sutherland's law

$$\mu = \mu_{ref}\left(\frac{T}{T_{ref}}\right)^{3/2}\frac{T_{ref} + S}{T + S}, \tag{2.2.12}$$

where T_{ref} is a reference temperature, μ_{ref} is the dynamic viscosity at the reference temperature and finally $S = 110.6$ is the Sutherland temperature.

The character of the whole system is mixed parabolic-hyperbolic. Since the viscosity of the air is relatively small in comparison with other fluids, it may have a negligible effect in some cases. This leads to a new model, whose solution is generally easier. If we neglect the internal friction, then $\mu = 0$ and at the same time, the heat conduction inside the fluid can also be neglected. The system of

the equations (2.2.1)–(2.2.3) then simplifies into the form

$$\frac{\partial \rho}{\partial t} + \sum_{j=1}^{3} \frac{\partial \rho v_j}{\partial x_j} = 0, \tag{2.2.13}$$

$$\frac{\partial (\rho v_i)}{\partial t} + \sum_{j=1}^{3} \frac{\partial \left(\rho v_i v_j + \delta_{ij} p\right)}{\partial x_j} = 0, \quad i = 1, 2, 3, \tag{2.2.14}$$

$$\frac{\partial E}{\partial t} + \sum_{j=1}^{3} \frac{\partial (E + p) v_j}{\partial x_j} = 0. \tag{2.2.15}$$

The symbol δ_{ij} is the standard Kronecker delta. This system is called the Euler equations. It is a hyperbolic system of differential equations.

2.3 Turbulence model

The description of the fluid motion by the system of conservation laws includes all important structures of the flow. However, it is very difficult to capturue all of them using numerical methods. The smallest turbulent eddies are much smaller than the largest eddies. Similarly, the time scales for the existence of the vortices are very different. The spatial discretization should be fine enough to capture the smallest eddies (the Kolmogorov length scale) and, of course, cover the entire area of interest. In addition, the scales depend on the Reynolds number so the demands grow rapidly when it is increasing. The length of the time step used in the numerical method should also respect the smallest time scales (the Kolmogorov time scale) present in the flow. Since the turbulence is generally a three-dimensional structure, this approach represents a very demanding task for common engineering applications. Their solution would take months on the most powerful computers. From this reason, the turbulence in practical problems is usually modeled by some statistical approach.

2.3.1 Averaged Navier-Stokes equations

In this standard approach [24] we can assume that the flow consists of a mean flow part and fluctuations caused by the turbulence. The mean flow is computed by the standard way and the fluctuations are modeled by a statistical model. Let θ be a time dependent flow variable. Since we assume a compressible flow, we will use two types of averaging, the Reynolds time averaging and the Favre mass averaging.

The flow variable θ is decomposed by the Reynolds averaging as $\theta = \overline{\theta} + \theta'$, where θ' is the fluctuation part and the mean average is given by

$$\overline{\theta}(x) = \lim_{T' \to \infty} \frac{1}{T'} \int_{t}^{t+T'} \theta(x, \tau) d\tau. \tag{2.3.1}$$

Using the Favre averaging we get $\theta = \tilde{\theta} + \theta''$, where θ'' represents the fluctuations and the mean average is given by

$$\tilde{\theta}(x) = \frac{1}{\overline{\rho}} \lim_{T' \to \infty} \frac{1}{T'} \int_t^{t+T'} \rho(x,\tau)\theta(x,\tau) d\tau, \tag{2.3.2}$$

where $\overline{\rho}$ is the Reynolds averaged density. The averages $\overline{\theta}$ and $\tilde{\theta}$ are strictly speaking time independent. Hence the use of the averaged equations (2.2.1)–(2.2.3) has sense only for steady solutions (which is our case). However, the averaged equations are commonly used even for unsteady problems. In that case, the time interval T' is chosen such that $T_1' \ll T' \ll T_2'$, where T_1' denotes the time scale of turbulent fluctuations and T_2' denotes the large-scale fluid motions. Using this approach, the averaged variables $\overline{\theta}$ and $\tilde{\theta}$ are treated as time-dependent. Unfortunately, it is usually difficult to set the right time scale T' separating the turbulence from the main flow. From this reason, the time accuracy of the unsteady model should be taken with care. We will formulate the averaged equations as time-dependent because it helps us to obtain the steady solution.

It is good to mention, that the average of a fluctuating part is zero. Using the Reynolds averaging, we decompose the instantaneous density and pressure,

$$\rho = \overline{\rho} + \rho', \quad p = \overline{p} + p' \tag{2.3.3}$$

and by the Favre averaging we decompose the instantaneous velocity and specific internal energy,

$$v_i = \tilde{v}_i + v_i'', \quad e = \tilde{e} + e''. \tag{2.3.4}$$

We denote by N the number of dimensions, which could be 2 or 3. Using the above mentioned, we obtain the averaged mean conservation equations

$$\frac{\partial \overline{\rho}}{\partial t} + \operatorname{div}\left(\overline{\rho}\tilde{\mathbf{v}}\right) = 0, \tag{2.3.5}$$

$$\frac{\partial \overline{\rho}\tilde{v}_i}{\partial t} + \operatorname{div}\left(\overline{\rho}\tilde{v}_i\tilde{\mathbf{v}}\right) = -\frac{\partial \overline{p}}{\partial x_i} + \operatorname{div}\left(\overline{\boldsymbol{\mathcal{T}}}\right)_i - \sum_{j=1}^{N} \frac{\partial}{\partial x_j}\left(\overline{\rho v_j'' v_i''}\right), \quad i = 1, 2, \ldots, N \tag{2.3.6}$$

$$\begin{aligned}\frac{\partial \tilde{E}}{\partial t} + \operatorname{div}\left((\tilde{E} + \overline{p})\tilde{\mathbf{v}}\right) &= \operatorname{div}\left(\overline{\boldsymbol{\mathcal{T}}}\tilde{\mathbf{v}}\right) - \operatorname{div}\left(\mathbf{q}_L + \mathbf{q}_T\right) \\ &\quad + \sum_{j=1}^{N} \frac{\partial}{\partial x_j}\left(\sum_{i=1}^{N} \overline{v_i'' \tau_{ji}} - \sum_{i=1}^{N} \tilde{v}_i \overline{\rho v_j'' v_i''} - \frac{1}{2}\sum_{i=1}^{N} \overline{\rho v_j'' v_i'' v_i''}\right).\end{aligned} \tag{2.3.7}$$

These equations are called the compressible Reynolds-Averaged Navier-Stokes equations (RANS, also termed the Favre-Averaged Navier-Stokes equations). Here $\overline{\tau}_{ij} = 2\mu S_{ij}^*$ are components of the averaged viscous stress tensor $\overline{\boldsymbol{\mathcal{T}}}$. The strain rate tensor $\boldsymbol{S}^*$ used in this expression is defined as

$$S_{ij}^* = \frac{1}{2}\left(\frac{\partial \tilde{v}_i}{\partial x_j} + \frac{\partial \tilde{v}_j}{\partial x_i} - \delta_{ij}\sum_{k=1}^{N} \frac{2}{3}\frac{\partial \tilde{v}_k}{\partial x_k}\right). \tag{2.3.8}$$

It is easy to show that this expression is in the correspondence with (2.2.5) and (2.2.6).

Symbols $\mathbf{q}_L$ and $\mathbf{q}_T$ are laminar and turbulent heat fluxes, $\mathbf{q}_L$ is given by (2.2.4) and $\mathbf{q}_T$ will be given bellow. The averaged total energy is given by

$$\tilde{E} = \overline{\rho}\tilde{e} + \frac{1}{2}\overline{\rho}\left|\tilde{v}\right|^2 + \overline{\rho}k, \tag{2.3.9}$$

$$\overline{\rho}k = \frac{1}{2}\sum_{i=1}^{N}\overline{\rho v_i'' v_i''}, \tag{2.3.10}$$

where k is the so-called turbulence kinetic energy. The term $-\overline{\rho v_i'' v_j''}$ in (2.3.6) and (2.3.7) is called the Reynolds stress tensor.

The turbulence modeling is in fact a way how to represent the unknown terms containing fluctuations by known quantities. The most important seems to be the matter of finding an expression for the Reynolds stress. This will be carried out in the following sections.

Unfortunately, the equations (2.3.5)–(2.3.7) still contain some unknown terms, so additional approximations of these terms are necessary in order to close the system. The turbulent heat flux vector is approximated as

$$\left(\mathbf{q}_T\right)_j = -\frac{\mu_T}{Pr_T}\gamma\frac{\partial\tilde{e}}{\partial x_j} \tag{2.3.11}$$

which is of the same form as the laminar heat flux $\mathbf{q}_L$. The turbulent Prandtl number Pr_T is assumed to be constant (e.g around 0.9 for air). The symbol μ_T denotes the so-called eddy viscosity (or turbulent viscosity) and its expression depends on the chosen turbulence model. The contribution of the turbulence kinetic energy to the total energy can be assumed very small. This is true especially for flows up to supersonic regimes. Therefore, the molecular diffusion, $\overline{v_i''\tau_{ji}}$, and turbulence transport, $\overline{\rho v_j'' v_i'' v_i''}$, terms are neglected in the energy equation (2.3.7) and also the turbulence energy k can be neglected in (2.3.9).

2.3.2 The $k-\omega$ model

One of the most widespread turbulence models is the two-equation $k-\omega$ model developed by Wilcox [24]. This model adds to the conservation equations (2.3.5)–(2.3.7) two additional transport equations to describe the turbulent properties of the flow. One equation for the turbulence kinetic energy k and the other for the specific dissipation rate ω. The first variable, k, specifies the amount of energy in the turbulence and the second one, ω, specifies the rate of dissipation of this energy in unit volume and time. These extra transport equations are

$$\frac{\partial\overline{\rho}k}{\partial t} + \operatorname{div}\left(\overline{\rho}k\tilde{\mathbf{v}}\right) = P_k - \beta^*\overline{\rho}\omega k + \operatorname{div}\left(\left(\mu + \sigma_k\mu_T\right)\nabla k\right), \tag{2.3.12}$$

$$\frac{\partial\overline{\rho}\omega}{\partial t} + \operatorname{div}\left(\overline{\rho}\omega\tilde{\mathbf{v}}\right) = P_\omega - \beta\overline{\rho}\omega^2 + \operatorname{div}\left(\left(\mu + \sigma_\omega\mu_T\right)\nabla\omega\right) + C_D. \tag{2.3.13}$$

The terms P_k and P_ω represent the production of the turbulence kinetic energy and the production of the specific dissipation, respectively. They are defined as

$$P_k = -\sum_{i,j=1}^{N} \overline{\rho v_i'' v_j''} \frac{\partial \tilde{v}_i}{\partial x_j} \tag{2.3.14}$$

and

$$P_\omega = \alpha_\omega \omega P_k / k. \tag{2.3.15}$$

The determination of the eddy viscosity μ_T is based on the Boussinesq approximation. The $k-\omega$ model formulates the Reynolds stresses and eddy viscosity coefficient as

$$-\overline{\rho v_i'' v_j''} = 2\mu_T S_{ij}^* - \frac{2}{3}\overline{\rho} k \delta_{ij}, \quad \mu_T = \frac{\overline{\rho} k}{\omega}. \tag{2.3.16}$$

If we are interested in the turbulence length scale l, it can be expressed as $l = \sqrt{k}/\omega$.

The values of the remaining parameters for the standard Wilcox model are

$$\begin{aligned} &\beta^* = 0.09, \quad \beta = 5\beta^*/6, \quad \alpha_\omega = \beta/\beta^* - \sigma_\omega \kappa^2/\sqrt{\beta^*}, \\ &\sigma_k = 0.5, \quad \sigma_\omega = 0.5 \quad \text{and} \quad C_D = 0, \end{aligned} \tag{2.3.17}$$

where $\kappa = 0.41$ is the Von Kármán constant.

Originally, the cross-diffusion term C_D was not included in the standard Wilcox model. However, this model suffers from the sensitivity on the free stream level of the turbulent dissipation ω. From this reason, Kok in his work [25] suggested to include a cross-diffusion term and to reset the model parameters. The cross-diffusion is defined by

$$C_D = \sigma_D \frac{\overline{\rho}}{\omega} \max\left(\sum_{i=1}^{N} \frac{\partial k}{\partial x_i} \frac{\partial \omega}{\partial x_i}, 0 \right). \tag{2.3.18}$$

The new Kok TNT (turbulent/non-turbulent) model has the following parameters:

$$\begin{aligned} &\beta^* = 0.09, \quad \beta = 5\beta^*/6, \quad \alpha_\omega = \beta/\beta^* - \sigma_\omega \kappa^2/\sqrt{\beta^*}, \\ &\sigma_k = 2/3, \quad \sigma_\omega = 0.5 \quad \text{and} \quad \sigma_D = 0.5. \end{aligned} \tag{2.3.19}$$

In practice, the turbulence production term defined by (2.3.14) may cause an unphysical growth of the turbulence level. Therefore, it is a good idea to limit the maximum value of the production by some proper limiter, for example

$$P_k^{lim} = \overline{\rho} k \sqrt{\sum_{i,j=1}^{N} S_{ij}^* S_{ji}^*}. \tag{2.3.20}$$

2.3.3 EARSM

The $k-\omega$ turbulence model based on the eddy viscosity assumption behaves well in many engineering applications. However, it can fail to predict true results in flows with strong adverse pressure gradients (i.e. the static pressure increases in the direction of the flow). In this case the fluid inside the boundary layer is slowed down and it can lead even to a reversion of the flow direction and to the separation of the boundary layer from the surface.

The Boussinesq approximation, which is used in the $k-\omega$ model, assumes that the eddy viscosity is isotropic, which is not generally true. An improvement is to incorporate individual Reynolds stresses into the transport equations. The Explicit Algebraic Reynolds-Stress Model (EARSM) according to Wallin [26] is formulated in the terms of the standard $k-\omega$ turbulence model. Therefore, this model can be considered as an extension to the standard model. The main differences are the expressions for the turbulent viscosity and Reynolds stresses. We will use the superscripts $^{(EARSM)}$ and $^{(\mathrm{k}-\omega)}$ to distinguish between the quantities from the standard $k-\omega$ model (Sec. 2.3.2) and from the new EARSM.

An extra anisotropy a_{ij} is introduced, which is added to the standard Reynolds stress formulation

$$-\overline{\rho v_i'' v_j''} = 2\mu_T^{(EARSM)} S_{ij}^* - \frac{2}{3}\overline{\rho} k \delta_{ij} - \overline{\rho} k a_{ij}. \tag{2.3.21}$$

The new eddy viscosity is formulated as

$$\mu_T^{(EARSM)} = -\frac{1}{2}(\beta_1 + \Pi_\Omega \beta_6) \max\left(\frac{\overline{\rho}k}{\beta^* \omega}, c_\tau \sqrt{\frac{\mu \overline{\rho} k}{\beta^* \omega}}\right) \tag{2.3.22}$$

with $c_\tau = 6$ a model constant. The other parameters are given bellow.

The modifications of the original model involves equations in the same form as (2.3.12)–(2.3.13) with new expressions of the turbulent viscosity coefficient $\mu_T^{(EARSM)}$, the production term

$$P_k^{(EARSM)} = P_k^{(\mathrm{k}-\omega)} - \sum_{i,j=1}^{N} \overline{\rho} k a_{ij} \frac{\partial \tilde{v}_i}{\partial x_j} \tag{2.3.23}$$

and the stress tensor

$$\tau_{ij}^{(EARSM)} = \tau_{ij} - \overline{\rho} k a_{ij}, \quad \tau_{ij} = 2(\mu + \mu_T^{(EARSM)}) S_{ij}^* - \frac{2}{3}\overline{\rho} k \delta_{ij}. \tag{2.3.24}$$

The extra anisotropy tensor is given by the relation

$$\begin{aligned} \boldsymbol{a} =& \beta_3(\boldsymbol{\Omega}^2 - \frac{\Pi_\Omega}{3}\boldsymbol{I}) + \beta_4(\boldsymbol{S\Omega} - \boldsymbol{\Omega S}) + \beta_6(\boldsymbol{S\Omega}^2 + \boldsymbol{\Omega}^2\boldsymbol{S} - \Pi_\Omega \boldsymbol{S} - \frac{2}{3}\Pi \boldsymbol{I}) \\ &+ \beta_9(\boldsymbol{\Omega S \Omega}^2 - \boldsymbol{\Omega}^2 \boldsymbol{S \Omega}). \end{aligned} \tag{2.3.25}$$

Here $\boldsymbol{S}$ and $\boldsymbol{\Omega}$ are normalized strain and rotation rate tensors,

$$\boldsymbol{S} = \tau \boldsymbol{S}^*, \quad \boldsymbol{\Omega} = \tau \boldsymbol{\Omega}^*, \tag{2.3.26}$$

where $\tau = \max\left(1/(\beta^*\omega), c_\tau\sqrt{\mu/(\overline{\rho}\beta^*\omega k)}\right)$ is the turbulent time scale $1/(\beta^*\omega)$ limited by the Kolmogorov time scale. The strain rate tensor S^*_{ij} is given by (2.3.8) and

$$\Omega^*_{ij} = \frac{1}{2}\left(\frac{\partial\tilde{u}_i}{\partial x_j} - \frac{\partial\tilde{u}_j}{\partial x_i}\right). \tag{2.3.27}$$

The strain rate tensor $\boldsymbol{S}$ is symmetric and the rotation rate tensor $\boldsymbol{\Omega}$ is antisymmetric. These properties can be employed with success in the evaluation of the equation (2.3.25).

The symbols $\Pi_S = \mathrm{tr}(\boldsymbol{S}^2)$, $\Pi_\Omega = \mathrm{tr}(\boldsymbol{\Omega}^2)$ and $\Pi = \mathrm{tr}(\boldsymbol{S\Omega}^2)$ denote traces (e.g. sums of the diagonal elements). The coefficients β are given by the relations

$$\begin{aligned}
&\beta_1 = -\frac{A(2A^2 - 7\Pi_\Omega)}{Q}, \quad \beta_3 = -\frac{12\Pi/A}{Q}, \quad \beta_4 = -\frac{2(A^2 - 2\Pi_\Omega)}{Q},\\
&\beta_6 = -\frac{6A}{Q}, \quad \beta_9 = \frac{6}{Q}, \quad Q = \frac{5}{6}(A^2 - 2\Pi_\Omega)(2A^2 - \Pi_\Omega).
\end{aligned} \tag{2.3.28}$$

The parameter A is evaluated as

$$A = \begin{cases} c_1/3 + (P_1 + \sqrt{P_2})^{1/3} + (P_1 - \sqrt{P_2})^{1/3} & \text{for } \mathrm{P}_2 \geq 0 \\ c_1/3 + 2(P_1^2 - P_2)^{1/6}\cos\left(\arccos\left(P_1/\sqrt{P_1^2 - P_2}\right)/3\right) & \text{for } \mathrm{P}_2 < 0 \end{cases} \tag{2.3.29}$$

where

$$P_1 = \left(\frac{c_1^2}{27} + \frac{9}{20}\Pi_S - \frac{2}{3}\Pi_\Omega\right)c_1, \tag{2.3.30}$$

$$P_2 = P_1^2 - \left(\frac{c_1^2}{9} + \frac{9}{10}\Pi_S + \frac{2}{3}\Pi_\Omega\right)^3, \tag{2.3.31}$$

$$c_1 = \frac{9}{4}(c_2 - 1), \quad c_2 = 1.8. \tag{2.3.32}$$

If we are dealing with a two-dimensional model, then the coefficients β are

$$\begin{aligned}
&\beta_1 = -\frac{6}{5}\frac{A}{A^2 - 2\Pi_\Omega}, \quad \beta_3 = 0, \quad \beta_4 = -\frac{6}{5}\frac{1}{A^2 - 2\Pi_\Omega},\\
&\beta_6 = 0, \quad \beta_9 = 0.
\end{aligned} \tag{2.3.33}$$

This means that the expression (2.3.25) for a two-dimensional flow simplifies to the relation

$$\boldsymbol{a} = \beta_4(\boldsymbol{S\Omega} - \boldsymbol{\Omega S}). \tag{2.3.34}$$

Values of the turbulence model parameters β^*, β, α_ω, σ_k, σ_ω and σ_D are the same as for the $k-\omega$ model (see (2.3.17) or (2.3.19)).

The comparison of the turbulence models is shown in Figure 2.6. This test case represents a flow around the RAE2822 airfoil with the free stream parameters $M_\infty = 0.754$ and $\alpha_\infty = 2.57°$. A shock wave arises on the upper surface of the airfoil (Figure 2.7). Behind this shock wave, the boundary layer separates from the surface and reattaches again. Even though it is a transonic flow, which our inverse method is not concerned with, this example shows the ability to

correctly capture the area of separation. Comparison of the results obtained by the software, which was developed by the author during his work on this thesis, with the data from the wind tunnel measurement [23] shows that EARSM turbulence model can quite accurately capture the position of the shock wave. The other models indicate its position further towards the trailing edge.

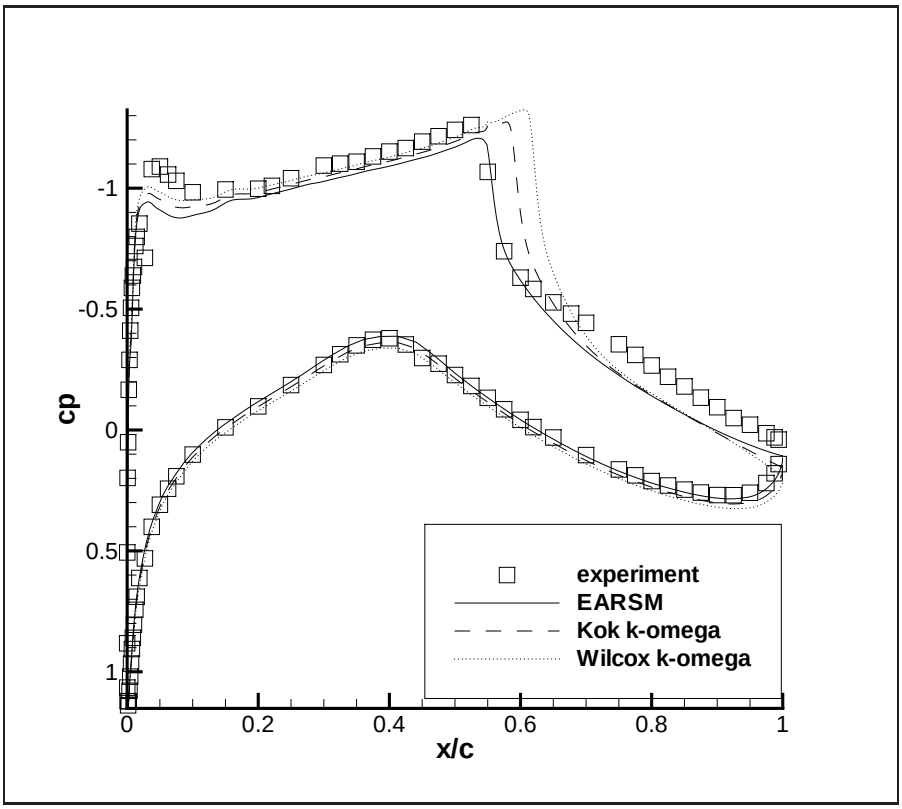

Figure 2.6: Comparison of c_p coefficient for flow around RAE2822, $\alpha_\infty = 2.57°$, $M_\infty = 0.754$. Obtained results for different turbulence models (Kok EARSM, Kok $k-\omega$, Wilcox $k-\omega$) compared with data from AGARD test case 10.

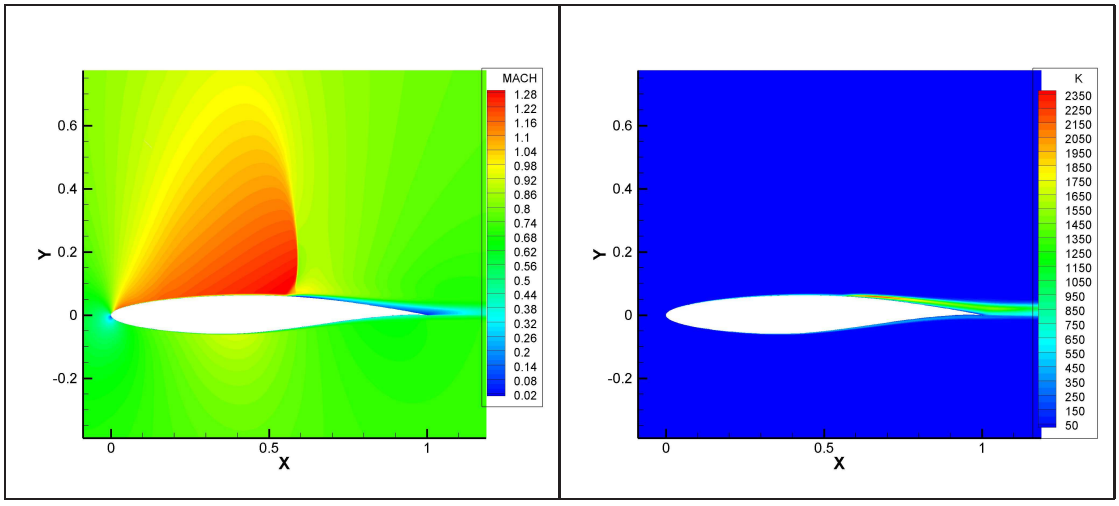

Figure 2.7: The Mach number and turbulence kinetic energy distribution around RAE2822, $\alpha_\infty = 2.57°$, $M_\infty = 0.754$ (Kok EARSM model).

2.4 Numerical solution

In the text above, the mathematical formulation of the flow model is presented. It can be seen that the system of conservation equations (2.2.1)–(2.2.3) has a similar form as the averaged equations (2.3.5)–(2.3.7). Due to the needs of our problem we will deal only with the two-dimensional model. We denote by Ω the bounded region around the airfoil, where the flow needs to be computed. In the following text, we will consider only the mean values of the state variables, so we will use the standard notation without overline and tilde. For the purpose of the numerical solution, it is useful to write the equations (2.3.5)–(2.3.7) and the turbulence model equations (2.3.12)–(2.3.13) in the vector form

$$\frac{\partial \mathbf{w}}{\partial t} + \sum_{i=1}^{2} \frac{\partial \mathbf{F}_i(\mathbf{w})}{\partial x_i} = \sum_{i=1}^{2} \frac{\partial \mathbf{R}_i(\mathbf{w}, \nabla \mathbf{w})}{\partial x_i}, \tag{2.4.1}$$

$$\frac{\partial \mathbf{q}}{\partial t} + \sum_{i=1}^{2} \frac{\partial \mathbf{G}_i(\mathbf{q})}{\partial x_i} = \sum_{i=1}^{2} \frac{\partial \mathbf{Q}_i(\mathbf{q}, \nabla \mathbf{q})}{\partial x_i} + \mathbf{S}\left(\mathbf{q}, \nabla \mathbf{q}\right), \tag{2.4.2}$$

where

$$\mathbf{w} = (\rho, \rho v_1, \rho v_2, E)^T, \tag{2.4.3}$$

$$\mathbf{F}_i(\mathbf{w}) = (\rho v_i, \rho v_1 v_i + \delta_{1i} p, \rho v_2 v_i + \delta_{2i} p, (E+p) v_i)^T, \tag{2.4.4}$$

$$\mathbf{R}_i(\mathbf{w}, \nabla \mathbf{w}) = \left(0, \tau_{i1}, \tau_{i2}, \tau_{i1} v_1 + \tau_{i2} v_2 + \left(\frac{\mu}{P_r} + \frac{\mu_T}{P_{rT}}\right) \gamma \frac{\partial e}{\partial x_i}\right)^T, \tag{2.4.5}$$

$$\mathbf{q} = (\rho k, \rho \omega)^T, \tag{2.4.6}$$

$$\mathbf{G}_i(\mathbf{q}) = (\rho k v_i, \rho \omega v_i)^T, \tag{2.4.7}$$

$$\mathbf{Q}_i(\mathbf{q}, \nabla \mathbf{q}) = \left((\mu + \sigma_k \mu_T) \frac{\partial k}{\partial x_i}, (\mu + \sigma_\omega \mu_T) \frac{\partial \omega}{\partial x_i}\right)^T, \tag{2.4.8}$$

$$\mathbf{S}(\mathbf{q}, \nabla \mathbf{q}) = \left(P_k - \beta^* \rho \omega k, P_\omega - \beta \rho \omega^2 + C_D\right)^T. \tag{2.4.9}$$

The symbol P_r denotes the Prandtl number which can be expressed as $P_r = \mu C_p/k_c$.

The components of the stress tensor $\boldsymbol{\mathcal{T}}$ can be written as

$$\begin{aligned}
\tau_{11} &= (\mu+\mu_T)\left(\frac{4}{3}\frac{\partial v_1}{\partial x_1} - \frac{2}{3}\frac{\partial v_2}{\partial x_2}\right) - \frac{2}{3}\rho k,\\
\tau_{22} &= (\mu+\mu_T)\left(-\frac{2}{3}\frac{\partial v_1}{\partial x_1} + \frac{4}{3}\frac{\partial v_2}{\partial x_2}\right) - \frac{2}{3}\rho k,\\
\tau_{12} = \tau_{21} &= (\mu+\mu_T)\left(\frac{\partial v_1}{\partial x_2} + \frac{\partial v_2}{\partial x_1}\right).
\end{aligned} \tag{2.4.10}$$

It follows from the above that if we set $k = 0$, the system (2.4.1) will be independent of the turbulence model (2.4.2). Therefore, we can solve only the first system in this situation. The mean flow equations thus describe a laminar flow. In addition, if we set $\mu = 0$, the resulting system will represent the Euler equations describing the inviscid flow.

We can obtain the requested velocity or pressure distribution needed for the solution of the inverse problem from the values $\mathbf{w}$ on the airfoil Γ_w. We deal either with the velocity distribution or with the pressure distribution so we will denote both by f. The velocity distribution on the airfoil surface can be expressed as

$$f = \sqrt{\left(\frac{w_2}{w_1}\right)^2 + \left(\frac{w_3}{w_1}\right)^2} \tag{2.4.11}$$

and the pressure distribution as

$$f = (\gamma-1)\left(w_4 - \frac{w_2^2+w_3^2}{2w_1}\right). \tag{2.4.12}$$

2.4.1 Dimensionless model

In practice, it is useful to deal with a dimensionless model. In order to do that, it is necessary to suitably transform all considered variables to new variables, denoted by hat, with respect to some specified reference values. These values are obtained with the use of the following relations for an isentropic flow. The Mach number M is defined as the ratio of the local speed of flow to the local speed of sound:

$$M = \frac{\sqrt{v_1^2+v_2^2}}{c}. \tag{2.4.13}$$

The speed of sound in a perfect gas can be expressed as

$$c = \sqrt{\gamma p/\rho}. \tag{2.4.14}$$

Then it is possible to express the density and static pressure by the formulae [27]:

$$\rho = \rho_0\left(1+\frac{\gamma-1}{2}M^2\right)^{-1/(\gamma-1)}, \tag{2.4.15}$$

$$p = p_0\left(1+\frac{\gamma-1}{2}M^2\right)^{-\gamma/(\gamma-1)}, \tag{2.4.16}$$

where the index zero denotes total values (values of a nonmoving gas). Using the previous relations we can also get the following expression for the speed of sound:

$$c^2 = c_0^2 \left(1 + \frac{\gamma - 1}{2} M^2\right)^{-1}. \tag{2.4.17}$$

Now using (2.4.15) and (2.4.16), we can define the critical values ρ_* and c_* of the density and the speed of sound for the unit Mach number. We get

$$\rho_* = \rho_0 \left(\frac{2}{\gamma + 1}\right)^{1/(\gamma-1)}, \qquad c_* = c_0 \sqrt{\frac{2}{\gamma + 1}}. \tag{2.4.18}$$

Next, let us set

$$\lambda = \frac{\sqrt{v_1^2 + v_2^2}}{c_*}. \tag{2.4.19}$$

We call this quantity the Laval number. The relation between the Laval number λ and the Mach number M is

$$\lambda^2 = \frac{\gamma + 1}{2/M^2 + \gamma - 1}. \tag{2.4.20}$$

Now we can transform the velocity vector $\mathbf{v}$ as

$$\hat{v}_1 = \frac{v_1}{c_*}, \quad \hat{v}_2 = \frac{v_2}{c_*}. \tag{2.4.21}$$

According to this, the Laval number is the transformed speed of flow,

$$\sqrt{\hat{v}_1^2 + \hat{v}_2^2} = \lambda. \tag{2.4.22}$$

Further we define $\hat{\rho} = \rho/\rho_*$:

$$\hat{\rho} = \hat{\rho}_0 \left(1 - \frac{\gamma - 1}{\gamma + 1} \lambda^2\right)^{1/(\gamma-1)}, \quad \hat{\rho}_0 = \left(\frac{2}{\gamma + 1}\right)^{-1/(\gamma-1)}. \tag{2.4.23}$$

It is necessary to preserve the equation for the speed of sound $c^2 = \gamma p/\rho$ in order to have the same form of the system of equations. Hence the pressure is transformed as

$$\hat{p} = \frac{p}{\rho_* c_*^2}, \quad \text{thus } \hat{p} = \hat{p}_0 \left(1 - \frac{\gamma - 1}{\gamma + 1} \lambda^2\right)^{\gamma/(\gamma-1)}, \tag{2.4.24}$$

where

$$\hat{p}_0 = \left(\left(\frac{2}{\gamma + 1}\right)^{1/(\gamma-1)} \frac{2\gamma}{\gamma + 1}\right)^{-1}. \tag{2.4.25}$$

Using this normalization we also get

$$\begin{gathered} \hat{E} = \frac{E}{\rho_* c_*^2}, \quad \hat{e} = \frac{e}{c_*^2}, \\ \hat{x} = \frac{x}{l_*}, \quad \hat{y} = \frac{y}{l_*}, \quad \hat{t} = \frac{c_* t}{l_*}, \\ \hat{k} = \frac{k}{c_*^2}, \quad \hat{\omega} = \frac{\omega l_*}{c_*}, \end{gathered} \tag{2.4.26}$$

where l_* is a characteristic length. In our case it is the real length of the chord of the airfoil. The coefficients of viscosity are normalized as

$$\hat{\mu} = \frac{\mu}{\rho_* c_* l_*}, \quad \hat{\mu}_T = \frac{\mu_T}{\rho_* c_* l_*} \tag{2.4.27}$$

and the stress tensor

$$\hat{\tau}_{ij} = \frac{\tau_{ij}}{\rho_* c_*^2}. \tag{2.4.28}$$

Using the mentioned transformation to a dimensionless system of equations, the formal notation of the system remains unchanged. Thus we can omit the hat symbol to simplify the notation in the following text.

2.4.2 Boundary and initial conditions

In order to use the differential equations (2.4.1) and (2.4.2) for a solution of a flow field inside the domain Ω, they should be completed with suitable boundary and initial conditions. Boundary conditions must be specified on all parts of the boundary Γ. In our case, it means conditions at the airfoil surface and at the far-field boundary.

Initial conditions

The biggest changes in the flow field are around the airfoil, with its increasing distance they go to zero. As a perfectly natural initial condition, it is suggested to use the free stream values.

Wall boundary conditions

The conditions on the wall depend on the selected flow model. If we consider the inviscid flow (the Euler equations), we require that the velocity vector is tangent to the boundary, i.e.

$$\mathbf{v} \cdot \mathbf{n} = 0 \quad \text{on } \Gamma_w, \tag{2.4.29}$$

where $\mathbf{n}$ is the unit normal vector to the boundary.

In the case of a viscous flow, the velocity very close to the wall can be considered to be zero. Therefore, we prescribe the so-called no-slip condition

$$\mathbf{v} = 0 \quad \text{on } \Gamma_w. \tag{2.4.30}$$

Since the equations contain heat fluxes, it is necessary to specify some boundary condition for the temperature. It can be given by the Dirichlet or Neumann boundary condition,

$$T = T_w \quad \text{or} \quad \nabla T \cdot \mathbf{n} = 0 \quad \text{on } \Gamma_w, \tag{2.4.31}$$

where T_w is a prescribed temperature.

Furthermore, in the case of a turbulent flow, it is necessary to specify conditions for k and ω. It follows from the physical properties of the flow that the values on the wall are

$$k_w = 0 \quad \text{and} \quad \omega_w \to \frac{6\mu}{\beta\rho y^2}, \tag{2.4.32}$$

where y is the distance from the wall. We assume smooth walls hence the value of the dissipation on the airfoil in the numerical method is given by

$$\omega_w = 120\frac{\mu}{\rho y_c^2}. \tag{2.4.33}$$

Here y_c is the distance between the wall and the centre of the current grid cell next to the wall from the considered discretization mesh.

Far-field boundary conditions

On the outer boundary of the domain Ω, which should be far enough, we prescribe the values of the free stream. To respect the mathematical properties of the equations we divide the boundary into two parts, the inlet and outlet part. This partitioning is performed on the basis of the free stream velocity direction.

Since we consider a subsonic flow, we prescribe the density and the velocity components of the free stream at the inlet part. If we solve a turbulent flow, it is necessary to prescribe the free stream turbulence intensity I_∞ and the ratio of the turbulent and molecular viscosity Re_T (the turbulent Reynolds number),

$$I_\infty = \sqrt{\frac{2}{3}\frac{k_\infty}{v_\infty^2}}, \tag{2.4.34}$$

$$\mathrm{Re}_T = \mu_T/\mu. \tag{2.4.35}$$

From these relations, we can derive the boundary conditions for k and ω:

$$k_\infty = \frac{3}{2}\left(v_\infty I_\infty\right)^2, \tag{2.4.36}$$

$$\omega_\infty = \frac{\rho k}{\mu}\left(\frac{\mu_T}{\mu}\right)^{-1}. \tag{2.4.37}$$

The other state variables are extrapolated from inside the computational domain.

On the outlet boundary, we prescribe only the free stream static pressure

$$p = p_\infty \tag{2.4.38}$$

and we extrapolate the remaining variables from inside the domain.

The values of the free stream can also be specified in the form of the total pressure p_0, total temperature T_0, Mach number M_∞ and the angle of attack α_∞. Then we determine the values of p_∞ and ρ_∞ using the equations for an isentropic flow (2.4.15) and (2.4.16). The velocity v_∞ is determined from the definition of the Mach number.

2.4.3 Boundary layer

Boundary layer is a thin layer of fluid near surfaces where the viscous effects are significant. To correctly capture the boundary layer near a wall, it is necessary to have a sufficiently refined discretization grid in the direction towards the wall. A typical velocity profile (magnitude of the velocity) across a turbulent boundary layer on a wall is shown in Figure 2.8. We can clearly distinguish four areas with different velocity behaviour, the viscous sublayer, buffer layer, logarithmic layer and the defect layer. The velocity profile is usually expressed using the dimensionless wall distance y^+ and the dimensionless velocity v^+ in order to eliminate the dependence on the position on the surface. These dimensionless variables are defined using the friction velocity $v_\tau = \sqrt{\tau_w/\rho}$, where τ_w is the surface shear stress. For a flat plate in the direction of the x_1-axis, $\tau_w = \mu(\partial v_1/\partial x_2)|_{x_2=0}$.

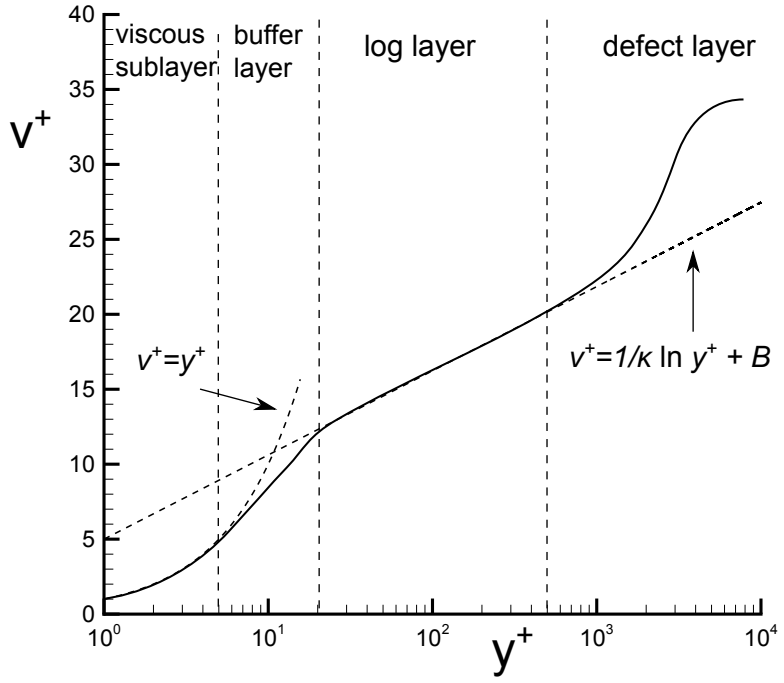

Figure 2.8: Typical velocity profile across a turbulent boundary layer.

Quantities y^+ and v^+ are expressed as

$$v^+ = \frac{v}{v_\tau}, \tag{2.4.39}$$

$$y^+ = \frac{\rho v_\tau y}{\mu}. \tag{2.4.40}$$

In the viscous sublayer, where the turbulence effects are negligible compared to the molecular viscosity effects, the velocity varies almost linearly with y^+. In the log layer, the velocity behaves according to the well-known law of the wall (for smooth surfaces) [24],

$$v^+ = \frac{1}{0.41} \ln y^+ + 5. \tag{2.4.41}$$

Therefore, the precision of capturing the boundary layer depends on the coverage of the viscous sublayer and the following regions by a sufficient number of grid cells. The height of the first row of cells is also very important. It is commonly recommended to set the height of the first layer of cells at $y^+ \approx 1$.

2.4.4 Finite volume method

The presented problem (2.4.1) and (2.4.2) is solved by a finite volume method (FVM). We discretize the computational domain $\Omega \subset \mathbb{R}^2$ by a mesh $\mathcal{D}_h = \{D_i,\ i = 1, \ldots, N_e\}$ formed by quadrilateral elements (cells). These elements satisfy the standard conditions, i.e.

- $\overline{\Omega}_h = \bigcup_{i=1}^{N_e} D_i$, where $\overline{\Omega}_h$ is the closure of a polygonal approximation of Ω,
- $\forall i \neq j,\ 1 \leq i, j \leq N_e :\ D_i \cap D_j$ is empty or a common vertex or a common edge.

The equations (2.4.1) and (2.4.2) are expressed as integral identities and using the Green's theorem rewritten into the form

$$\frac{\partial}{\partial t}\int_{D_j} \mathbf{w} dx + \int_{\partial D_j} \sum_{i=1}^{2} \mathbf{n}_i \mathbf{F}_i(\mathbf{w}) dS - \int_{\partial D_j} \sum_{i=1}^{2} \mathbf{n}_i \mathbf{R}_i\left(\mathbf{w}, \nabla \mathbf{w}\right) dS = 0 \tag{2.4.42}$$

and

$$\frac{\partial}{\partial t}\int_{D_j} \mathbf{q} dx + \int_{\partial D_j} \sum_{i=1}^{2} \mathbf{n}_i \mathbf{G}_i(\mathbf{q}) dS - \int_{\partial D_j} \sum_{i=1}^{2} \mathbf{n}_i \mathbf{Q}_i\left(\mathbf{q}, \nabla \mathbf{q}\right) dS = \int_{D_j} \mathbf{S}\left(\mathbf{q}, \nabla \mathbf{q}\right) dx. \tag{2.4.43}$$

These equations are valid on each element $D_j \in \mathcal{D}_h$.

The symbol $\mathbf{w}_i$ will denote the integral average of the vector $\mathbf{w}$ on the element D_i and it will represent the value of the approximate solution on this element. The vector $\mathbf{w}_h$, $\mathbf{w}_h|_{D_i} = \mathbf{w}_i$ will denote the approximate solution of the problem for the entire domain Ω_h. The symbols $\mathbf{q}_i$ and $\mathbf{q}_h$ are defined in the same way. Then we can define the vector functions $\mathbf{\Phi}(\mathbf{w}_h)$ and $\mathbf{\Phi}^t(\mathbf{q}_h)$ as

$$\begin{aligned}\mathbf{\Phi}_i(\mathbf{w}_h) =& \frac{1}{|D_i|}\Bigg(\sum_{j\in S(i)} \mathbf{H}\left(\mathbf{w}_i, \mathbf{w}_j, \mathbf{n}_{ij}\right)|\Gamma_{ij}| - \\ & \sum_{j\in S(i)}\sum_{s=1}^{2} \left(\mathbf{n}_{ij}\right)_s \mathbf{R}_s\left(\mathbf{w}|_{\Gamma_{ij}}, \left(\nabla \mathbf{w}\right)|_{\Gamma_{ij}}\right)|\Gamma_{ij}|\Bigg),\end{aligned} \tag{2.4.44}$$

$$\begin{aligned}\mathbf{\Phi}_i^t(\mathbf{q}_h) =& \frac{1}{|D_i|}\Bigg(\sum_{j\in S(i)} \mathbf{H}^t\left(\mathbf{q}_i, \mathbf{q}_j, \mathbf{n}_{ij}\right)|\Gamma_{ij}| - \\ & \sum_{j\in S(i)}\sum_{s=1}^{2} \left(\mathbf{n}_{ij}\right)_s \mathbf{Q}_s\left(\mathbf{q}|_{\Gamma_{ij}}, \left(\nabla \mathbf{q}\right)|_{\Gamma_{ij}}\right)|\Gamma_{ij}|\Bigg) - \mathbf{S}(\mathbf{q}_i, \nabla \mathbf{q}_i).\end{aligned} \tag{2.4.45}$$

By the symbol $S(i)$ we denote here the index set of neighbouring elements, $|\cdot|$ denotes the area of the element D_i, respectively the length of the common edge

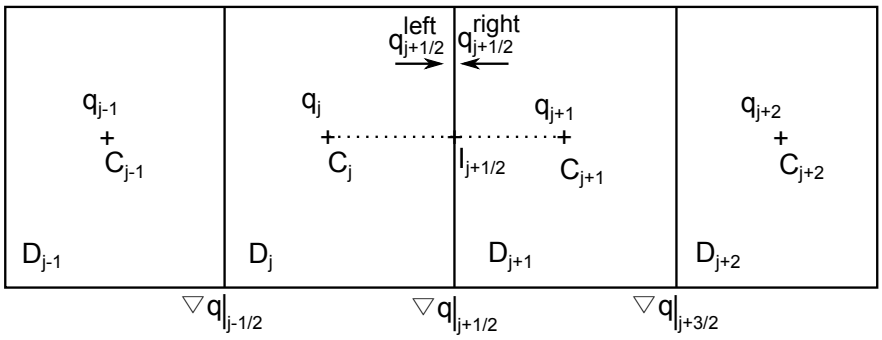

Figure 2.9: Scheme for higher order reconstruction.

Γ_{ij} between elements D_i and D_j, $\mathbf{n}_{ij}$ is the unit normal to Γ_{ij} pointing towards D_j and $\mathbf{H}(\mathbf{w}_i, \mathbf{w}_j, \mathbf{n}_{ij})$, $\mathbf{H}^t(\mathbf{q}_i, \mathbf{q}_j, \mathbf{n}_{ij})$ denote numerical fluxes.

The gradients on the common edges Γ_{ij} are approximated from the values of $\mathbf{w}_h$ or $\mathbf{q}_h$ on the neighbouring elements to Γ_{ij}. More details about this evaluation is presented in Section 2.4.5. The numerical flux $\mathbf{H}$ is expressed according to Osher and Solomon and the turbulent numerical flux $\mathbf{H}^t$ is expressed by the Vijayasundaram scheme [28]:

$$\mathbf{H}^t(\mathbf{q}_i, \mathbf{q}_j, \mathbf{n}_{ij}) = \left(\sum_{s=1}^{2} (\mathbf{n}_{ij})_s \frac{(\mathbf{v}_i)_s + (\mathbf{v}_j)_s}{2} \right)^+ \begin{pmatrix} \rho_i k_i \\ \rho_i \omega_i \end{pmatrix} + \left(\sum_{s=1}^{2} (\mathbf{n}_{ij})_s \frac{(\mathbf{v}_i)_s + (\mathbf{v}_j)_s}{2} \right)^- \begin{pmatrix} \rho_j k_j \\ \rho_j \omega_j \end{pmatrix}, \quad (2.4.46)$$

where $(\cdot)^+$ and $(\cdot)^-$ are the positive and negative parts of $(\cdot)$.

The numerical flux $\mathbf{H}$ (resp. $\mathbf{H}^t$) computes the flux across the edge Γ_{ij} from the values of $\mathbf{w}$ (resp. $\mathbf{q}$) on the left and right side of Γ_{ij}. The mentioned formulation of $\mathbf{\Phi}$ uses the values $\mathbf{w}_i$ and $\mathbf{w}_j$ because these are the approximate values of $\mathbf{w}$ on the corresponding elements. However, this formulation yields only a first order of accuracy. To increase the order of accuracy it is necessary to reconstruct the values of the solution on the edges. If we consider the situation in Figure 2.9 where C_j are centres of elements, $I_{j+1/2}$ centres of edges, q_j values on elements and $\nabla q|_{j+1/2}$ approximations of gradients on edges, then the reconstructed edge values $q^{left}_{j+1/2}$ and $q^{right}_{j+1/2}$ can be approximated using the following:

$$q^{left}_{j+1/2} = q_j + \Psi(R_j) \nabla q|_{j-1/2} (I_{j+1/2} - C_j), \quad (2.4.47)$$

$$q^{right}_{j+1/2} = q_{j+1} + \Psi\left(\frac{1}{R_{j+1}}\right) \nabla q|_{j+3/2} (I_{j+1/2} - C_{j+1}), \quad (2.4.48)$$

where

$$R_j = \frac{\nabla q|_{j+1/2} (C_{j+1} - I_{j+1/2})}{\nabla q|_{j-1/2} (I_{j+1/2} - C_j)}. \quad (2.4.49)$$

We substitute for q the values of ρ, v_1, v_2, p, k and ω. The function $\Psi : \mathbb{R} \to \mathbb{R}$ is called a (slope) limiter. If we choose the limiter in the form

$$\Psi(R) = \frac{1+2R}{3}, \tag{2.4.50}$$

we obtain the Van Leer κ-scheme for $\kappa = 1/3$, which yields a third order of accuracy in 1-D. However, this scheme suffers from spurious oscillations near discontinuities. Another possibility is to choose the limiter according to Van Albada, which eliminates this problem:

$$\Psi(R) = \frac{R^2+R}{R^2+1}. \tag{2.4.51}$$

Using the newly reconstructed values on the edges in the expressions of numerical fluxes, we obtain a scheme with a second order of accuracy in space.

The numerical solution of both systems (2.4.1) and (2.4.2) is carried out in the similar way so we will describe only the solution of the first system.

The semi-discrete formulation (the method of lines) of the FVM for the equation (2.4.1) can be written in the form

$$\frac{\partial \mathbf{w}_i}{\partial t} + \mathbf{\Phi}_i(\mathbf{w}_h) = 0, \quad 1 \le i \le N_e. \tag{2.4.52}$$

This system of ordinary differential equations can be solved by explicit methods, such as the forward Euler or the Runge-Kutta method, or by implicit methods. It is known that the stability region of explicit methods is rather limited. It means that the maximum possible time step τ is small.

We are interested in the steady state solution $\mathbf{w}_h^*$. This solution will be obtained by the pseudo-transient method, which solves the steady state problem as an unsteady problem for a sufficiently long time period, i.e. $\mathbf{w}_h \to \mathbf{w}_h^*$ for $t \to \infty$. Therefore, the computation with a small time step can be very time consuming. This is why an implicit method was chosen, which allows us to use a considerably larger time step without loosing the numerical stability.

If we know the solution $\mathbf{w}_h^k$ at the time t^k, $k \in \mathbb{N}_0$, we can obtain the solution at the new time level $t^{k+1} = t^k + \tau^k$ as

$$\mathbf{w}_i^{k+1} = \mathbf{w}_i^k - \tau^k \mathbf{\Phi}_i(\mathbf{w}_h^{k+1}). \tag{2.4.53}$$

This is the backward Euler method, which has a first-order accuracy. The length of the time step τ^k is given by the modified CFL-stability condition:

$$\tau^k = \min_{1 \le i \le N_e} \left\{ \mathrm{CFL}^k \cdot \frac{|D_i|}{\max_{j \in S(i)} \left\{ \lambda_{max}(\mathbf{w}_i^k, \mathbf{n}_{ij}) \right\} \sum_{j \in S(i)} |\Gamma_{ij}| + \mu} \right\}, \tag{2.4.54}$$

where CFL^k is a positive number and

$$\lambda_{max}(\mathbf{w}, \mathbf{n}) = \max(|\mathbf{v} \cdot \mathbf{n} - c|, |\mathbf{v} \cdot \mathbf{n}|, |\mathbf{v} \cdot \mathbf{n} + c|). \tag{2.4.55}$$

We define the residuum

$$\mathrm{res}^{k+1}(\rho_h) = \frac{1}{\tau^k}\sqrt{\frac{1}{N_e}\sum_{i=1}^{N_e}\left(\rho_i^{k+1}-\rho_i^k\right)^2} \tag{2.4.56}$$

which will serve as the measure of convergence. In the beginning of the iteration process (2.4.53), we start with $\mathrm{CFL}^0 \sim 1$ and determine the value of CFL^{k+1} from the value in the previous time level t^k and the progress of the residuum $\mathrm{res}(\rho_h)$. The CFL number is increased in a favourably converging situation and reduced otherwise, e.g.

$$\mathrm{CFL}^{k+1} = \mathrm{CFL}^k \frac{\mathrm{res}^k(\rho_h)}{\mathrm{res}^{k+1}(\rho_h)}. \tag{2.4.57}$$

Of course, it is necessary to imply limits on the rate of change and set the minimum and maximum CFL values. The CFL number can grow up to the order of 10^4 and the ratio $\mathrm{CFL}^{k+1}/\mathrm{CFL}^k$ should not be larger than 1.2.

For a given time level t^k, the expression (2.4.53) represents a nonlinear system of equations which is solved by the Newton method. Hence the approximate solution at t^{k+1} can be obtained as a result of another iterative process

$$\mathbf{w}_h^{k+1,0} = \mathbf{w}_h^k, \tag{2.4.58}$$

$$\left(\boldsymbol{I} + \tau^k \frac{D\boldsymbol{\Phi}(\mathbf{w}_h^{k+1,r})}{D\mathbf{w}}\right)\left(\mathbf{w}_h^{k+1,r+1} - \mathbf{w}_h^{k+1,r}\right) = \mathbf{w}_h^k - \mathbf{w}_h^{k+1,r} - \tau^k \boldsymbol{\Phi}(\mathbf{w}_h^{k+1,r}), \tag{2.4.59}$$

for $r = 0, 1, 2, \ldots, s$, $s \in \mathbb{N}$. The symbol $D\,\boldsymbol{\Phi}(\mathbf{w})/D\mathbf{w}$ denotes the Jacobi matrix of the function $\boldsymbol{\Phi}$.

The result is the sequence $\left\{\mathbf{w}_h^{k+1,r}\right\}_{r=0}^{s}$ and we set $\mathbf{w}_h^{k+1} = \mathbf{w}_h^{k+1,s}$. For the sake of the speed of computation, only one iteration of this method is used. It has of course an impact on the time precision of the solution, but since we are interested in the steady state solution, this drawback can be neglected. Hence setting $s = 1$, we get the following linearization of (2.4.53):

$$\left(\boldsymbol{I} + \tau^k \frac{D\boldsymbol{\Phi}(\mathbf{w}_h^k)}{D\mathbf{w}}\right)\left(\mathbf{w}_h^{k+1} - \mathbf{w}_h^k\right) = -\tau^k \boldsymbol{\Phi}(\mathbf{w}_h^k). \tag{2.4.60}$$

The values of k and ω needed to evaluate the function $\boldsymbol{\Phi}(\mathbf{w}_h^k)$ are taken from the solution of the system (2.4.2) at the time t^k.

We solve the system of linear algebraic equations in the form

$$(\boldsymbol{I} + \tau \boldsymbol{A})\mathbf{x} = \mathbf{b}. \tag{2.4.61}$$

The matrix $\boldsymbol{A}$ is sparse and non-symmetric. This leads us to the use of iterative Krylov methods, namely GMRES. As the implementation of GMRES the software SPARSKIT2 [29] is used. Since it is an iterative method, it is necessary to determine a stopping criterion when a sufficient precision is reached. One possible choice of this criterion is $\|residuum\| < 10^{-2}\left\|\boldsymbol{\Phi}(\mathbf{w}_h^k)\right\|$.

It is useful to precondition the system in order to accelerate the convergence of GMRES. The preconditioning used in this case is an incomplete LU factorization, ILU.

The pseudo-transient method allows us to escape local minima or to cross regions where the residuum is rising. When the residuum $\mathrm{res}^l(\rho_h)$ at the time level t^l, $l \in \mathbb{N}$ is sufficiently low, we can speed up the convergence by switching to the steady problem

$$\mathbf{w}_h^{l,0} = \mathbf{w}_h^l, \tag{2.4.62}$$

$$\frac{D\boldsymbol{\Phi}(\mathbf{w}_h^{l,m})}{D\mathbf{w}} \left(\mathbf{w}_h^{l,m+1} - \mathbf{w}_h^{l,m}\right) = -\boldsymbol{\Phi}(\mathbf{w}_h^{l,m}), \quad m = 0, 1, \ldots. \tag{2.4.63}$$

If the sequence $\left\{\mathbf{w}_h^{l,m}\right\}_m$ converges, we will put $\mathbf{w}_h^* = \lim_{m\to\infty} \mathbf{w}_h^{l,m}$. Otherwise we return back to the pseudo-transient method and try to switch again after the residuum achieves a lower value.

2.4.5 Implementation in a computer code

The implicit formulation of the method needs a construction of the Jacobi matrices for the functions (2.4.44) and (2.4.45). In the first case, the contribution of inviscid fluxes is computed by forward differences. The viscous terms contribution is derived by an analytical way. In the case of turbulence equations, the Jacobi matrix of inviscid fluxes (2.4.46) is easily evaluated. The contribution of viscous part is derived by an analytical way. Since we are interested in the steady state solution, it is sufficient to use some approximation of the Jacobi matrix. Hence the contribution of source terms is very simplified, it is approximated by a diagonal matrix

$$\frac{\mathrm{D}\boldsymbol{S}(\mathbf{w}_i, \nabla\mathbf{w}_i)}{\mathrm{D}\mathbf{w}} = -\begin{pmatrix} 2\beta^*\omega & 0 \\ 0 & 2\beta\omega + C_D/(\rho\omega) \end{pmatrix}. \tag{2.4.64}$$

The values of gradients of the state variables on the edges of the elements D_i, $i = 1, \ldots, N_e$ are evaluated by the following technique. We construct a dual mesh $\tilde{\mathcal{D}}_h = \left\{\tilde{D}_j,\ j = 1, \ldots, \tilde{N}_e\right\}$ by connecting the centres of the elements D_i with their vertices. An example of a part of this dual mesh is shown in Figure 2.10 for an edge inside the domain and in Figure 2.11 for a part of the boundary. Then we evaluate the average value of the gradient in each dual element $\tilde{D}_j$. This value will be used as an approximation of the gradient on the edge in the FVM method (e.g. in (2.4.44) and (2.4.45)).

If the considered edge is inside the domain, we denote the vertices of the dual element $\tilde{D}_j$ according to the Figure 2.10, i.e. V^1, V^2, V^3, V^4. Let q be some function defined in the domain Ω and q^1, q^2, q^3, q^4 be the values of q in these vertices. We will denote by $q_{x_1}|_{\tilde{D}_j}$ and $q_{x_2}|_{\tilde{D}_j}$ the average value of derivatives

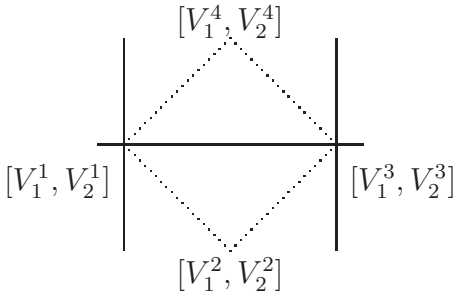

Figure 2.10: Scheme for a derivative inside the domain

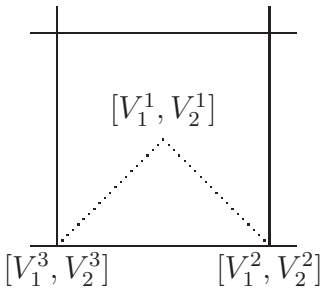

Figure 2.11: Scheme for a derivative on a wall

$\partial q/\partial x_1$ and $\partial q/\partial x_2$ on $\tilde{D}_j$. These approximations should satisfy:

$$(V_1^2 - V_1^4)q_{x_1}|_{\tilde{D}_j} + (V_2^2 - V_2^4)q_{x_2}|_{\tilde{D}_j} = q^2 - q^4, \tag{2.4.65}$$

$$(V_1^1 - V_1^3)q_{x_1}|_{\tilde{D}_j} + (V_2^1 - V_2^3)q_{x_2}|_{\tilde{D}_j} = q^1 - q^3. \tag{2.4.66}$$

The solution of this system for the unknowns $q_{x_1}|_{\tilde{D}_j}$ and $q_{x_2}|_{\tilde{D}_j}$ is given by:

$$\begin{aligned} q_{x_1}|_{\tilde{D}_j} &= \frac{(q^3 - q^1)(V_2^4 - V_2^2) - (q^4 - q^2)(V_2^3 - V_2^1)}{|(V_1^3 - V_1^1)(V_2^4 - V_2^2) - (V_1^4 - V_1^2)(V_2^3 - V_2^1)|}, \\ q_{x_2}|_{\tilde{D}_j} &= -\frac{(q^3 - q^1)(V_1^4 - V_1^2) - (q^4 - q^2)(V_1^3 - V_1^1)}{|(V_1^3 - V_1^1)(V_2^4 - V_2^2) - (V_1^4 - V_1^2)(V_2^3 - V_2^1)|}. \end{aligned} \tag{2.4.67}$$

If the considered edge is on a boundary, we get by a similar approach the expressions for derivatives:

$$\begin{aligned} q_{x_1}|_{\tilde{D}_j} &\approx \frac{-(V_2^3 - V_2^2)\left(q^1 - q^{wall}\right)}{|(V_1^2 - V_1^1)(V_2^3 - V_2^1) - (V_1^3 - V_1^1)(V_2^2 - V_2^1)|}, \\ q_{x_2}|_{\tilde{D}_j} &\approx \frac{(V_1^3 - V_1^2)\left(q^1 - q^{wall}\right)}{|(V_1^2 - V_1^1)(V_2^3 - V_2^1) - (V_1^3 - V_1^1)(V_2^2 - V_2^1)|}, \end{aligned} \tag{2.4.68}$$

where q^{wall} is a prescribed value.

Thus, the gradients of the values of state variables ρ, v_1, v_2, e, k and ω on an edge of the element D_i are obtained by substitution for q in the above expressions. The values q^2 and q^4 are values of state variables in these cells. The values q^1 and q^3 are obtained as an arithmetic mean of values from the four neighbouring cells.

3. Operator equation

Our goal is to find a geometric curve ψ which represents the shape of an airfoil. This airfoil should correspond to the given velocity or pressure distribution $f = (f_u, f_l)$, where f_u, f_l are distributions along the upper and lower side of the airfoil, parametrized along the chord line ($x \in [0, C]$). In the Chapter 2 two different direct operators $f = \mathbf{P}(\psi)$ were derived (potential model and Navier-Stokes equations), which map an airfoil ψ to a velocity/pressure distribution f on its surface. As it will be shown in the next chapter, it is possible to consider a simplified potential flow model and use the presented algorithm to construct an operator $\mathbf{L}$, which maps a velocity/pressure distribution f to some airfoil ψ, $\psi = \mathbf{L}(f)$. The operator $\mathbf{L}$ is explicitly given and is also continuous, as can be shown. We compose these two operators $\mathbf{P}$ and $\mathbf{L}$ together and solve the operator equation

$$\mathbf{P}(\mathbf{L}u) = f \tag{3.0.1}$$

for an unknown velocity/pressure distribution u. If the operator $\mathbf{L}$ was a precise inversion to $\mathbf{P}$, it would be true that $u = f$. But $\mathbf{L}$ is only an inexact inversion, so the solution u is different from f. The distribution u will be called a fictitious distribution. From the equation (3.0.1) it is clear, that if we apply the operator $\mathbf{L}$ on u, we obtain an airfoil, whose velocity/pressure distribution on its surface corresponds to the given f. The solution is based on the fixed point theorem.

Definition. *Let $F : X \to X$ be some mapping in a space X. Then we say that u is a fixed point of the mapping F, if the following holds true:*

$$F(u) = u.$$

Definition. *The mapping $F : X \to X$ is a contractive mapping with respect to the norm $\|.\|$ in a space X, if there exists some constant $q \in [0, 1)$ such that*

$$\|F(x) - F(y)\| \leq q \|x - y\| \quad \forall x, y \in X.$$

Theorem 2. *Let X be a Banach space, $F : X \to X$ be a contractive mapping. Than there exists a unique fixed point $u \in X$ of the mapping F. This fixed point can be constructed with the following algorithm:*

$$u = \lim_{k \to \infty} u_k,$$

where u_0 is an arbitrary starting point and

$$u_{k+1} = F(u_k) \quad \text{for } k \geq 0.$$

Our equation $\mathbf{P}(\mathbf{L}u) = f$ can be rewritten in the form

$$u = u + \eta \left(f - \mathbf{P}\mathbf{L}u\right), \quad \eta \in (0, 1]. \tag{3.0.2}$$

If we choose the coefficient η such that the sequence

$$\{u_k\}_{k=0}^{\infty}\,,\ u_{k+1} = u_k + \eta\,(f - \mathbf{PL}u_k)\,,\ u_0 = f \tag{3.0.3}$$

converges, the sought fictitious velocity/pressure distribution u will be the limit of this sequence. The resulting airfoil $\psi = \mathbf{L}(u)$ will satisfy the equation

$$\mathbf{P}(\psi) = f. \tag{3.0.4}$$

It needs to be said that due to the complexity of the mentioned operators it is difficult to determine the right value of the coefficient η analytically. From this reason, the value of the parameter $\eta \in (0, 1]$ is chosen on the basis of the experimental results.

If we choose a small value of η, the probability of convergence is higher. On the other hand, the convergence speed can be slower. Practical results suggest that the value $\eta = 0.6$ is sufficient for the most cases. Some of the examples presented in this work even use the value $\eta = 0.9$.

According to the formulation of the inversion, it is necessary to deal with velocity/pressure distributions which are represented by continuous functions. This is achieved by assuming a subsonic flow. In order to have an airfoil with an acceptable geometry, the distributions u_k should be smooth. From the numerical point of view, this restriction is not so strong. However, the new fictitious distribution u_{k+1} is created from the pointwise difference between the target distribution f and the computed distribution $\mathbf{PL}u_k$. So it may happen after a few iterations that some spurious oscillations occur. From this reason it is good to use some kind of smoothing. For example a method based on moving averages which shifts the value at some point towards the average of its neighboring points.

4. Approximate inverse operator

As mentioned in the previous chapter, the method of solving the inverse problem of the flow around an airfoil described in this thesis is based on finding an approximate inverse operator, denoted by $\mathbf{L}$. This operator assigns an airfoil shape to a given velocity or pressure distribution. The operator is derived on the basis of the thin airfoil theory, proposed by Max Munk and Hermann Glauert [30]. The theory given bellow serves only as a basis for the development of the operator $\mathbf{L}$. Although it is capable to solve the flow to some extent, it uses a lot of simplifications and therefore it is worse comparing to other models described in this work, namely the integral formulation in Section 2.1 and the Navier-Stokes equations in Section 2.2.

4.1 Thin airfoil theory

The thin airfoil theory describes an idealized two-dimensional flow, which is assumed to be stationary, inviscid, incompressible and potential. Therefore, a potential Φ can be constructed to the velocity $\mathbf{V} = (V_x, V_y)$ and this potential satisfies the Laplace equation

$$\Delta\Phi = 0 \tag{4.1.1}$$

in the domain Ω which is the exterior of an airfoil. We suppose, that the airfoil is given by a pair of functions $\psi_u^y(x)$ and $\psi_l^y(x)$ for $x \in [0, C]$. These functions represent the y-coordinates of the upper and lower airfoil parts. Here C is again the length of the chord line. The description of the geometry is shown in Figure 4.1. We will assume that the airfoil has a small thickness and that the camber line has a small curvature.

Since the Laplace operator is linear, we can write the potential Φ as the sum of the free stream potential and the perturbation potential ϕ arising due to insertion of the airfoil into the free stream. The free stream velocity will be denoted again as $\mathbf{v}_\infty = v_\infty(\cos\alpha_\infty, \sin\alpha_\infty)$. So we can write

$$\Phi(x, y) = v_\infty x\cos(\alpha_\infty) + v_\infty y\sin(\alpha_\infty) + \phi(x, y), \quad (x, y) \in \Omega. \tag{4.1.2}$$

Due to the definition of the potential, velocity components are the partial derivatives of the potential,

$$\frac{\partial\Phi(x,y)}{\partial x} = V_x(x,y), \quad \frac{\partial\Phi(x,y)}{\partial y} = V_y(x,y), \text{ similarly,} \tag{4.1.3}$$

$$\frac{\partial\phi(x,y)}{\partial x} = v_x(x,y), \quad \frac{\partial\phi(x,y)}{\partial y} = v_y(x,y). \tag{4.1.4}$$

As well as for the total potential Φ, the Laplace equation is true for the induced potential,

$$\Delta\phi = 0 \text{ in } \Omega. \tag{4.1.5}$$

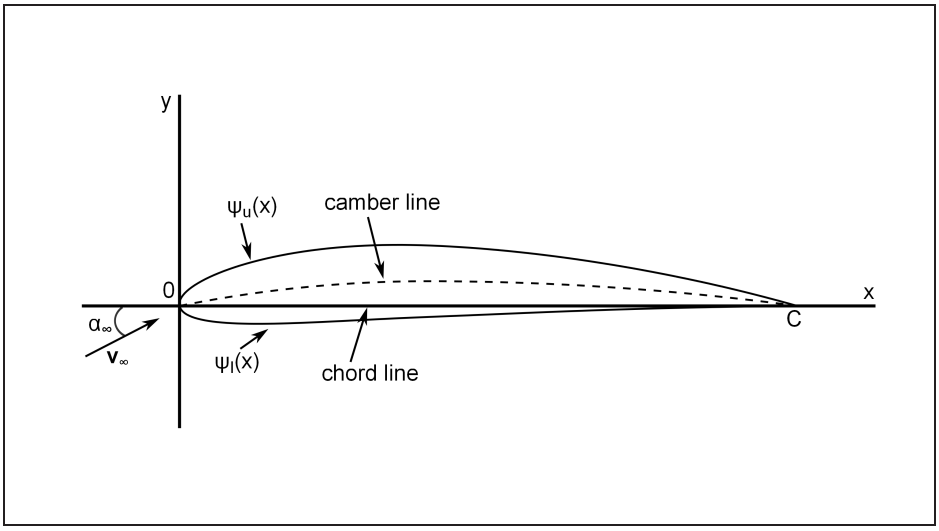

Figure 4.1: Description of an airfoil.

Boundary conditions are added to this equation,

$$\begin{aligned}
\frac{\partial \phi}{\partial x} &\to 0, \quad \text{at } \infty, \\
\frac{\partial \phi}{\partial y} &\to 0, \quad \text{at } \infty, \\
\left.\frac{\partial \phi(x,y)}{\partial y}\right|_{y=\psi_u^y(x)} &= v_\infty \left(\psi_u^{y\prime}(x) - \tan(\alpha_\infty)\right), \quad \text{for } x \in [0, C], \\
\left.\frac{\partial \phi(x,y)}{\partial y}\right|_{y=\psi_l^y(x)} &= -v_\infty \left(\psi_l^{y\prime}(x) - \tan(\alpha_\infty)\right), \quad \text{for } x \in [0, C].
\end{aligned} \tag{4.1.6}$$

The last two conditions on the airfoil surface ensure that the flow is tangential to the surface and thus the airfoil forms an impermeable boundary. In the context of the thin airfoil, these conditions can be linearized and be considered for $y \to 0^{\pm}$ instead of on the actual surface. Thus

$$v_y(x, 0^+) = v_\infty \left(\psi_u^{y\prime}(x) - \tan(\alpha_\infty)\right), \quad \text{for } x \in [0, C], \tag{4.1.7}$$

$$v_y(x, 0^-) = -v_\infty \left(\psi_l^{y\prime}(x) - \tan(\alpha_\infty)\right), \quad \text{for } x \in [0, C]. \tag{4.1.8}$$

Further, we express a function describing the mean camber line $s(x)$ and a thickness function $t(x)$ for $x \in [0, C]$. We measure the airfoil thickness perpendicular to the camber line. However, we suppose that this line has small curvature and thus we can express the thickness as perpendicular to the chord line with small error. Hence, the functions $s(x)$ and $t(x)$ are given by the relations

$$s(x) = \left(\psi_u^y(x) + \psi_l^y(x)\right)/2 \tag{4.1.9}$$

and

$$t(x) = \left(\psi_u^y(x) - \psi_l^y(x)\right)/2. \tag{4.1.10}$$

This makes it possible to define the linearized problem for the induced potential

$$\begin{aligned} &\Delta\phi = 0 \quad \text{in } \mathbb{R}^2 - \{(x,0),\ x \in [0,C]\}\,, \\ &\frac{\partial\phi}{\partial x} \to 0, \qquad \text{at } \infty, \\ &\frac{\partial\phi}{\partial y} \to 0, \qquad \text{at } \infty, \end{aligned} \tag{4.1.11}$$

$$\left.\frac{\partial\phi(x,y)}{\partial y}\right|_{y=0^+} = v_\infty s'(x) + v_\infty t'(x) - v_\infty \tan\alpha_\infty, \quad x \in [0,C]\,, \tag{4.1.12}$$

$$\left.\frac{\partial\phi(x,y)}{\partial y}\right|_{y=0^-} = v_\infty s'(x) - v_\infty t'(x) - v_\infty \tan\alpha_\infty, \quad x \in [0,C]\,. \tag{4.1.13}$$

We may notice that the conditions (4.1.12)–(4.1.13) contain terms representing the influence of the camber line, thickness and angle of attack α_∞. Therefore, we can use the principle of superposition and decompose the potential ϕ into independent potentials ϕ_s, ϕ_{α_∞} and ϕ_t corresponding to the camber, angle of attack and thickness:

$$\phi = \phi_s + \phi_{\alpha_\infty} + \phi_t. \tag{4.1.14}$$

These potentials are solved as three independent problems, described further.

The influence of the mean camber line $s(x)$ is determined by assuming a flow, which is parallel to the x-axis, around an airfoil with an infinitesimal thickness. The effect of the angle of attack is studied by assuming a flow, which forms the angle α_∞ with the x-axis, around the chord line. Finally, to determine the effect of the airfoil thickness, we consider a flow parallel to the axis x, which goes around a symmetrical airfoil with the corresponding thickness $t(x)$. The scheme of these three problems is in Figure 4.2.

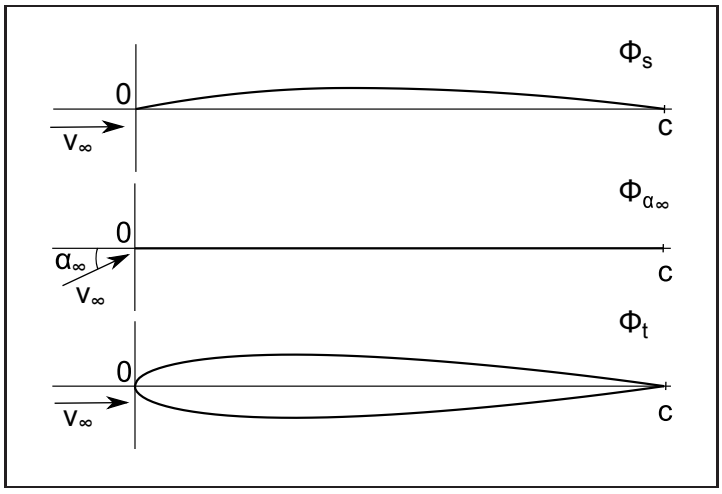

Figure 4.2: New problems solved in the thin airfoil theory: the flow around the camber line, flow around the chord line with α_∞ and flow around the thick symmetric airfoil.

4.1.1 Potential induced by the camber

To determine the velocity potential induced by the camber we solve the problem (4.1.11) for the unknown function ϕ_s with boundary conditions

$$\left.\frac{\partial \phi_s(x,y)}{\partial y}\right|_{y=0^+} = v_\infty s'(x), \tag{4.1.15}$$

$$\left.\frac{\partial \phi_s(x,y)}{\partial y}\right|_{y=0^-} = v_\infty s'(x), \quad x \in [0, C]\,. \tag{4.1.16}$$

That means we consider a flow around the mean camber line representing the airfoil with a zero angle of attack α_∞. The chord line of an infinitesimally thin airfoil, as shown in the upper part of Figure 4.2, lies on the axis x. The velocity field corresponding to the mean camber line will be imitated by a velocity field caused by some distribution of vortices on the chord.

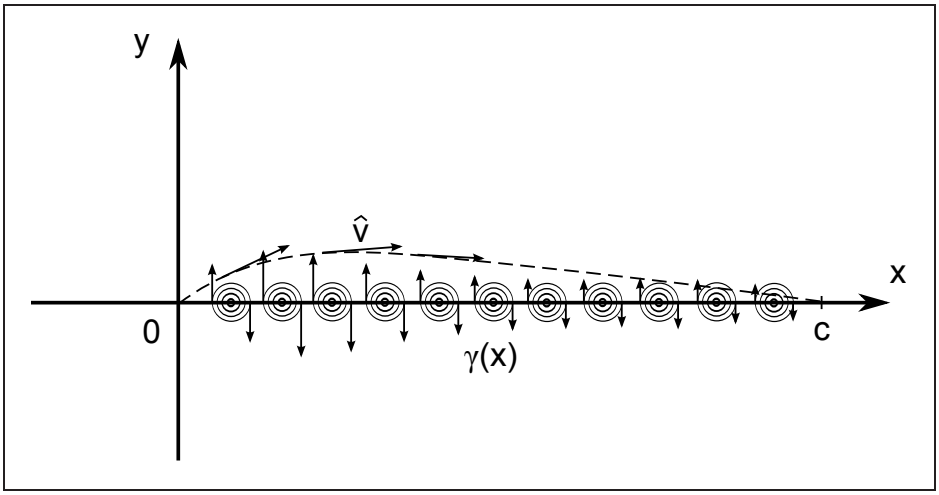

Figure 4.3: Velocity induced by a system of vortices.

The solution of our problem is solved by the use of the Biot-Savart law. In two dimensions, the velocity potential ϕ_s^e excited by an elementary vortex of an intensity Γ^e, located at some point $\xi \in [0, C]$ on the chord, can be expressed in the form

$$\phi_s^e(x,y) = -\frac{\Gamma^e}{2\pi} \arctan\left(\frac{y}{x-\xi}\right), \quad x, y \in \mathbb{R}. \tag{4.1.17}$$

If we consider a continuous distribution of vortices along the chord line, we obtain the following expression for the velocity potential:

$$\phi_s(x,y) = -\frac{1}{2\pi} \int_0^C \gamma(\xi) \arctan\left(\frac{y}{x-\xi}\right) d\xi, \quad x, y \in \mathbb{R}, \tag{4.1.18}$$

where $\gamma(\xi)$ is the specific circulation of the vortex distribution per unit length. The function $\gamma(\xi)$, $\xi \in [0, C]$ is unknown at this moment. It needs to be determined from the conditions (4.1.15)–(4.1.16).

Since we are interested in the velocity more than in the potential, we differentiate the potential ϕ_s with respect to x and y. We obtain expressions for the

induced velocity components

$$\hat{v}_x(x,y) = \frac{1}{2\pi}\int_0^C \gamma(\xi)\frac{y}{(x-\xi)^2+y^2}d\xi, \tag{4.1.19}$$

$$\hat{v}_y(x,y) = -\frac{1}{2\pi}\int_0^C \gamma(\xi)\frac{x-\xi}{(x-\xi)^2+y^2}d\xi. \tag{4.1.20}$$

The integrated functions have singularities on the interval $[0, C]$. From this reason, the integration process is defined in the sense of the Cauchy principal value.

Definition. *Let $f(x)$ be a function defined on the interval $[a, b]$. Let $c \in [a, b]$ be a point where the function f has a singularity. Then we define the Cauchy principal value of the integral as*

$$(PV)\ \int_a^b f(x)dx = \lim_{\epsilon\to 0+}\left(\int_a^{c-\epsilon} f(x)dx + \int_{c+\epsilon}^b f(x)dx\right). \tag{4.1.21}$$

All the integrals are treated in this way. The commonly used sign (PV) will be omitted for the simplicity of notation.

From the boundary conditions (4.1.15)–(4.1.16) we get the following conditions for the y-component of the perturbation velocity:

$$\lim_{y\to 0^{\pm}} \hat{v}_y(x,y) = v_\infty s'(x), \quad x \in [0, C] \tag{4.1.22}$$

This corresponds to the requirement that the velocity vector is tangent to the airfoil surface, i.e. the mean camber line $s(x)$. Since it is assumed that the mean camber line has a small curvature and therefore its points lie near the axis x, the error arising from the shift to the chord line (i.e. $y \to 0^{\pm}$) is negligible.

Taking the limit in the relation (4.1.22) we get

$$s'(x) = \frac{1}{2\pi v_\infty}\int_0^C \frac{\gamma(\xi)}{\xi - x}d\xi, \quad x \in [0, C]\,. \tag{4.1.23}$$

This important relation will also be further used to derive the equation describing the mean camber line in the searched inverse operator.

We can also derive a relation between the specific circulation γ and the perturbation velocity. We start from the expression (4.1.19) for the perturbation velocity $\hat{v}_x$ and evaluate it for $y \to 0^{\pm}$. It can be seen that the only significant contribution to the integral comes from a very close neighbourhood of x. For this reason, it is possible to approximate the function γ by its value at x and move it in front of the integral. For the remaining integral we get

$$\lim_{y\to 0^{\pm}} \int_0^C \frac{y}{(x-\xi)^2+y^2}d\xi = \pm\pi. \tag{4.1.24}$$

The result is

$$\lim_{y\to 0^{\pm}} \hat{v}_x(x,y) = \pm\frac{\gamma(x)}{2}, \quad x \in [0, C]\,. \tag{4.1.25}$$

Hence, we get the relation

$$\gamma(x) = \hat{v}_x(x, 0^+) - \hat{v}_x(x, 0^-). \tag{4.1.26}$$

Now we have enough information to derive one part of the inverse operator **L**, which describes the construction of the mean camber line. Nevertheless, we will finish the solution of the problem stated at the beginning of this section.

To evaluate the velocity increments (4.1.19) and (4.1.20) (or the potential (4.1.18)) caused by the camber we have only to determine the specific circulation $\gamma(x)$. This means to solve the equation

$$\int_0^C \frac{\gamma(\xi)}{\xi - x} d\xi = 2\pi v_\infty s'(x), \quad x \in [0, C] \tag{4.1.27}$$

for the unknown γ. Like in the Chapter 2.1 about the potential flow, it is necessary to ensure the uniqueness of the solution by adding a condition for the circulation. The Kutta condition ensuring the correct position of the stagnation point at the trailing edge requires $\gamma(C) = 0$.

The equation (4.1.27) is solved using the coordinate transformation

$$x = \frac{C}{2}(1 - \cos(\theta)), \quad \xi = \frac{C}{2}(1 - \cos(\zeta)), \tag{4.1.28}$$

$x, \xi \in [0, C]$, $\theta, \zeta \in [0, \pi]$. Using this transformation, we convert the equation to the form

$$\frac{1}{2\pi} \int_0^\pi \frac{\gamma(\zeta)\sin(\zeta)}{\cos(\zeta) - \cos(\theta)} d\zeta = -v_\infty \frac{ds(\theta)}{dx}, \quad \theta \in [0, \pi]\,. \tag{4.1.29}$$

We use the same notation for the original and transformed functions γ and s here. In the next step, the distribution of vorticity is expressed through the expansion into a Fourier sine series with an additional term ensuring a non-zero value on the leading edge [22]

$$\gamma(\zeta) = 2\left(A_0 \cot\frac{\zeta}{2} + \sum_{n=1}^{\infty} A_n \sin n\zeta \right). \tag{4.1.30}$$

The trailing edge is due to the coordinate transformation located at $\zeta = \pi$ and it is obvious that $\gamma(\pi) = 0$. Hence, the Kutta condition is automatically satisfied in this expansion.

This expansion is substituted into the equation (4.1.29), where each integral, after some necessary adjustments, is evaluated using the Glauert integral [31]

$$\int_0^\pi \frac{\cos n\zeta}{\cos\zeta - \cos\theta} d\zeta = \pi \frac{\sin n\theta}{\sin\theta}. \tag{4.1.31}$$

The result is

$$A_0 - \sum_{n=1}^{\infty} A_n \cos n\theta = -v_\infty \frac{ds(\theta)}{dx}, \tag{4.1.32}$$

from which the values of the series coefficients can be determined. To do this, the orthogonality of the basis functions $\cos n\theta$ will be used. Then we get

$$A_0 = -\frac{v_\infty}{\pi}\int_0^\pi \frac{ds(\theta)}{dx}d\theta, \tag{4.1.33}$$

$$A_n = \frac{2v_\infty}{\pi}\int_0^\pi \frac{ds(\theta)}{dx}\cos n\theta \; d\theta. \tag{4.1.34}$$

4.1.2 Potential induced by the angle of attack

The effect of the angle of attack on the velocity potential is determined by assuming a flow with the given angle α_∞ around an airfoil represented by its chord line. The layout of the problem is in the middle part of Figure 4.2.

The problem we are solving is the problem (4.1.11) for the potential ϕ_{α_∞} with boundary conditions

$$\left.\frac{\partial\phi_{\alpha_\infty}(x,y)}{\partial y}\right|_{y=0^+} = -v_\infty\tan(\alpha_\infty), \tag{4.1.35}$$

$$\left.\frac{\partial\phi_{\alpha_\infty}(x,y)}{\partial y}\right|_{y=0^-} = -v_\infty\tan(\alpha_\infty), \quad x\in[0,C]\,. \tag{4.1.36}$$

The solution of this problem can be transformed to the problem dealt with in the previous section. For this moment we denote the straight line representing the airfoil by $s(x)$. The coordinate system is rotated so that the flow is parallel to the axis x, and thus the line $s(x)$ is rotated by an angle $-\alpha_\infty$. So we have the same problem as was solved above, now with

$$s'(x) = -\tan\alpha_\infty. \tag{4.1.37}$$

By substituting into relations (4.1.33)–(4.1.34), the expression for the circulation corresponding to the potential ϕ_{α_∞} is obtained,

$$\gamma_{\alpha_\infty}(\theta) = 2v_\infty\tan\alpha_\infty\cot\frac{\theta}{2}. \tag{4.1.38}$$

4.1.3 Potential induced by the thickness

To determine the velocity potential ϕ_t, which is caused by the influence of the airfoil thickness, a symmetric airfoil is considered. Its thickness is given by the thickness function $t(x)$ defined by (4.1.10). The flow is, as previously mentioned, considered with a zero angle of attack, i.e. parallel to the axis x.

The problem can be formulated as follows: Find a function ϕ_t satisfying (4.1.11) with conditions

$$\left.\frac{\partial\phi_t(x,y)}{\partial y}\right|_{y=0^+} = v_\infty t'(x), \tag{4.1.39}$$

$$\left.\frac{\partial\phi_t(x,y)}{\partial y}\right|_{y=0^-} = -v_\infty t'(x), \quad x\in[0,C]\,. \tag{4.1.40}$$

As in the previous cases where the velocity field was imitated by a continuous distribution of vortices along the chord line, this time the approach is similar. Instead of the distribution of vortices, however, the distribution of sources is considered.

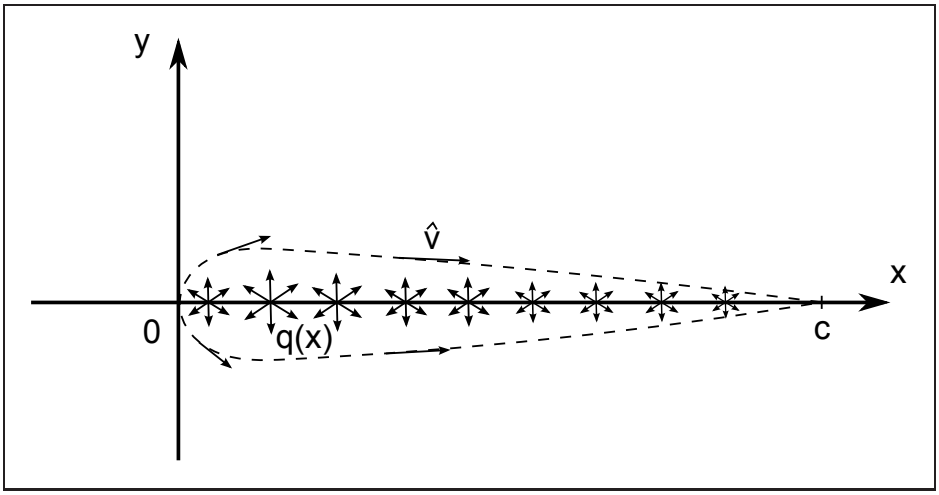

Figure 4.4: Velocity induced by a system of sources.

It is known that an elementary point source of an intensity Q^e located at a point $[\xi, 0]$, $\xi \in \mathbb{R}$, induces by its presence a velocity potential

$$\phi_t^e(x,y) = \frac{Q^e}{2\pi} \ln \sqrt{(x-\xi)^2 + y^2}, \quad x, y, \in \mathbb{R}. \tag{4.1.41}$$

Therefore, if considering the continuous distribution of sources along the chord of the length C, the resulting potential is equal to

$$\phi_t(x,y) = \frac{1}{2\pi} \int_0^C q(\xi) \ln \sqrt{(x-\xi)^2 + y^2} d\xi, \quad x, y \in \mathbb{R}, \tag{4.1.42}$$

where $q(\xi)$ is a specific source intensity per unit length.

Differentiating ϕ_t by individual variables, we obtain velocity components along the axis x and y, denoted again by $\hat{v}_x$, $\hat{v}_y$:

$$\hat{v}_x(x,y) = \frac{1}{2\pi} \int_0^C q(\xi) \frac{x-\xi}{(x-\xi)^2 + y^2} d\xi, \tag{4.1.43}$$

$$\hat{v}_y(x,y) = \frac{1}{2\pi} \int_0^C q(\xi) \frac{y}{(x-\xi)^2 + y^2} d\xi. \tag{4.1.44}$$

Based on the requirements (4.1.39)–(4.1.40), the surface condition

$$\hat{v}_y(x, 0^{\pm}) = \pm v_\infty t'(x), \quad x \in [0, C] \tag{4.1.45}$$

is prescribed.

Now, we take the limit in the equation (4.1.44) for $y \to 0^{\pm}$. We use the same approximation as was used in the derivation of (4.1.25). That means we

approximate the function q by its value at x and move it in front of the integral. This leads to the relation between the induced velocity and source intensity:

$$\hat{v}_y(x, 0^{\pm}) = \pm\frac{q(x)}{2}, \quad x \in [0, C]\,. \tag{4.1.46}$$

Substituting the condition (4.1.45) into this relation, we obtain the relation between the derivative of the thickness function and the source intensity. It is also clear that the total source intensity is zero because

$$\int_0^C q(\xi)d\xi = \int_0^C 2v_\infty t'(\xi)d\xi = 0 \tag{4.1.47}$$

by the fact that the airfoil is closed ($t(0) = t(C) = 0$).

The induced potential can be written in the form

$$\phi_t(x, y) = \frac{v_\infty}{\pi}\int_0^C t'(\xi)\ln\sqrt{(x-\xi)^2 + y^2}d\xi, \quad x, y \in \mathbb{R}. \tag{4.1.48}$$

4.2 Derivation of the inverse operator

In the previous section, the thin airfoil theory was described. Its primary use is to calculate the velocity of the flow in the vicinity of the given airfoil or to determine its relevant characteristics. In the case of thinking about the inverse problem, however, the shape of the airfoil is of course not known. On the contrary, the velocity distribution or pressure distribution (in case of viscous flow) along the surface is known. The corresponding airfoil shape is the searched unknown.

Knowing the velocity distribution on the surface of the airfoil, we will use the same procedure as in the above-mentioned theory. The airfoil can thus be described using the camber line $s(x)$ and the thickness function $t(x)$. The derivation of relations defining these functions will use the already obtained results. In the case when a pressure distribution instead of a velocity distribution is given, we need to evaluate an equivalent velocity. This transformation will be described at the end of this chapter.

The inverse operator $\mathbf{L}$ is applied on the fictitious velocity distribution u. This distribution is given by a pair of functions u_u and u_l, which represent the velocity magnitude on the upper and lower part of the airfoil along the chord line. By an airfoil we understand a closed curve ψ, which has its beginning and end located at the trailing edge and which is oriented counterclockwise. To the prescribed velocity distribution we assign a sign plus or minus, according to the direction of flow. If the velocity is in the opposite direction of the curve ψ, then we consider the minus sign and otherwise the plus sign. Hence, on the upper surface, the velocity is mostly negative and on the lower surface mostly positive. The sign is changing at the stagnation point near the leading edge.

4.2.1 Mean camber line

To derive the relation determining the mean camber line $s(x)$ we start from the equations (4.1.23) and (4.1.37). Their sum leads to an expression for the

derivative of the camber line, depending on the circulation,

$$s'(x) = \tan\alpha_\infty + \frac{1}{2\pi v_\infty}\int_0^C \frac{\gamma(\xi)}{\xi - x}\,d\xi, \quad x \in [0, C]\,. \tag{4.2.1}$$

This equation for the unknown function $s(x)$ will be completed by the boundary conditions $s(0) = s(C) = 0$. Since this is a first order differential equation, the requirement of two conditions is generally impossible. In order to achieve that, it is necessary to consider the angle of the free stream α_∞ as an unknown parameter.

As already mentioned in the previous chapter, the circulation can be expressed as a difference of velocities on both sides of the surface. These velocities are the given velocity distribution u_u and u_l. If we consider the sign of the velocity, the specific circulation can be expressed as

$$\gamma(x) = -(u_u(x) + u_l(x)). \tag{4.2.2}$$

To meet the Kutta condition, it is necessary $u_u(C) = -u_l(C)$, i.e. $\gamma(C) = 0$.

For simplicity, we will consider the unit velocity at infinity, $v_\infty = 1$, in the following text. This can be done without loss of generality by normalizing the velocity distribution. We denote here $a = \tan\alpha_\infty$ for this moment. The solution of (4.2.1) is written in the form

$$s(x) = ax - \frac{1}{2\pi}\int_0^x \left(\int_0^C \frac{\gamma(\xi)}{t - \xi}d\xi\right) dt, \tag{4.2.3}$$

where we used the requirement $s(0) = 0$.

Further, we change the order of integrations and evaluate the newly formed integral

$$\int_0^x \frac{1}{t - \xi}dt = \ln\left|\frac{x - \xi}{\xi}\right|. \tag{4.2.4}$$

It remains to determine the parameter a so as to fulfil the second condition $s(C) = 0$. This is determined by substituting into the equation (4.2.3), which gives

$$a = \frac{1}{2\pi C}\int_0^C \gamma(\xi)\ln\left|\frac{C - \xi}{\xi}\right| d\xi. \tag{4.2.5}$$

Thus we finally derive the equation for the mean camber line and its derivative

$$s'(x) = \frac{1}{2\pi C}\int_0^C \gamma(\xi)\ln\left|\frac{C - \xi}{\xi}\right| d\xi - \frac{1}{2\pi}\int_0^C \frac{\gamma(\xi)}{x - \xi}d\xi, \tag{4.2.6}$$

$$s(x) = \frac{x}{2\pi C}\int_0^C \gamma(\xi)\ln\left|\frac{C - \xi}{\xi}\right| d\xi - \frac{1}{2\pi}\int_0^C \gamma(\xi)\ln\left|\frac{x - \xi}{\xi}\right| d\xi. \tag{4.2.7}$$

4.2.2 Thickness function

To derive the thickness function, we come out again from relations previously derived in Chapter 4.1. Specifically, differentiating the relation (4.1.48) with respect to x gives us the expression of the induced velocity:

$$\hat{v}_x(x, 0) = \frac{v_\infty}{\pi}\int_0^C t'(\xi)\frac{1}{x - \xi}d\xi, \quad x \in [0, C]\,. \tag{4.2.8}$$

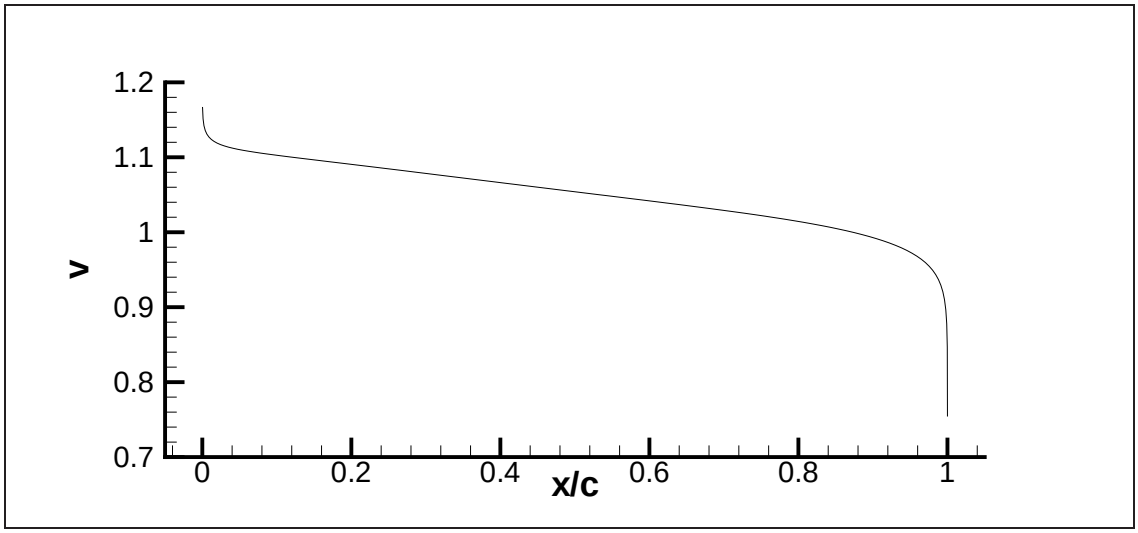

Figure 4.5: Velocity distribution $u_u(x) = -u_l(x)$ evaluated from NACA0012 airfoil ($v_\infty = 1$).

To derive this expression, we considered a symmetric airfoil at a zero angle of attack. Therefore, we can expect that the velocity along both sides of the airfoil will be of the same size. However, in our case we have a general velocity distribution that is either desired by engineers or obtained by the direct operator $\mathbf{P}$. Thus, we define a new function v_t obtained by averaging the velocities on both sides of the airfoil and subtracting the free stream velocity. While respecting the signs, as described above, this function can be expressed in the form

$$v_t(x) = \frac{-u_u(x) + u_l(x)}{2} - v_\infty. \tag{4.2.9}$$

In the following, for simplicity, we will again consider a unit velocity at infinity, $v_\infty = 1$.

Substituting (4.2.9) into the relation (4.2.8) we obtain the integral equation

$$v_t(x) = \frac{1}{\pi} \int_0^C t'(\xi) \frac{1}{x - \xi} d\xi, \quad x \in [0, C] \tag{4.2.10}$$

for an unknown function $t'(x)$.

An illustrative example how function $u_u(x) = -u_l(x)$ can look can be found in Figure 4.5. This function is determined on the basis of this equation for an existing airfoil. It is a symmetric airfoil NACA0012, whose analytical expression is given in Appendix 6. The figure shows that there is a singularity on the leading edge, which causes that the velocity goes to infinity. This is caused besides other by the fact that the derivative of the thickness at the point 0 is equal to infinity. In practice, using a discrete distribution of points and numerical integration, this problem is avoided.

Our goal is to express the unknown function $t'(x)$ using the given function $v_t(x)$. This can be achieved if we realize that the equation (4.2.10) can be considered as a special case of a more general integral equation in the complex domain. The solution will use the following statement [20]:

Theorem 3. *Let L be a smooth simple curve in the complex domain and $\varphi, f \in H(\langle L\rangle)$ (see Definition in Sec. 2.1.1) are complex functions defined on this curve. Let a and b be the endpoints of the curve L and $\alpha, \beta \in \mathbb{C}$ satisfy $\alpha^2 - \beta^2 \neq 0$. Then the singular integral equation*

$$\alpha\varphi(\vartheta) + \frac{\beta}{\pi \mathrm{i}} \int_L \frac{\varphi(z)}{z-\vartheta} dz = f(\vartheta), \quad \vartheta \in \langle L\rangle$$

for the unknown function φ has a solution

$$\begin{aligned}\varphi(\vartheta) =& \frac{\alpha}{\alpha^2-\beta^2} f(\vartheta) - \\ & \frac{\beta}{\pi \mathrm{i}(\alpha^2-\beta^2)(\vartheta-a)^{1-m}(\vartheta-b)^m} \int_L \frac{(z-a)^{1-m}(z-b)^m}{z-\vartheta} f(z)dz + \\ & \frac{A}{(\vartheta-a)^{1-m}(\vartheta-b)^m},\end{aligned}$$

where $\vartheta \in \langle L\rangle$, A is an arbitrary constant and the coefficient m is given by

$$m = \frac{1}{2\pi \mathrm{i}} \log \frac{\alpha+\beta}{\alpha-\beta}.$$

In our case, $\alpha = 0$, $\beta = -\mathrm{i}$ and the curve L is the chord line. Thus, we obtain the solution

$$t'(x) = -\frac{1}{\pi} \int_0^C \frac{v_t(\xi)}{x-\xi} \sqrt{\frac{\xi(C-\xi)}{x(C-x)}}\, d\xi + \frac{A}{\sqrt{x(C-x)}}. \tag{4.2.11}$$

In this expression an arbitrary constant A occurs, which must be further defined.

In the next step, we will integrate with respect to the variable x. After changing the order of integration we obtain

$$\begin{aligned}t(x) =& -\frac{1}{\pi} \int_0^C \left(v_t(\xi)\sqrt{\xi(C-\xi)} \int_0^x \frac{dy}{\sqrt{y(C-y)}(y-\xi)} \right) d\xi + \\ & + A \arctan\left(\frac{x-C/2}{\sqrt{x(C-x)}} \right) - B,\end{aligned} \tag{4.2.12}$$

where B is a new integration constant.

The second integral in the expression can be calculated as

$$\int_0^x \frac{dy}{\sqrt{y(C-y)}(y-\xi)} = -\frac{1}{\sqrt{\xi(C-\xi)}} \ln \left| \frac{1+\sqrt{\frac{\xi}{C-\xi}}\sqrt{\frac{C-x}{x}}}{1-\sqrt{\frac{\xi}{C-\xi}}\sqrt{\frac{C-x}{x}}} \right|. \tag{4.2.13}$$

Substituting into (4.2.12) we obtain the equation determining the thickness function of the airfoil,

$$t(x) = \frac{1}{\pi} \int_0^C v_t(\xi) \ln \left| \frac{1+\sqrt{\frac{\xi}{C-\xi}}\sqrt{\frac{C-x}{x}}}{1-\sqrt{\frac{\xi}{C-\xi}}\sqrt{\frac{C-x}{x}}} \right| d\xi + A \arctan\left(\frac{x-C/2}{\sqrt{x(C-x)}} \right) + B. \tag{4.2.14}$$

All these integrals are understood as improper integrals in the sense of the Cauchy principal value, defined in Section 4.1.1.

Finally, it remains to determine the values of the parameters A and B. To do this, we use the requirements on the thickness, i.e. that at both ends of the chord the thickness is zero. If we put $x = 0$ or $x = C$, the above integral is always equal to zero. The second term containing A is a monotone function that takes the value $-A\pi/2$ at the origin and the value $A\pi/2$ at the trailing edge for $x = c$. Therefore, we set $A = B = 0$.

This choice is entirely consistent with the case when the velocity function $v_t(x)$ is zero. Then the velocity on the surface is equal to the free stream velocity and for a symmetric airfoil, it must be of a zero thickness. If we, purely theoretically, prescribe $v_t(x) = 1$ along the chord, we get an airfoil in the shape of a circle, as

$$\frac{1}{\pi}\int_0^C \ln\left|\frac{1+\sqrt{\frac{\xi}{C-\xi}}\sqrt{\frac{C-x}{x}}}{1-\sqrt{\frac{\xi}{C-\xi}}\sqrt{\frac{C-x}{x}}}\right| d\xi = \sqrt{\left(\frac{C}{2}\right)^2 - \left(x-\frac{C}{2}\right)^2}. \tag{4.2.15}$$

Under these assumptions, the mapping between the velocity distribution $v_t(x)$ and the thickness function $t(x)$ is well defined. Although our method deals with airfoils which have a sharp trailing edge, from the above it is evident that a suitable choice of parameters A and B can give a description of airfoils with a non-zero thickness of their trailing edge $t(C)$.

The resulting equation for the thickness function is therefore

$$t(x) = \frac{1}{\pi}\int_0^C v_t(\xi) \ln\left|\frac{1+\sqrt{\frac{\xi}{C-\xi}}\sqrt{\frac{C-x}{x}}}{1-\sqrt{\frac{\xi}{C-\xi}}\sqrt{\frac{C-x}{x}}}\right| d\xi. \tag{4.2.16}$$

Finally, it is worth to mention one comment. The thickness function should, of course, be positive on the whole range of the chord line, except its endpoints. However, the above-described equation cannot guarantee this property for any arbitrary distribution $v_t(x)$. It could happen that at some points the resulting airfoil thickness will be negative. During the iterative process of the inverse method, this problem is fortunately not so frequent. If it happens, it is mainly during the first iterations and it occurs mostly in the vicinity of the trailing edge. For this reason, it is necessary to implement a control mechanism to check the positivity of the thickness. If the thickness at some point is negative then the magnitude of the fictitious velocity distribution u is raised at this point to achieve a positive thickness.

4.2.3 Construction of the airfoil

Points belonging to the airfoil surface are constructed from the camber line function $s(x)$ and the thickness function $t(x)$. Both functions depend on the velocity distribution, denoted as $u = \{u_u, u_l\}$. The airfoil ψ can be replaced by a pair of

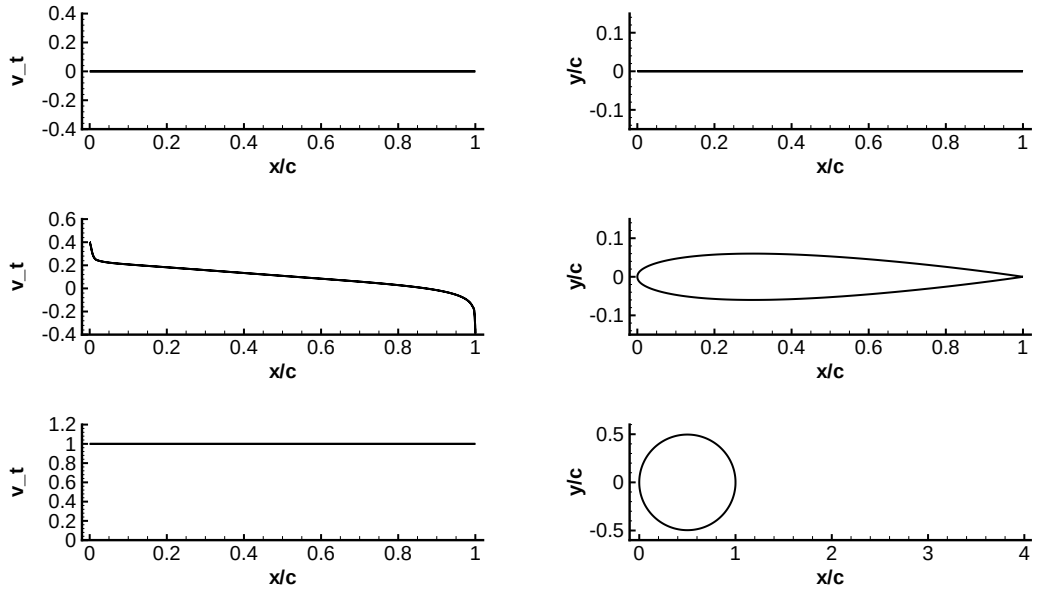

Figure 4.6: Example of airfoil shapes according to distribution $v_t(x)$.

curves $\psi_u(x)$ and $\psi_l(x)$, $x \in [0, C]$, representing the upper and lower part of the airfoil parametrized along the chord line.

The construction of the airfoil geometry is shown in Figure 4.7. The thickness is measured perpendicular to the mean camber line $s(x)$ (notice we use a simplification in Section 4.1). Therefore, the coordinates of the upper and lower airfoil surface are written as:

$$\psi_u^x(x) = x - t(x)\frac{s'(x)}{\sqrt{1+s'^2(x)}}, \quad \psi_u^y(x) = s(x) + t(x)\frac{1}{\sqrt{1+s'^2(x)}}, \tag{4.2.17}$$

$$\psi_l^x(x) = x + t(x)\frac{s'(x)}{\sqrt{1+s'^2(x)}}, \quad \psi_l^y(x) = s(x) - t(x)\frac{1}{\sqrt{1+s'^2(x)}}, \tag{4.2.18}$$

where $x \in [0, C]$.

By the above procedure, an airfoil can be designed according to the given velocity distribution. The approximate inverse operator $\mathbf{L}$ is thus the mentioned mapping $\mathbf{L}(u) = \mathbf{L}(u_u, u_l) = (\psi_u, \psi_l)$.

It is possible to prove that the operator $\mathbf{L}$ is continuous. To prove this statement it is sufficient to swap the limits and integrals, as well as use the relations for the sum and product of limits.

4.3 Numerical realization

The computation of the curves $\psi_u(x)$, $\psi_l(x)$, respectively $s(x)$ and $t(x)$ from (4.2.7) and (4.2.16), includes the evaluation of integrals, which is carried out with the aid of a suitable numerical quadrature. The integrands are functions of two variables x and ξ and have singularities for $x = \xi$. From this reason it

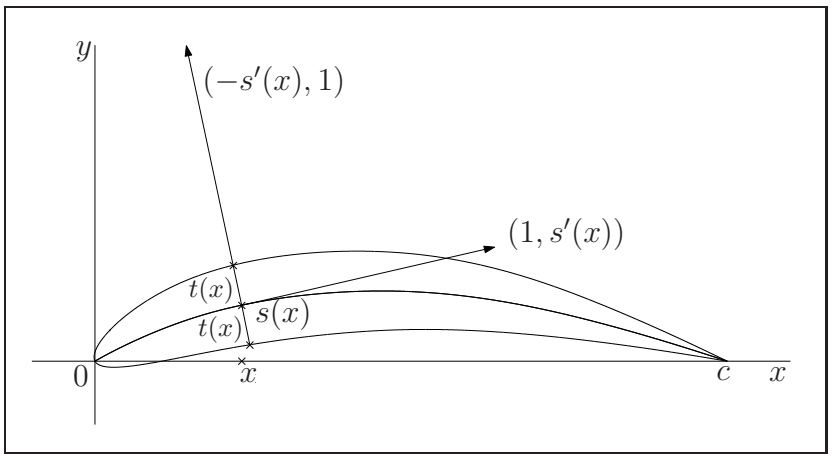

Figure 4.7: Construction of the airfoil

is necessary to avoid these points. The quadrature used in this method is the Chebyshev-Gauss quadrature [32], formulated for some function $f(x)$ as:

$$\int_{-1}^{1} \frac{f(x)}{\sqrt{1-x^2}} dx = \sum_{k=1}^{N/2} w_k f(\hat{x}_k) + R_N, \tag{4.3.1}$$

where N is an even number and $w_k = 2\pi/N$ are quadrature weights. The points $\hat{x}_k$ are roots of the Chebyshev polynomial

$$T_{N/2}(x) = \cos\left(\frac{N}{2} \arccos x\right) \tag{4.3.2}$$

and are given by

$$\hat{x}_k = \cos\left(\frac{(2k-1)\pi}{N}\right). \tag{4.3.3}$$

The error of the quadrature formula is expressed as

$$R_N = \frac{2\pi}{2^N N!} f^{(N)}(\eta). \tag{4.3.4}$$

Hence, if we denote the integrands in (4.2.6), (4.2.7) and (4.2.16) by $g(x, \xi)$, the integrals can be computed as

$$\int_0^C g(x,\xi)\, d\xi \approx \sum_{k=1}^{N/2} w_k g(x, \xi_k) \sqrt{\xi_k (C - \xi_k)}, \tag{4.3.5}$$

where $x \in [0, C]$ and $\xi_k = (C + C\hat{x}_k)/2$ are the quadrature nodes.

Based on this we can define the sequence $\{x_i\}_{i=0}^{N}$ as

$$x_i = \frac{C}{2}\left(1 + \cos\frac{i\pi}{N}\right). \tag{4.3.6}$$

Thus the nodes of the quadrature formula (4.3.5) are x_i, $i = 1, 3, \ldots, N-1$, and if we put for x the values x_i, $i = 0, 2, \ldots, N$, we avoid the problems with

singularities. The resulting formula for the evaluation of the integrals is of the form

$$\int_0^C g(x_i,\xi)\,d\xi \approx \frac{2\pi}{N}\sum_{k=1}^{N/2} g(x_i,x_{2k-1})\sqrt{x_{2k-1}(C-x_{2k-1})}, \quad i=0,2,4\ldots,N. \tag{4.3.7}$$

The distribution of nodes using the Chebyschev polynomial has a favourable property. The density of nodes is higher near the ends of the chord. From this reason the shape of the airfoil is expressed more precisely. The velocity is needed to be known at points x_i, $i=1,3,\ldots,N-1$ and the approximation of the airfoil is obtained at points x_i, $i=0,2,4,\ldots,N$. The number of evaluated points along one side of the airfoil is $N/2+1$ and the total number of different points of the airfoil is $2(N/2+1)-2=N$.

4.4 Pressure distribution

The so far derived approximate operator $\mathbf{L}$ assigns a new airfoil shape to a specified velocity distribution along the chord line. This can be in many cases sufficient. But if we consider, for example, viscous flow, this approach should be changed appropriately. Because of the molecular viscosity, the adhesion of particles on the surface of the airfoil occurs and so there is a zero velocity. For this reason, it does not make sense to consider a velocity distribution. As more appropriate it appears to prescribe a pressure distribution. In addition, the pressure is associated with many significant features such as the lift, drag and moment. Therefore, the ability to design the shape of the airfoil with a given pressure distribution is much more important.

In order to make maximum use of the so far obtained results, it is necessary to determine the relationship between the velocity and pressure. The approximate inversion $\mathbf{L}$, defined by (4.2.17) and (4.2.18), was derived on the basis of a simplified model for a potential incompressible flow. It is therefore possible to use the Bernoulli's equation for the incompressible, irrotational, steady flow, through which the relationship for the velocity is

$$v^2 = \frac{2(p_\infty - p)}{\rho_\infty} + v_\infty^2. \tag{4.4.1}$$

However, because the determination of the pressure on the airfoil is mainly done by models based on the solution of the Navier-Stokes equations for a compressible flow, this relationship is burdened with an error.

The pressure is assumed to be constant across the boundary layer in the normal direction to the airfoil. Hence, the velocity on the edge of a boundary layer is computed from the pressure on the airfoil. The transformation is derived

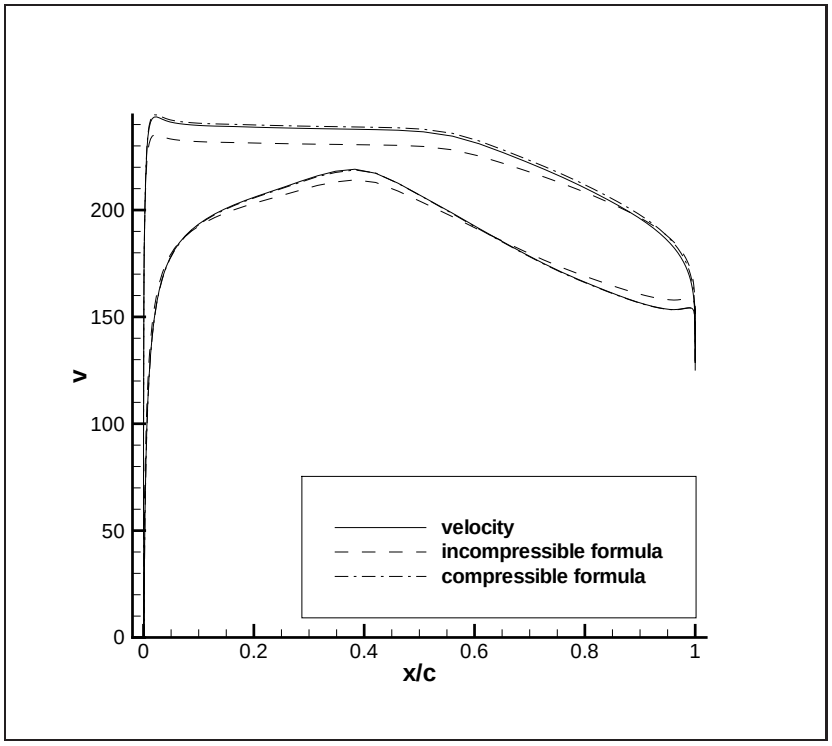

Figure 4.8: Comparison of a real velocity and transformed velocity from pressure (RAE2822, $\alpha_\infty = 1.96°$, $M_\infty = 0.604$, inviscid flow).

from relations for the pressure, density, Mach number and speed of sound [27],

$$p = p_0 \left(1 + \frac{\gamma - 1}{2} M^2\right)^{-\gamma/(\gamma-1)},$$
$$\rho = \rho_0 \left(1 + \frac{\gamma - 1}{2} M^2\right)^{-1/(\gamma-1)},$$
$$c^2 = \gamma p/\rho.$$

The derived formula for the velocity related to the velocity in the free stream is

$$\left(\frac{v}{v_\infty}\right)^2 = \frac{2/M_\infty^2 + \gamma - 1}{\gamma - 1} \frac{(p_0/p)^{(\gamma-1)/\gamma} - 1}{(p_0/p)^{(\gamma-1)/\gamma}}, \tag{4.4.2}$$

where p_0 is the stagnation pressure at zero velocity, M_∞ is the Mach number of the free stream, γ is the Poisson adiabatic constant and p is the given pressure distribution. The velocity defined by (4.4.2) will be used to design the airfoil shape. This transformed inverse operator, which maps a pressure distribution to an airfoil shape, will be denoted, for simplicity, again by $\mathbf{L}$.

5. Numerical validation of the method

The developed method is based on several ideas. It is well-known that the inverse problems belong to the class of the ill-posed problems. Therefore, in order to obtain physically applicable results, it was necessary to combine rigorous mathematical techniques with heuristic ideas based on the combination of several models. Therefore, it is necessary to carry out the validation of the developed technique which would guarantee its reliability and give bounds and limitations of its applicability. To this end, we present several numerical examples of the solution of inverse problems using various models of flow.

To remind, we solve the iteration process

$$u_k = u_{k-1} + \eta \left(f - \mathbf{PL} u_{k-1} \right), \tag{5.0.1}$$

where u_k denotes the fictitious distribution of the velocity or pressure on the upper and lower airfoil surface, given along the chord line. The direct operator $\mathbf{P}$ is either the potential flow model described in Section 2.1 or the compressible turbulent model described in Sections 2.2 and 2.3. The operator $\mathbf{L}$ is the approximate inversion derived in Chapter 4, either mapping a velocity distribution or a pressure distribution to an airfoil shape. The initial distribution u_0 is set equal to the target distribution f. In each step, we determine the airfoil shape $\psi_{k-1} = \mathbf{L} u_{k-1}$ and then compute the velocity/pressure distribution $u = \mathbf{P}(\mathbf{L} u_{k-1})$.

5.1 Potential flow

5.1.1 NACA0012

One of the ways to validate the new method is to consider a problem with a known solution and to see if using this method we obtain the same solution. To start with the simplest problem, we consider flow around the symmetric NACA0012 airfoil, with the potential flow model described in Section 2.1, yet without compressibility corrections. The target velocity distribution f on the airfoil is obtained by the calculation for a given velocity of the free stream and the selected angle of attack. The initial fictitious velocity distribution u_0 is chosen the same as the target distribution f.

First, we test a case for a symmetric flow with the angle $\alpha_\infty = 0°$. Figure 5.1 shows in the left part the initial fictitious distribution u_0 and the newly evaluated velocity distribution $\mathbf{PL} u_0$ corresponding to the newly created airfoil. On the right side, there is a comparison of the new design with the original shape. The scales of the image were adjusted to highlight the differences between the shapes. It can be seen that the initial design of the shape of the airfoil is very close to

the target shape. After ten iterations we get the NACA0012 original shape with the corresponding velocity distribution (see Figure 5.2).

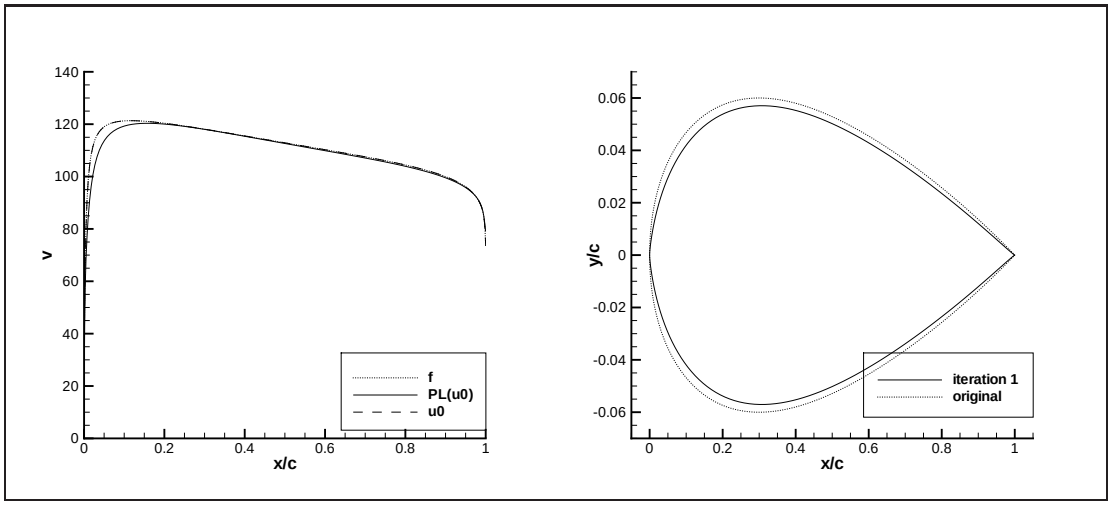

Figure 5.1: NACA0012, $\alpha_\infty = 0°$, $M_\infty = 0.3$ - after first iteration.

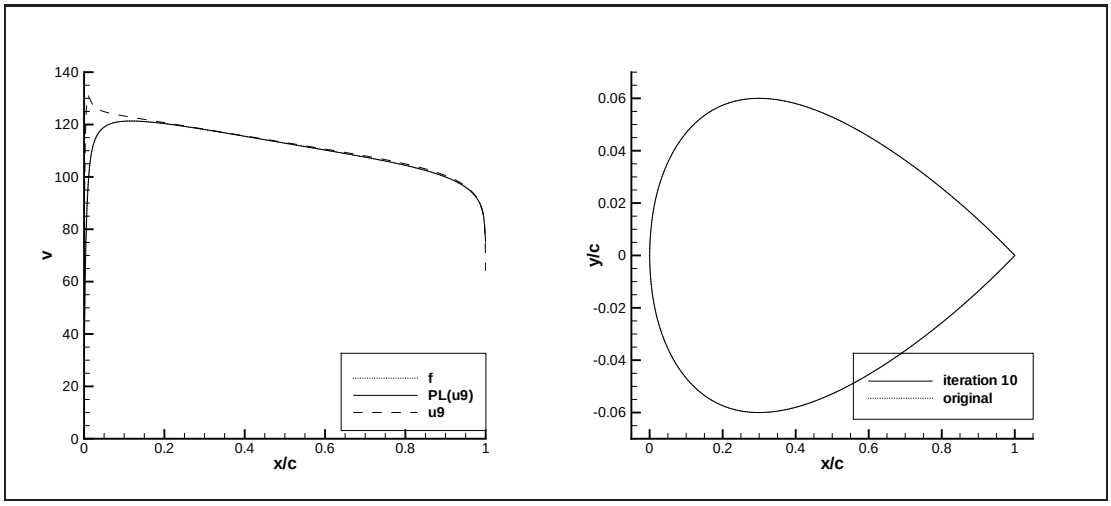

Figure 5.2: NACA0012, $\alpha_\infty = 0°$, $M_\infty = 0.3$ - after 10th iteration.

Another test is then a flow with a non-zero angle of attack. For selected different angles α_∞ we determine the velocity distribution, from which we create first approximations of the airfoil shapes using the inverse operator. Using an iterative process, we should get back the original symmetric NACA0012 airfoil. Figure 5.3 shows the result after the first iteration for the angle $\alpha_\infty = -2.5°$. It can be seen that the initial approximation already has a different shape. This is due to the fact that we use the asymmetric velocity distribution as the initial distribution u_0. Therefore, it is necessary to do more iterations to converge than in the previous case, when the fictitious target distribution was very close to the desired distribution. After fifteen iterations we obtain a shape which is very close to the original one. After thirty iterations we finish with the desired result (Figure 5.4).

Comparison of different choices for angles of attack can be found in Figure 5.5. The results show that the number of iterations depends on how large is the difference between each target velocity distribution (and hence initial fictitious distribution) and the fictitious distribution corresponding to the target shape. The speed of convergence, therefore, depends on how is the prescribed angle of attack distant from the so-called ideal angle of attack. This is such an angle, when the stagnation point is located in the beginning on the leading edge. For a symmetric NACA0012 airfoil, the ideal angle of attack is zero and therefore this configuration has the highest rate of convergence. The value of the parameter is $\eta = 0.9$.

The solution of the inverse problem using the potential flow model is very fast. It takes few seconds to get the results.

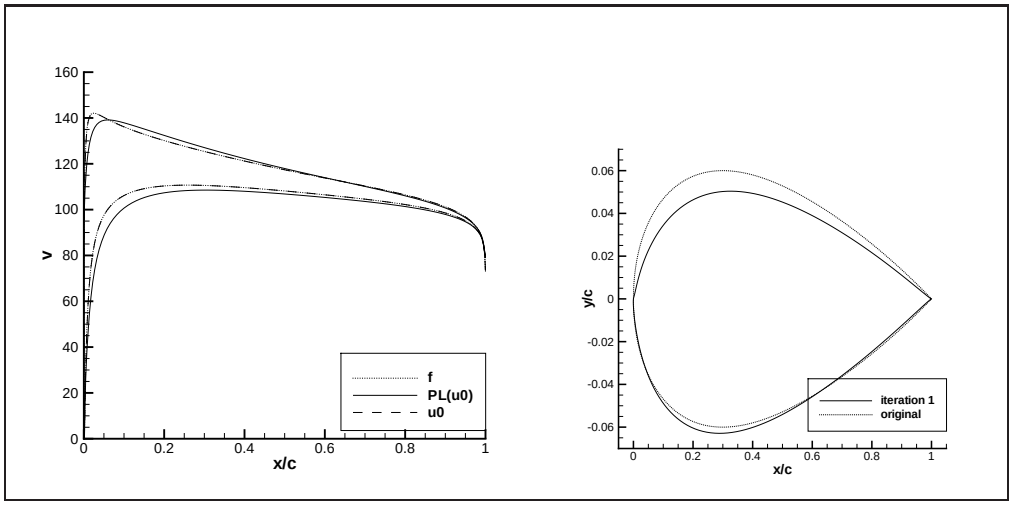

Figure 5.3: NACA0012, $\alpha_\infty = -2.5°$, $M_\infty = 0.3$ - after first iteration.

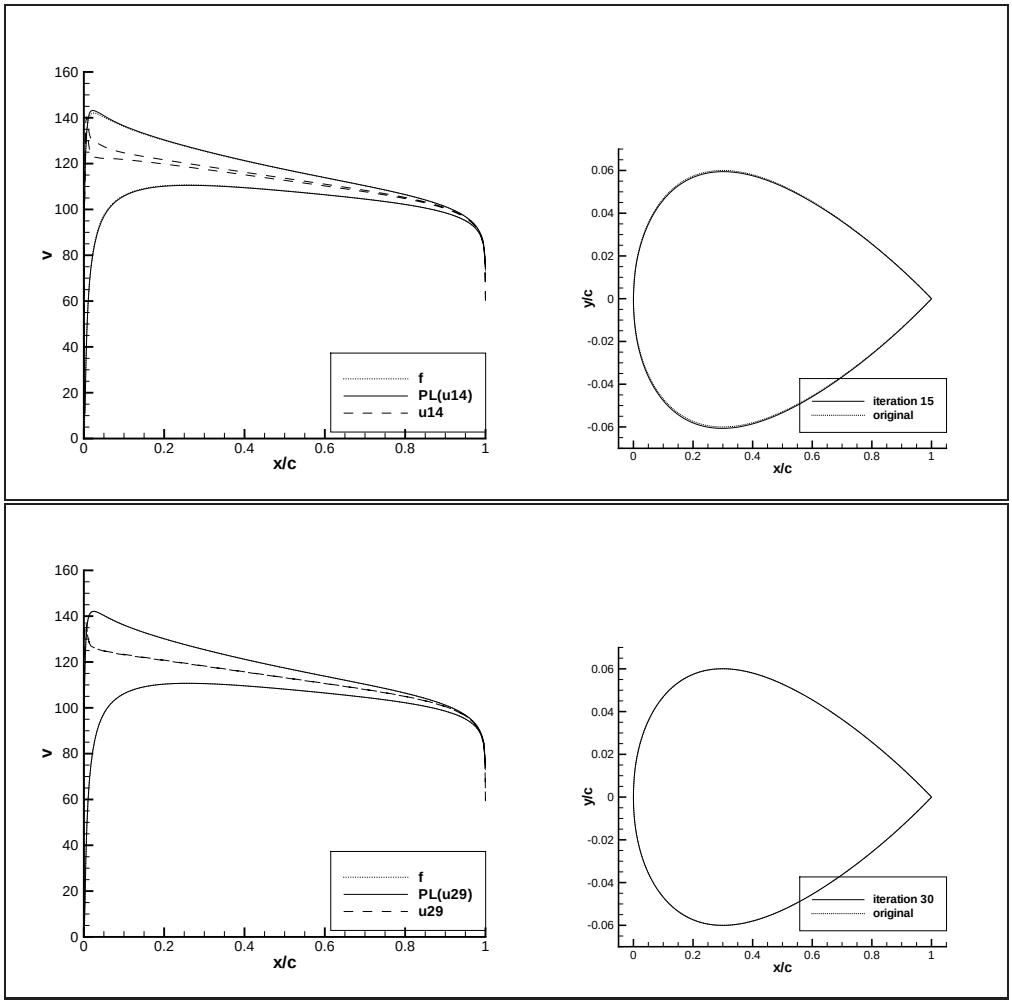

Figure 5.4: NACA0012, $\alpha_\infty = -2.5°$, $M_\infty = 0.3$ - after 15th and 30th iteration.

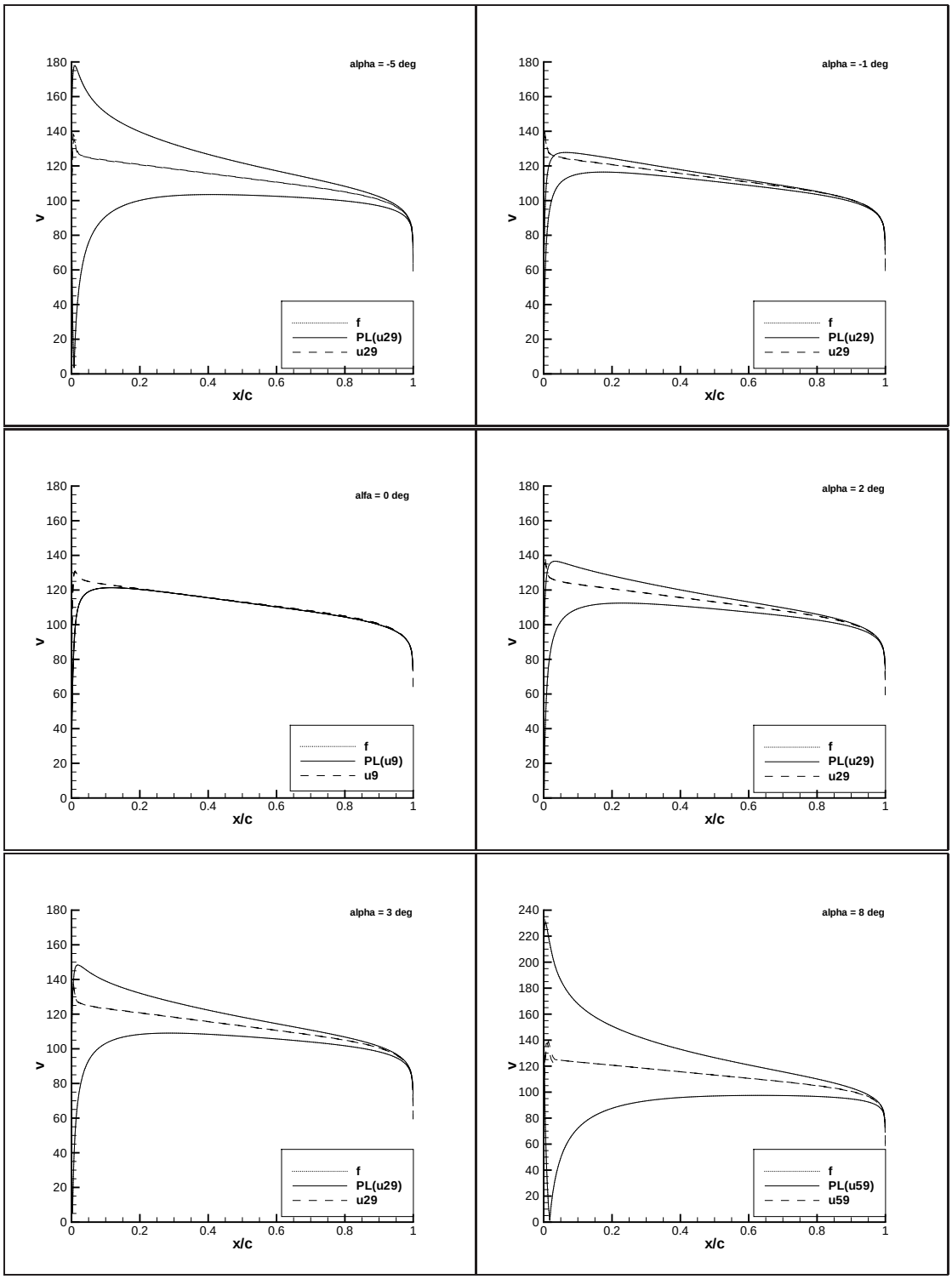

Figure 5.5: NACA0012, various angles of attack, $M_\infty = 0.3$ - results from the inverse method.

5.1.2 Eppler e337

The next example is an asymmetric airfoil Eppler e337, whose shape is shown in Figure 5.6. This test case illustratively shows the ability of convergence even

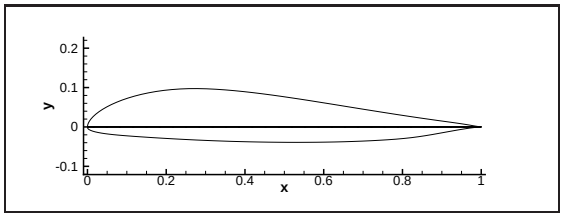

Figure 5.6: Shape of the Eppler e337 airfoil.

for asymmetric airfoils. Every time, the initial shape is obtained from the target distribution, which turns during iterations into the desired target shape.

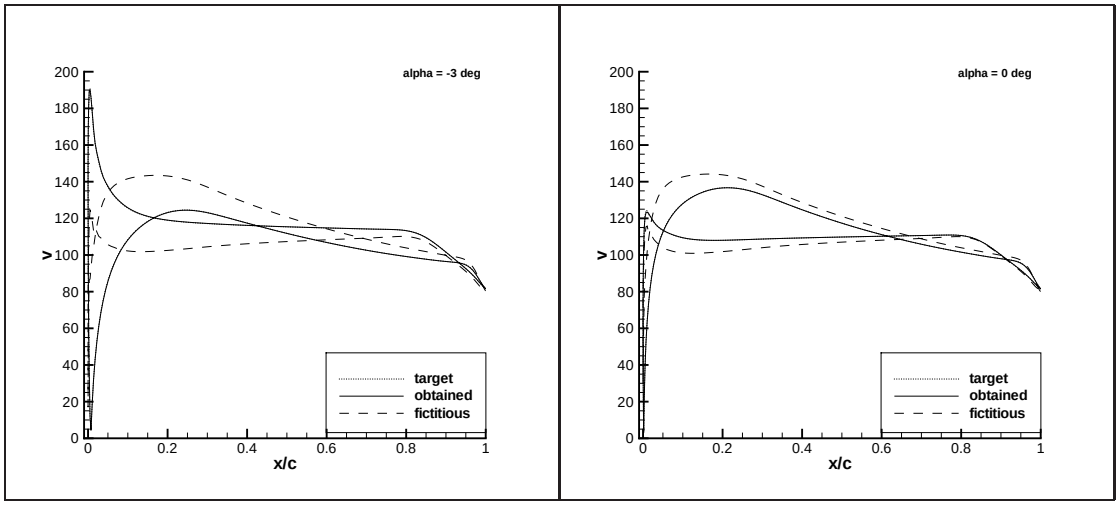

Figure 5.7: Eppler e337, various angles of attack, $M_\infty = 0.3$ - results from the inverse method.

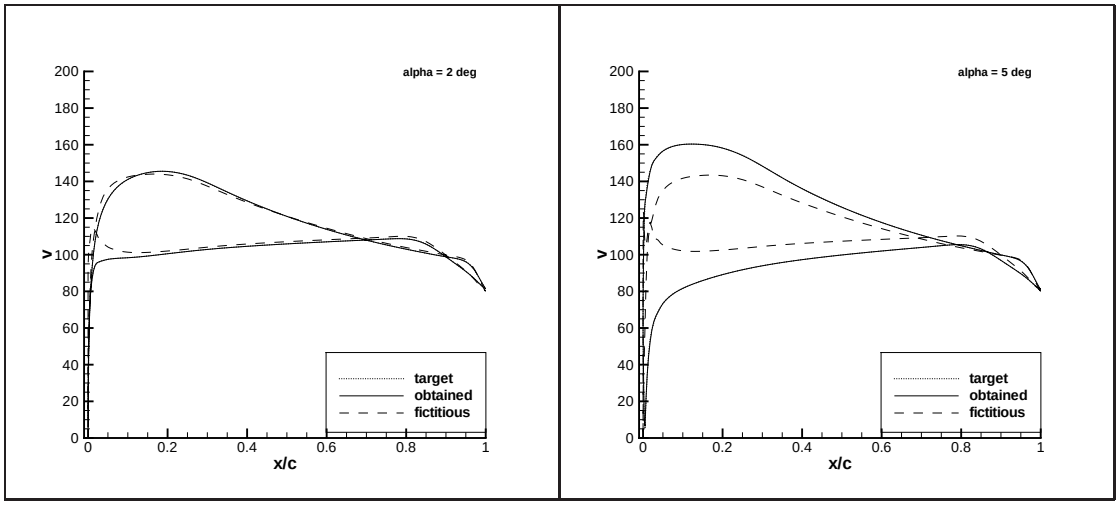

Figure 5.8: Eppler e337, various angles of attack, $M_\infty = 0.3$ - results from the inverse method.

5.2 Viscous flow

Now it is necessary to test the method for the viscous, compressible, turbulent flow described in Sections 2.2 and 2.3. Since the velocity on the airfoil surface is zero, we consider the pressure distribution instead of this.

5.2.1 NACA0012

At first, we test again a symmetric NACA0012 airfoil at zero angle of attack. The free stream velocity was selected so that $M_\infty = 0.6$. The Reynolds number for the presented examples has the value $Re = 6300000$. In Figure 5.9 we can see the initial design of the airfoil shape. Unlike for the incompressible flow, there is a much greater difference caused by the compressibility effects of the air. Also, the greater thickness near the trailing edge caused by the boundary layer is noticeable. After a few dozen iterations, we get again the original shape of the

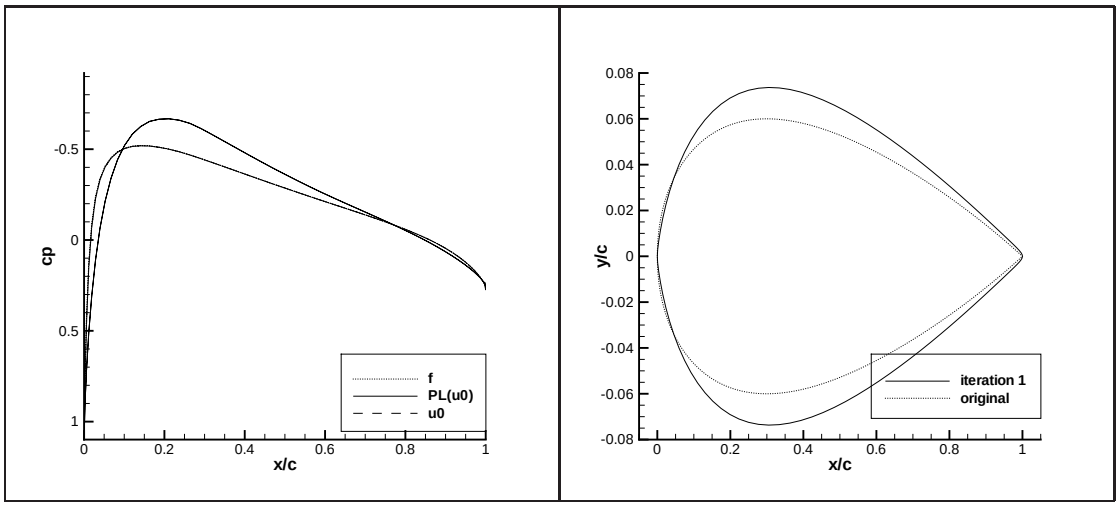

Figure 5.9: NACA0012, $\alpha_\infty = 0°$, $M_\infty = 0.6$, viscous flow - after first iteration.

airfoil. The result is shown in Figure 5.11, the following pictures show the rate of convergence of the solution and the flow field around the airfoil.

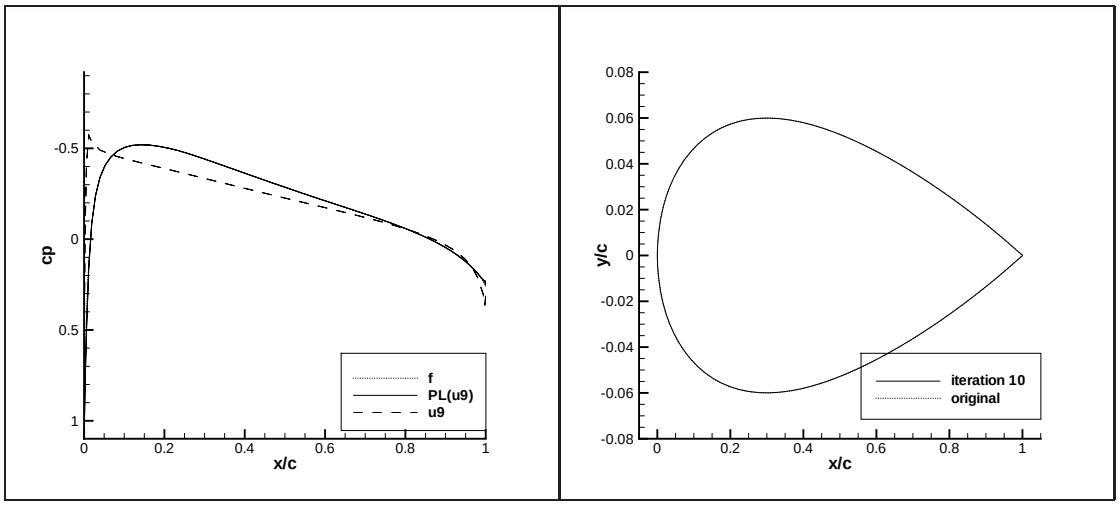

Figure 5.10: NACA0012, $\alpha_\infty = 0°$, $M_\infty = 0.6$, viscous flow - after 10th iteration.

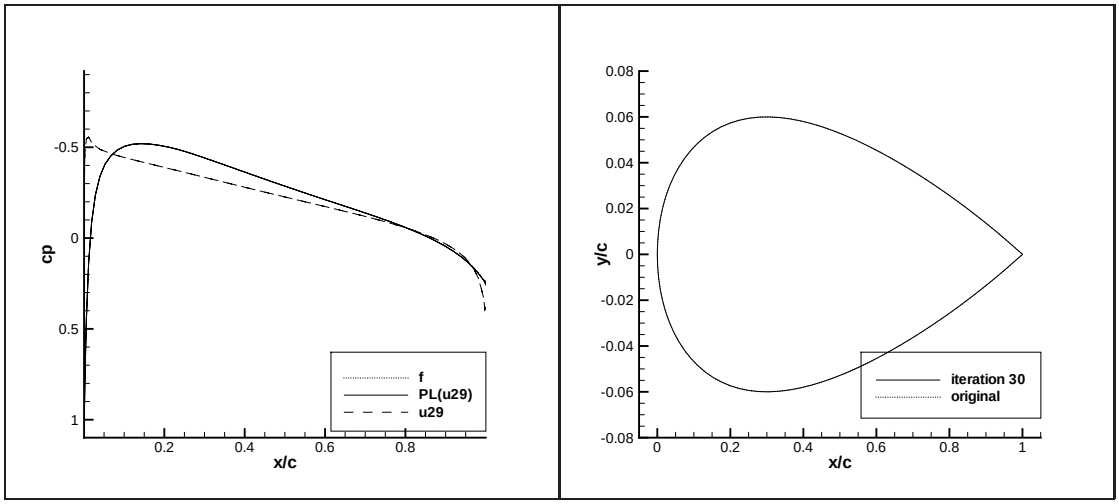

Figure 5.11: NACA0012, $\alpha_\infty = 0°$, $M_\infty = 0.6$, viscous flow - after 30th iteration.

The relative error of the solution is defined as the L_2-norm of the difference between the target and calculated pressure distribution, divided by the norm of the target distribution and evaluated on each airfoil side separately. Recall that the distribution on the upper and lower part is denoted by u_u and u_l (resp. f_u and f_l). The error on the upper part after (k+1)-th iteration is computed according to the formula

$$\epsilon_{rel,u} = \frac{\sqrt{\int_0^C \left(f_u(x) - \mathbf{PL}u_{k,u}(x)\right)^2 dx}}{\sqrt{\int_0^C f_u(x)^2 dx}}. \tag{5.2.1}$$

The maximum of $\epsilon_{rel,u}$ and $\epsilon_{rel,l}$ for our test case is shown in Figure 5.12.

The iteration process (5.0.1) is stopped when a sufficiently low error is achieved or the maximum number of iterations is exceeded. As a check of the result, the comparison of the target and calculated distributions can also serve.

The solution of the inverse problem using the model of the flow based on the Navier-Stokes equations take more time than using the potential model. However, depending on the number of elements in the FVM method, it is possible to get the solution in half an hour.

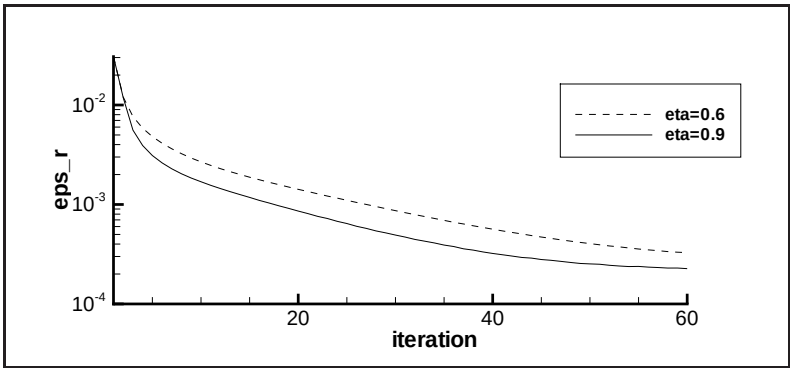

Figure 5.12: NACA0012, $\alpha_\infty = 0°$, $M_\infty = 0.6$, viscous flow - history of convergence for different η.

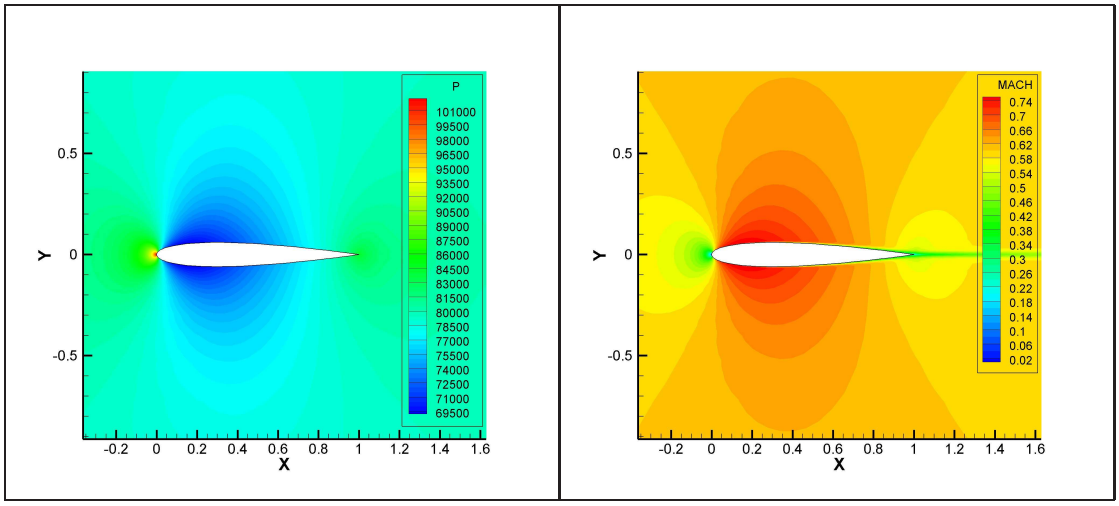

Figure 5.13: NACA0012, $\alpha_\infty = 0°$, $M_\infty = 0.6$, viscous flow - pressure and Mach number field.

The next step is to verify the method by solving problems for non-zero angles of attack. These angles were selected as 2 and 4 degrees, the free stream velocity and the Reynolds number remained the same. For smaller angles of attack the method works as expected, as in the case of a symmetric pressure distribution. In the first iteration, an airfoil corresponding to the specified pressure distribution is created. This shape is asymmetric, and as indicated above, has a greater thickness. Then it transforms step by step by the iterative process back into the initial symmetric shape (see Figure 5.14). The history of convergence is shown in Figure 5.15.

The case with the angle of attack $\alpha_\infty = 4°$ is more complicated. Due to the free stream velocity and the angle of attack and also because the initial airfoil design has a greater thickness, a transonic region on the upper surface occurs.

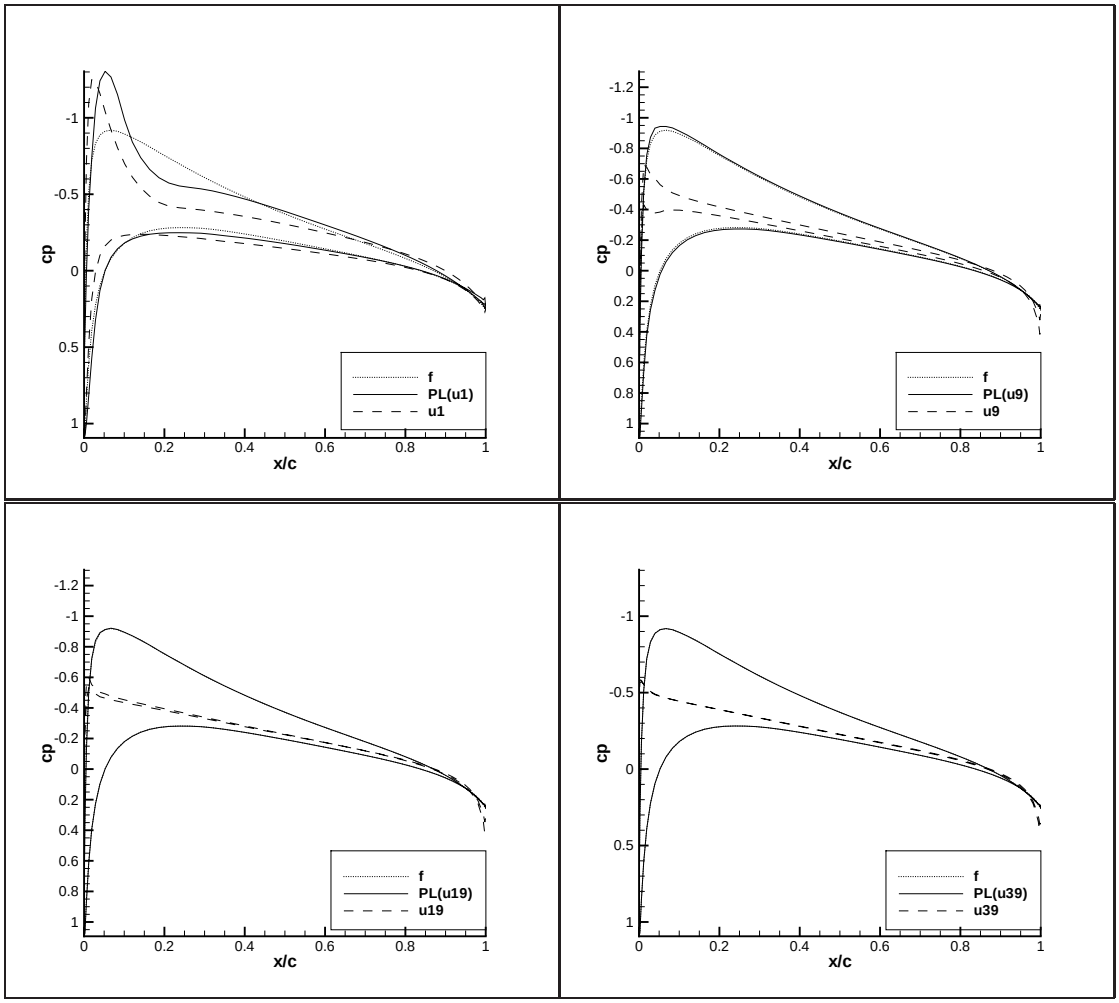

Figure 5.14: NACA0012, $\alpha_\infty = 2°$, $M_\infty = 0.6$, viscous flow - pressure distribution development.

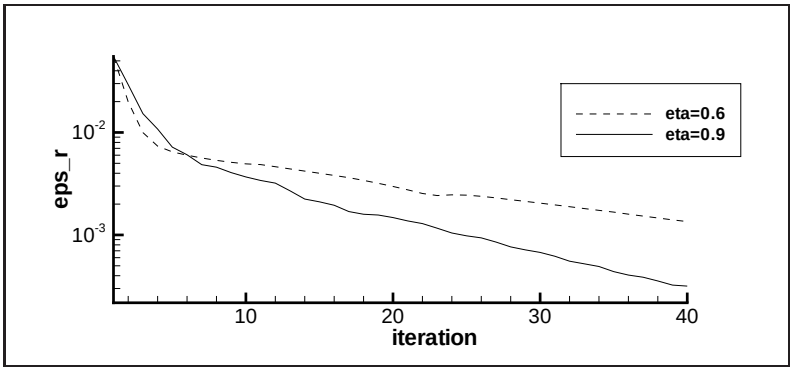

Figure 5.15: NACA0012, $\alpha_\infty = 2°$, $M_\infty = 0.6$, viscous flow - history of convergence.

This leads to the formation of a shock wave. The shock wave in Figure 5.16 is not so sharply captured because it is not our intention and so the computational grid is quite coarse in this area. The thin airfoil theory, of course, does not allow for the existence of shock waves that cause jumps in the pressure and velocity distribution. These jumps must be, according to this theory caused only by changing the thickness or the mean camber line of the airfoil. This leads to the fact that the designed airfoils could have very non-aerodynamic shapes, as shown in Figures 5.17 and 5.18. Fortunately, if the effect of shock waves is not too strong, the method is able to smooth slowly these bumps and return the airfoil back into the subsonic flow regime. Thus, we again finish with the NACA0012 airfoil, whose pressure distribution corresponds to the specified one (Figure 5.20). The history of convergence is in Figure 5.21. The relative error ceased to decrease after 85 iterations because it apparently reached the limit given by the number of discretization points.

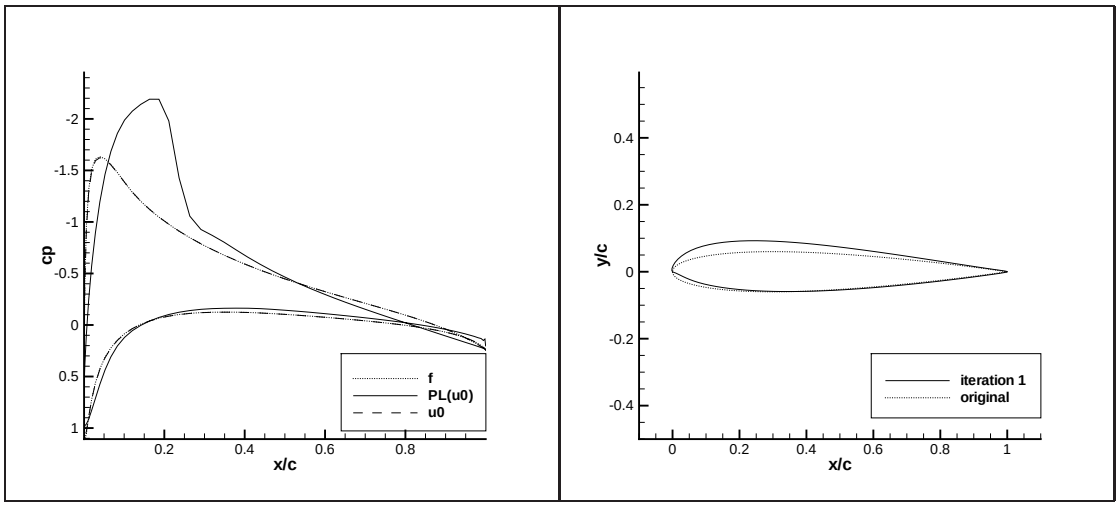

Figure 5.16: NACA0012, $\alpha_\infty = 4°$, $M_\infty = 0.6$, viscous flow - arising of transonic region.

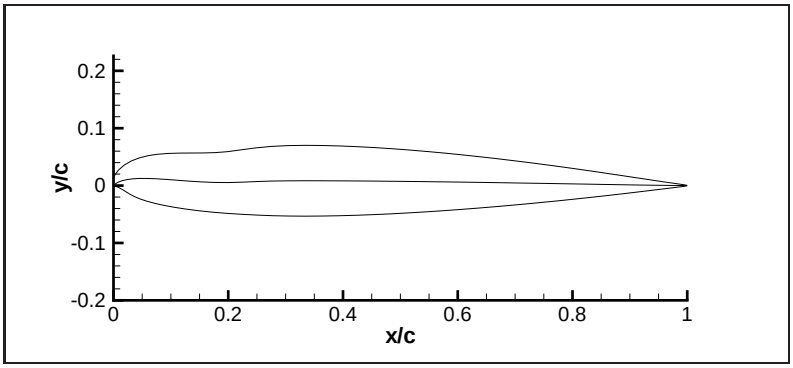

Figure 5.17: NACA0012, $\alpha_\infty = 4°$, $M_\infty = 0.6$, viscous flow - shape after two iterations.

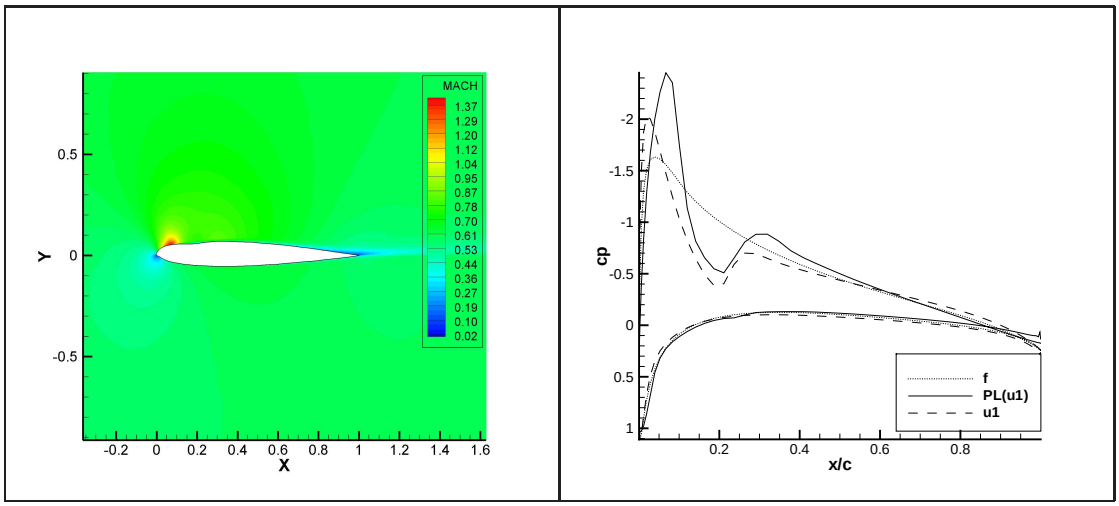

Figure 5.18: NACA0012, $\alpha_\infty = 4°$, $M_\infty = 0.6$, viscous flow - after second iteration.

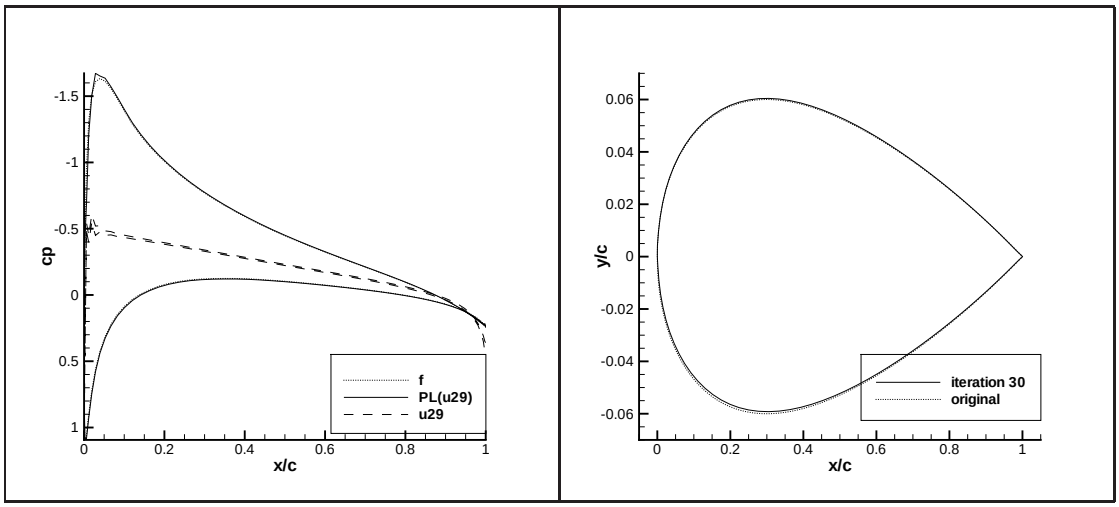

Figure 5.19: NACA0012, $\alpha_\infty = 4°$, $M_\infty = 0.6$, viscous flow - after 30th iteration.

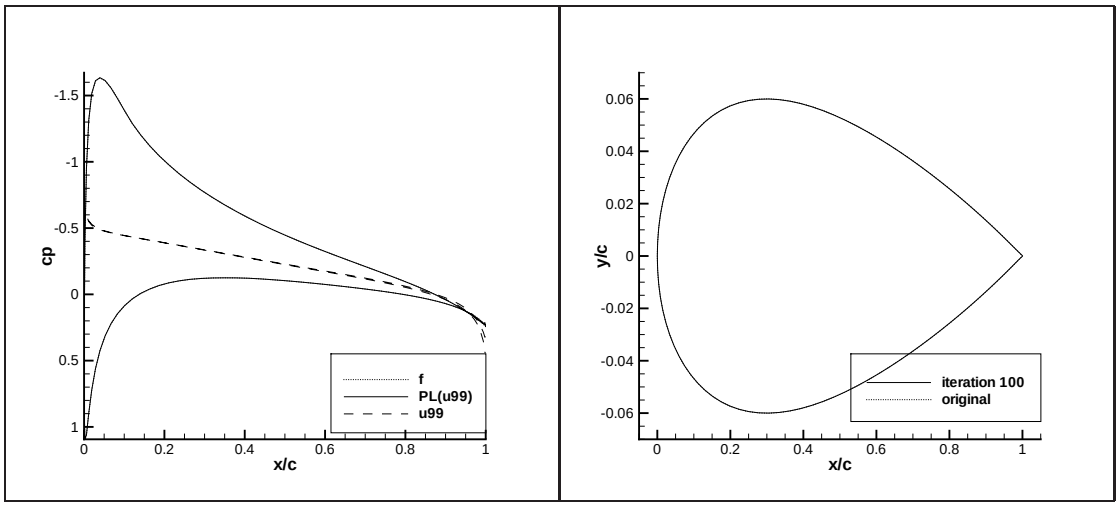

Figure 5.20: NACA0012, $\alpha_\infty = 4°$, $M_\infty = 0.6$, viscous flow - after final iteration.

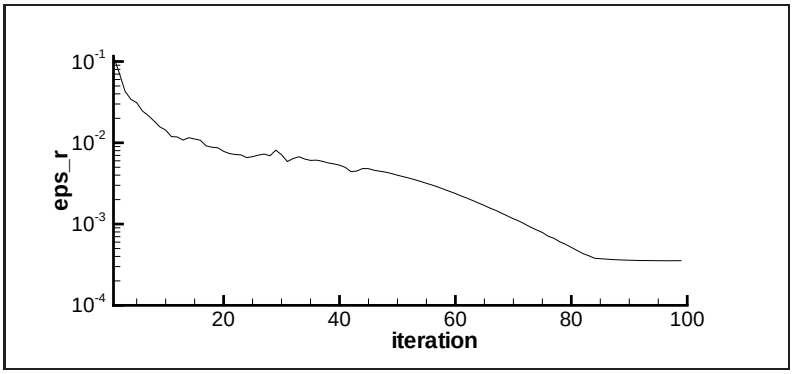

Figure 5.21: NACA0012, $\alpha_\infty = 4°$, $M_\infty = 0.6$, viscous flow - history of convergence, $\eta = 0.6$.

5.2.2 RAE2822

Another example is the pressure distribution obtained from RAE2822 airfoil for the selected flow regime $M_\infty = 0.604$, $\alpha_\infty = 1.96°$ and $Re = 6300000$. The results are on the following Figures 5.22–5.24.

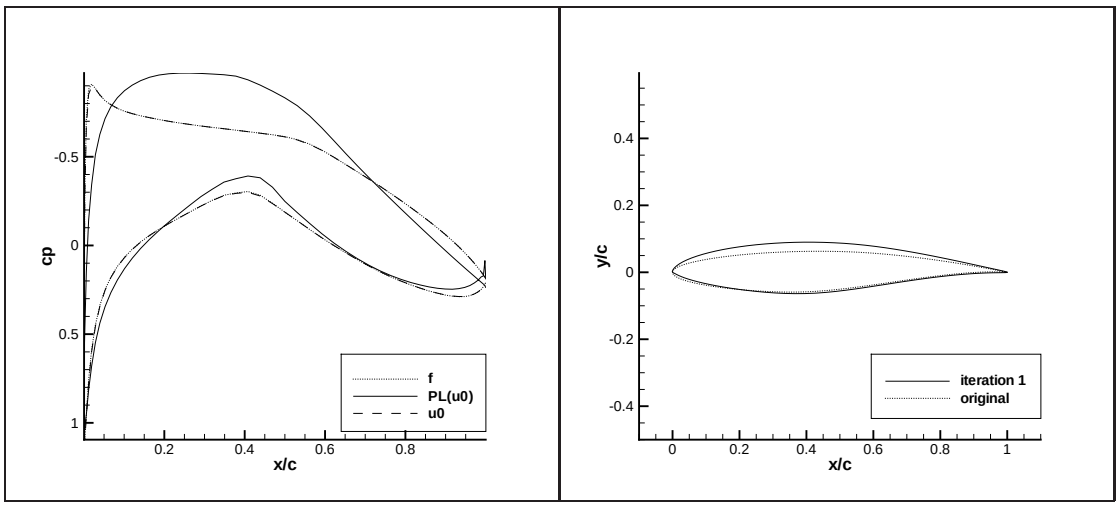

Figure 5.22: RAE2822, $\alpha_\infty = 1.96°$, $M_\infty = 0.604$, viscous flow - after first iteration.

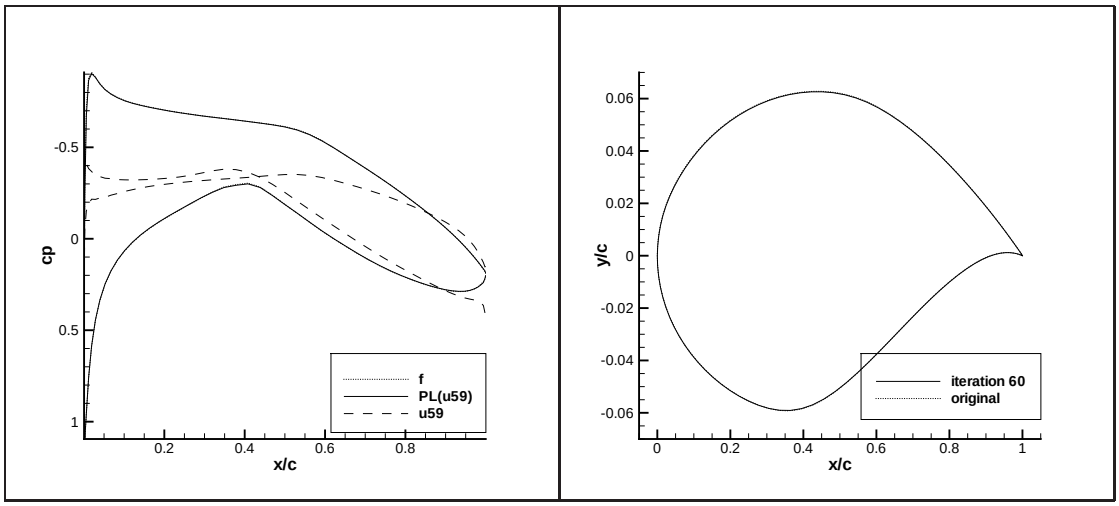

Figure 5.23: RAE2822, $\alpha_\infty = 1.96°$, $M_\infty = 0.604$, viscous flow - after final iteration.

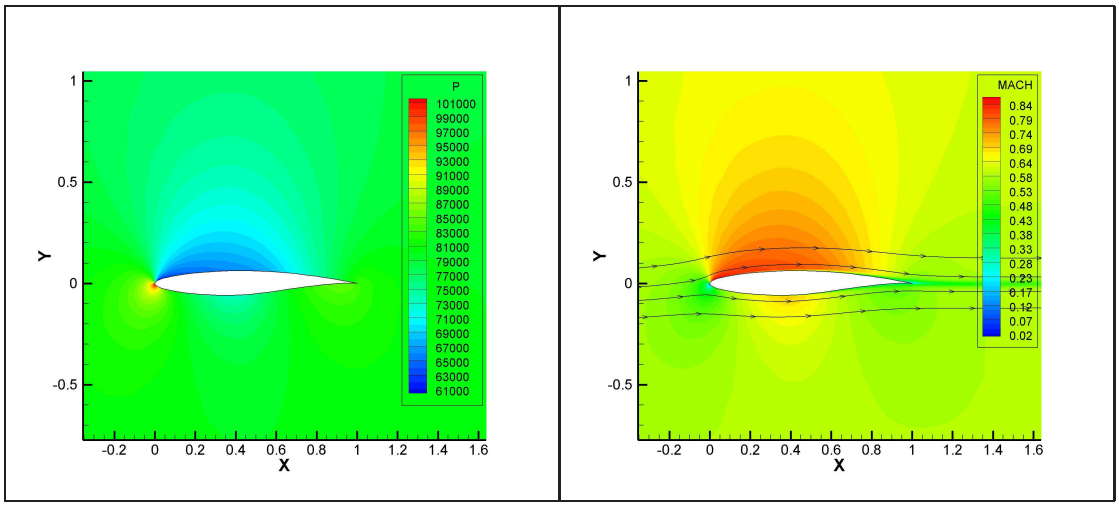

Figure 5.24: RAE2822, $\alpha_\infty = 1.96°$, $M_\infty = 0.604$, viscous flow - pressure and Mach number field.

5.2.3 Modification of the given pressure

So far, we have been looking for airfoil shapes with a velocity/pressure distribution that exactly match a known shape. Now, we need to validate that the method is able to find shapes with other distributions. Since the inverse problem is generally ill-posed, it is necessary to specify the target pressure distribution with caution.

The first test case represents a slight modification of an existing airfoil. The initial distribution is obtained from the NACA0012 airfoil for the angle of attack $\alpha_\infty = 2°$, $M_\infty = 0.6$ and $Re = 6300000$. This distribution was then manually modified so that the peak on the upper surface at the leading edge was cut. The results are on the following Figures 5.25–5.27.

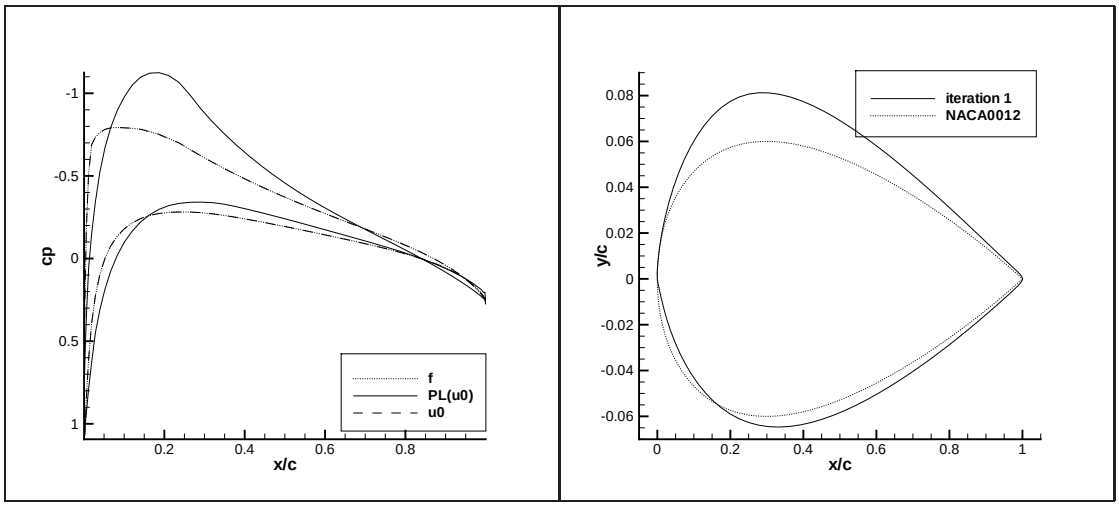

Figure 5.25: Modified distribution, $\alpha_\infty = 2°$, $M_\infty = 0.6$, viscous flow - after first iteration.

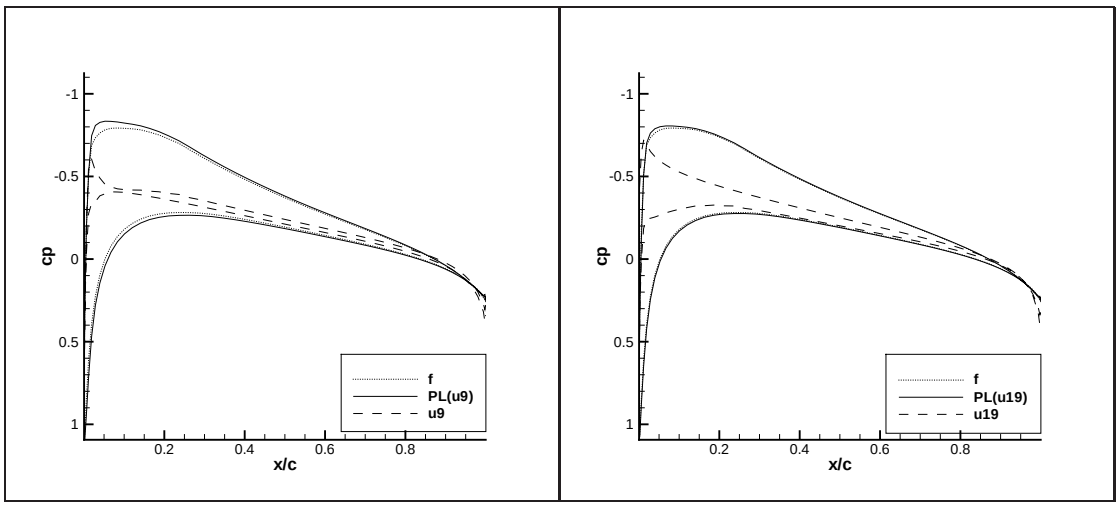

Figure 5.26: Modified distribution, $\alpha_\infty = 2°$, $M_\infty = 0.6$, viscous flow - after 10th and 20th iteration.

The other test case shows the ability of the presented method to design an airfoil shape to a completely new pressure distribution. We would like to obtain

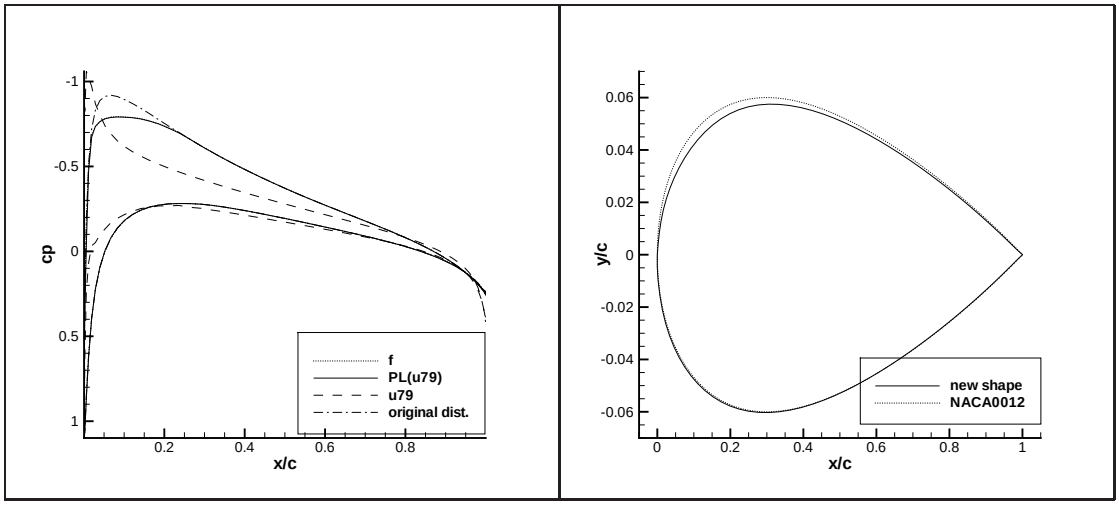

Figure 5.27: Modified distribution, $\alpha_\infty = 2°$, $M_\infty = 0.6$, viscous flow - final iteration.

a shape meeting the target c_p distribution with the angle of attack $\alpha_\infty = 1°$ and the free stream Mach number $M_\infty = 0.6$. We can also obtain a shape which satisfies the same c_p distribution for a different Reynolds number and Mach number $M_\infty = 0.5$.

The obtained results show a good agreement. The computed pressure coefficient distribution corresponds to the target distribution, except at the trailing edge where it is slightly distorted. This is caused by the fact that the new airfoil is rather thick near the trailing edge and the target pressure seems to be unrealistic in this area.

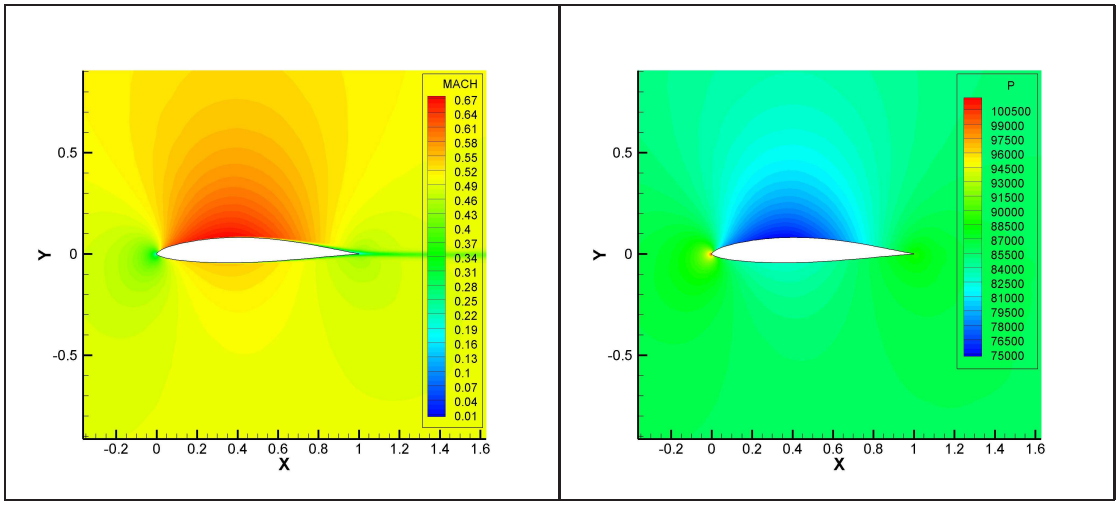

Figure 5.28: Mach number and pressure around the airfoil (newly prescribed distribution, $\alpha_\infty = 1°$, $M_\infty = 0.5$, $Re = 5 \cdot 10^6$).

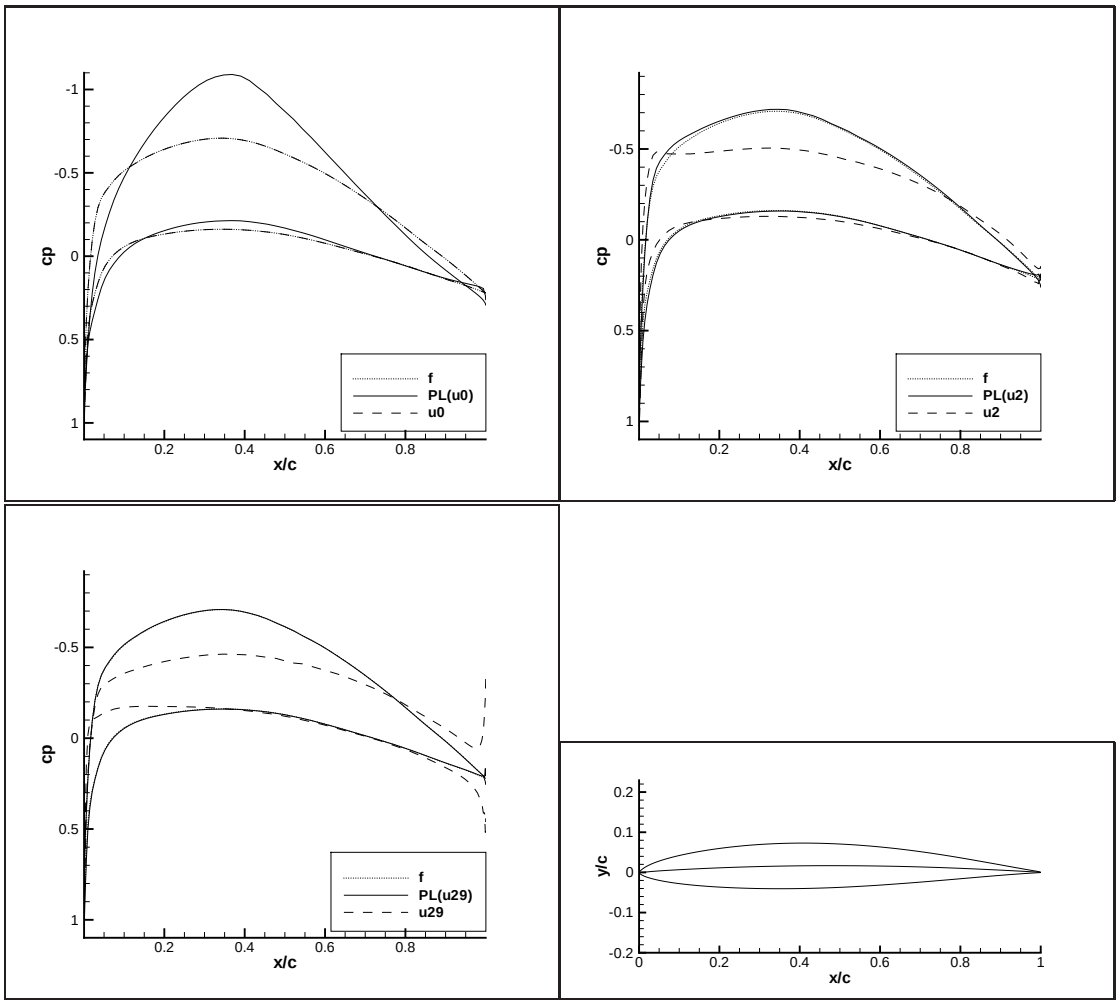

Figure 5.29: Completely new prescribed distribution, $\alpha_\infty = 1°$, $M_\infty = 0.6$, $Re = 12.8 \cdot 10^6$.

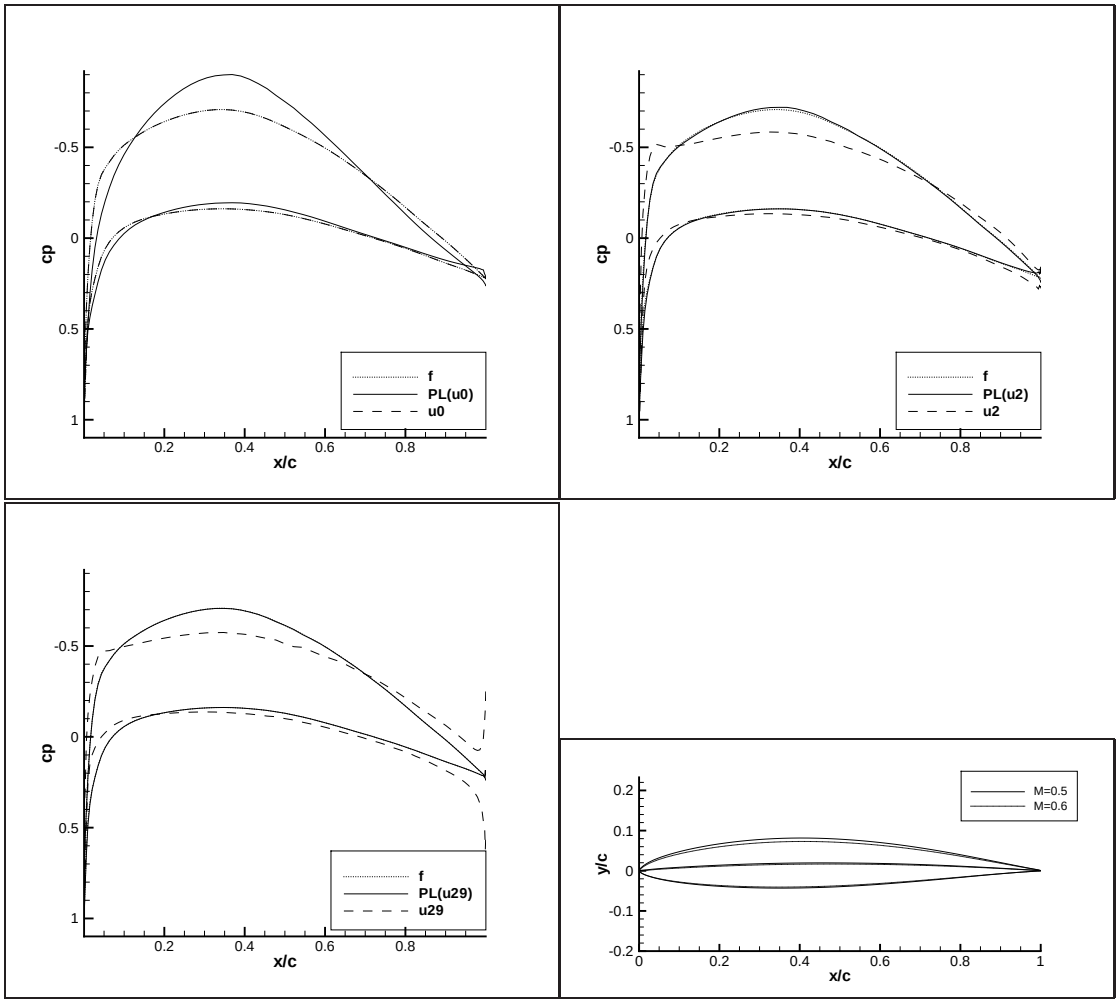

Figure 5.30: Completely new prescribed distribution, $\alpha_\infty = 1°$, $M_\infty = 0.5$, $Re = 5 \cdot 10^6$. Comparison with the airfoil designed with the same c_p distribution for $M_\infty = 0.6$.

Conclusion

A novel method for a solution of an inverse problem of a flow around an airfoil was described in this work. Its purpose is to determine the shape of an airfoil based on the specified velocity or pressure distribution on its surface, given along the chord line. Therefore, it can be used in modifications of existing airfoils or be applied in optimization methods.

The presented method consists of two parts. The first part solves the flow problem and the second part is responsible for the shape design. The advantage of this method is that these parts may be independent of each other. Therefore, it is possible to combine the various models of flow depending on which suits better our requirements. The potential flow model solved by the Fredholm integral equation represents a fast solution which is suitable for problems with low velocity and small angles of attack. Thanks to its speed it is used mostly in applications where it is necessary to evaluate many airfoils. The integral formulation allows an effective solution of the problem.

On the other hand, the flow described by the system of the averaged Navier-Stokes equations with the $k-\omega$ turbulence model provides a sufficiently accurate description of the reality. The use of the EARSM turbulence model significantly improves the accuracy of the numerical simulation at the cost of a slight increase in computational demands. The numerical method of the solution is fast enough due to the implicit formulation and also robust for the considered problem. The way of solving the systems of the Navier-Stokes equations and the turbulence equations in a sequential approach makes the implementation of the turbulence model into the existing source code easier.

The approximate inverse operator is derived on the basis of the thin airfoil theory. This allows us to create the initial approximation of the airfoil shape directly from the prescribed velocity or pressure distribution. If the angle of attack is close to the ideal angle of attack, the initial approximation will be very close to the desired shape. Thanks to this, the major shape changes are done within a few iterations. In the subsequent iterations, only the shape refinement is performed. The solution of the flow problem is considered as a restarted problem with changing geometry. Hence due to small changes in the shape in later iterations, only a few dozen of time steps in the CFD solver are necessary.

The examples given at the end of this work demonstrate the ability of the method. Based on the known airfoil shapes and their velocity/pressure distributions, the presented method designed the corresponding airfoil shapes. By comparing these shapes the method was validated. Also the examples of new pressure distributions were presented, where the method was also successful.

The iterative process is treated as a fixed point problem. Although the practical results proved the correctness of this approach, it is not optimal with respect to the convergence speed. A more sophisticated technique would better utilize the potential of the method.

The method is intended for subsonic problems. However, as the presented examples indicate, the method can also handle the situations when the flow changes to transonic during the iteration process. On the other hand, the method may have problems if there would be a significant flow separation.

Bibliography

[1] Drela, M. *Pros and Cons of Airfoil Optimization*. Frontiers of Computational Fluid Dynamics 1998. D. A. Caughey, M. M. Hafez, Eds. World Scientific Publishers, 1998. ISBN 981-02-3707-3

[2] Theodorsen, T. and I. E. Garrick. *General Potential Theory of Arbitrary Wing Sections*. NACA Report No. 452. NACA, 1933.

[3] Jacobs, E. N. *Preliminary Report on Laminar-Flow Airfoils and New Methods Adopted for Airfoil and Boundary-Layer Investigations*. NACA WR L-345. NACA, 1939.

[4] Lighthill, M. J. *A New Method of Two-Dimensional Aerodynamic Design*. R&M 2112. London: Aeronautical Research Council, 1945.

[5] Takanashi, S. *Iterative Three-Dimensional Transonic Wing Design Using Integral Equations*. Journal of Aircraft, Vol. 22, No. 8. August 1985, pp. 655–660.

[6] Campbell, R. L. and L. A. Smith. *A Hybrid Algorithm for Transonic Airfoil and Wing Design*. AIAA Paper 87-2552, 1987.

[7] Eppler, R. and D. M. Somers. *A Computer Program for the Design and Analysis of Low-Speed Airfoils*. NASA Technical Memorandum 80210. August 1980.

[8] Drela, M. *Elements of Airfoil Design Methodology*. Applied Computational Aerodynamics, edited by P. A. Henne, Vol. 125 of Progress in Astronautics and Aeronautics, AIAA. Washington DC: AIAA, 1990, pp. 167–189.

[9] Garabedian, P. and G. McFadden. *Design of Supercritical Wings*. AIAA Journal, Vol. 20, No. 3. 1982, pp 289–291.

[10] Jameson, A. *Aerodynamic Design via Control Theory*. Journal of Scientific Computing, Vol. 3, No. 3, 1988.

[11] Campbell, R. L. *Efficient Viscous Design of Realistic Aircraft Configurations*. AIAA Paper 98-2539, 29th Fluid Dynamics Conference, Albuquerque, USA, 1998.

[12] Pelant, J. *Inverse Problem for Two-dimensional Flow around a Profile*. VZLÚ Report Z-69. Praha: Výzkumný a zkušební letecký ústav, 1998.

[13] Šimák, J. *Řešení inverzní úlohy obtékání leteckého profilu*. Master thesis. Charles University in Prague, 2005.

[14] Pelant, J., K. Adámek and J. Šimák. *Inverse problem for two-dimensional flow around a profile*. 6th World Congresses of Structural and Multidisciplinary Optimization. Rio de Janeiro, 30 May - 03 June 2005, Brazil.

[15] Šimák, J., J. Pelant. *A contractive operator solution of an airfoil design inverse problem*. *PAMM*, 7, 2007 (DOI: 10.1002/pamm.200700136).

[16] Šimák, J., J. Pelant. *Solution of an Airfoil Design Problem With Respect to a Given Pressure Distribution for a Viscous Laminar Flow*. VZLÚ Report R–4186. Praha: Výzkumný a zkušební letecký ústav, 2007.

[17] Šimák, J., J. Pelant. *Design of an Airfoil from a Given Pressure Distribution Using an Approximate Inverse Operator*. 2nd International Conference on Engineering Optimization, September 6-9, 2010, Lisbon, Portugal.

[18] Drela, M., *XFOIL: An Analysis and Design System for Low Reynolds Number Airfoils*. Conference on Low Reynolds Number Airfoil Aerodynamics, University of Notre Dame, June 1989.

[19] Černý, I. *Základy analysy v komplexním oboru*. Praha: Academia, 1967.

[20] Michlin, S. G. *Integral Equations*. Oxford: Pergamon Press, 1964.

[21] Pelant, J. *The Application of Integral Equations on Potential Flow around Profiles at Low Speed at Given Circulations*. VZLÚ Report Z-35. Praha: Výzkumný a zkušební letecký ústav, 1980.

[22] Anderson J. *Fundamentals of aerodynamics*. 5th ed. New York: McGraw-Hill, 2011.

[23] Cook, P. H., M. A. McDonald and M. C. P. Firmin. *Aerofoil RAE 2822 - Pressure distributions and boundary layer and wake measurements*. AGARD AR-138. November, 1979.

[24] Wilcox, D. C. *Turbulence Modeling for CFD*. 2nd ed. DCW Industries Inc., 1998.

[25] Kok, J. C. Resolving the Dependence on Freestream Values for the $k-\omega$ Turbulence Model. *AIAA Journal*. vol. 38. 2000, No. 7, pp. 1292–1295.

[26] Wallin, S. *Engineering turbulence modelling for CFD with a focus on explicit algebraic Reynolds stress models*. Doctoral thesis. Stockholm: Royal Institute of Technology, 2000.

[27] Shapiro, A. H. *The dynamics and thermodynamics of compressible fluid flow*. Reprint ed., with corrections. Krieger Pub. Co, June 1983. ISBN 0-89874-566-7.

[28] Feistauer, M., J. Felcman and I. Straškraba. *Mathematical and Computational Methods for Compressible Flow*. Oxford: Clarendon Press, 2003.

[29] Saad, Y. *Iterative Methods for Sparse Linear Systems*. 2nd ed. SIAM, 2003.

[30] Glauert, H. *Die Grundlagen der Tragflügel und Luftschraubentheorie*. Berlin: Julius Springer, 1929.

[31] Milne-Thomson L. M. *Theoretical Aerodynamics*. 2nd ed. London: Macmillan, 1952.

[32] Ralston, A. *Základy numerické matematiky*. Praha: Academia, 1973.

[33] Jacobs E. N., K. E. Ward and R. M. Pinkerton. *The characteristics of 78 related airfoil sections from tests in the variable-density wind tunnel*. NACA Report No. 460. NACA, 1933.

[34] Jacobs E. N., R. M. Pinkerton. *Test in the variable-density wind tunnel of related airfoils having the maximum camber unusually far forward*. NACA Report No. 537. NACA, 1936.

[35] Abbot I. H., A. E. von Doenhoff and L. S. Stivers. *Summary of airfoil data*. NACA Report No. 824. NACA, 1945.

Attachments

6. NACA airfoils

Under the name NACA airfoils we mean a group of airfoil shapes developed by the National Advisory Committee for Aeronautics since the first half of the previous century. Each of the shapes is labelled by NACA letters and an appropriate code number, which means particular design parameters. Generally, these airfoils are designed using a mean camber line and an appropriate thickness. Expressions of these functions are analytic.

One of the first shape groups are the so-called four-digit series airfoils, which were designed from given geometrical properties. The first digit indicates a maximum camber expressed as a percentage of the chord line. Then the second digit indicates a position of the camber maximum on the chord away from the leading edge, given in tenths of the chord length. Finally, the last two digits indicate the maximum thickness of the airfoil, indicated as a percentage of the chord.

Airfoils are specified using the formulas for the camber line $s(x)$ and the thickness function $t(x)$ [33] normalized on the chord,

$$s(x) = m\frac{x}{p^2}\left(2p - x\right), \quad 0 \leq x \leq p, \tag{6.0.1}$$

$$s(x) = m\frac{1-x}{(1-p)^2}\left(1 + x - 2p\right), \quad p \leq x \leq 1 \tag{6.0.2}$$

and

$$t(x) = \frac{q}{0.2}\left(0.2969\sqrt{x} - 0.1260x - 0.3516x^2 + 0.2843x^3 - 0.1015x^4\right). \tag{6.0.3}$$

The thickness for $x = 1$ is not zero. If we would like to have a zero thickness trailing edge, the last coefficient is changed to -0.1036. Individual points on the top and bottom sides are then obtained as

$$\psi_u^x = x - t\sin\theta, \qquad \psi_u^y = s + t\cos\theta, \tag{6.0.4}$$

$$\psi_l^x = x + t\sin\theta, \qquad \psi_l^y = s - t\cos\theta, \tag{6.0.5}$$

where $\theta = \arctan\left(ds/dx\right)$.

The parameter meanings are as follows:

m - maximum camber (100 m is the first digit),

p - position of the maximum camber (10 p is the second digit),

q - maximum thickness (100 q are the last two digits).

Another group of airfoils include a five-digits series [34], where the camber line is determined by the formula

$$s(x) = \frac{1}{6}k_1\left(x^3 - 3mx^2 + m^2(3-m)x\right), \quad 0 \leq x \leq p, \tag{6.0.6}$$

$$s(x) = \frac{1}{6}k_1(1-x)m^3, \quad p \leq x \leq 1. \tag{6.0.7}$$

The thickness function is the same as in the previous case. The first digit determines after multiplying by 0.15 the desired theoretical lift coefficient, the second two digits divided by two give the value of p and finally the last couple of digits determines the thickness q. The coefficient k_1 is to be determined so as to achieve the desired theoretical lift coefficient for an ideal angle of attack.

There are other groups of NACA airfoils, such as modified 4-/5-digits series or 6-digits, 7-digits and 8-digits series. Their description is beyond the scope of this work, but it can be found in the literature, if necessary. See, e.g. [35].